Synthesis and characterization of folate-PEG-conjugated polysaccharide nanoparticles for potential use as a targeted DNA carrier.

Simone Houng, B. Eng.

Department of Biomedical Engineering
McGill University, Montreal, QC, Canada
February 2009

A thesis submitted to McGill University in partial fulfillment of the requirements of the degree of Master's of Engineering.

ACKNOWLEDGEMENTS

I would like to give my sincere thanks to my supervisor, Dr. Maryam Tabrizian, and the members of the Biomaterials research group of the Biomat'x Research Laboratories for over 2 years of support, advice, and encouragement through a sometimes challenging project.

In particular, I am thankful to Christina Holmes, my partner in the night shift, as a sounding board and guidance counselor during all my cell work. Her fine eye for details and tactful critical review was priceless in the editing of this document. Marinella Sandros was an invaluable and patient resource that I turned to often in deciphering unknown synthetic chemistry protocols while Line Mongeon's expertise with electronic microscopy was very much needed and very much appreciated. Fereshteh Azari very kindly helped perform agarose gel retention of pDNA in nanoparticles. I would like to thank Nicolas Duceppe for advice on cell protocols and transfection. I could not forget Anna Hillberg for extensive advice and editing of this document.

In rough times with chemical synthesis, Dr. Francoise Winnik (Department of Chemistry, University of Montreal) came to my rescue with generous help from her lab. Xingping Qiu is an expert and a savior with the design and extensive help with revised synthetic methods. I would also like to thank Zhimei Miao and Satu Strandman for their patience with gel permeation chromatography analysis.

NMR experiments were recorded at the Québec/Eastern Canada High Field NMR Facility, supported by grants from the Canada Foundation for Innovation, the Québec ministère de la recherche en science et technologie, and McGill University. I would like to recognize Tara Sprules, the facility manager, for making time for me and my samples.

Marie-Helene Lacombe of the flow cytometry facility guided me in performing my transfection analysis with great patience towards an inexperienced user and was a great help with translation. HEK 293T cells were obtained from Valerie Hay, under the supervision of Ciriaco A. Piccirillo, in the Department of Microbiology and Immunology of McGill University. Dr. Jay Nadeau (Department of Biomedical Engineering, McGill) kindly allowed the use of restriction enzymes as well as use of the UV spectrophotometer. Dieter P Reinhart and his PhD student Laetitia Sabatier (Department of Anatomy and Cell Biology, McGill) were kind enough to allow us to use their facilities for amplifying pDNA.

Finally, I would like to acknowledge Karen, I-Yuan, Caroline, Brian, Wendy and Katherine; my family, friends and a great support behind me throughout these years.

This work was possible through generous funding from the Fonds de recherche sur la nature et les technologies de Quebec (FRQNT), the National Sciences and Engineering Research Council of Canada (NSERC), and the Canadian Institutes of Health Research (CIHR).

TABLE OF CONTENTS

LIST OF FIGURES

LIST OF EQUATIONS

LIST OF TABLES

LIST OF SCHEMA

ABSTRACT

Designing an effective gene delivery carrier, combining good transfection potential with material properties such as biocompatibility, non-immunogenicity, and nontoxicity, is a challenging problem under active research. Non-viral vectors attempt to match the transfection efficiency of viral vectors without the issues of immunogenicity and mutagenicity. The aim of this study was to synthesize a biopolymer-based DNA carrier modified to enhance circulation times *in vivo* and incorporating a targeting moiety to certain cancerous cells. This carrier is made of chitosan linked to folate as a targeting ligand through a poly(ethylene glycol) molecule. Nanoparticles formed by chitosan-PEG-folate linked to a secondary polymer, alginate, were further complexed with plasmid DNA. Successful synthesis of chitosan-PEG-folate was confirmed and particles formed in the desired size range with positive surface charge. Transfection was optimized in HEK 293T cells but preliminary evaluation in Caov-3 and MDA-MB-231 cells were not successful. Further investigation of chitosan-PEG-folate/alginate complexes should be undertaken to assess the full potential of this material as a DNA carrier.

RÉSUMÉ

Le design d'un transporteur efficace pour le largage du matériel génétique ayant à la fois un bon potentiel de transfection ainsi que des bonnes propriétés physicochimiques et biologiques telles que la biocompatibilité, non-immunogénicité et non-toxicité, suscite beaucoup d'intérêt en recherche biomédicale. Les efforts majeurs concentrés sur développement des vecteurs non-viraux tentent d'égaler des vecteurs viraux en termes d'efficacité de transfection, mais éviter les problèmes d'immunogénicié et de mutagénicité associés a ceux-ci. Le but de cette étude était de développer une véhicule de livraison de gène à base de biopolymères modifiés afin d'augmenter d'une part le temps de circulation *in vivo* et d'autre part de pouvoir cibler certaines cellules cancéreuses. Ce système constitue de chitosan liée au folate, comme ligand pour le ciblage, via d'un bras séparateur à base de poly éthylène glycol. Les nanoparticules formées par complexation de chitosan-PEG-folate et de l'alginate, au moyen d'interactions électrostatiques, sont par la suite chargées avec un plasmide d'ADN. La synthèse des chitosans modifiés ainsi que la formation des complexes ayant la taille et le chargement désirés ont été suivies avec des techniques adéquates de caractérisation. Par ailleurs, le protocole de transfection a été optimisé pour les cellules HEK 293T. Cependant, les résultats préliminaires avec les cellules Caov-3 et MDA-MB-231 ne semblent pas confirmer l'efficacité de ce système pour la transfection de ces dernières lignées cellulaires. Une étude plus approfondie du complexe chitosan-PEG-folate/alginate s'avère nécessaire afin de déterminer son plein potentiel comme transporteur d'ADN.

CHAPTER 1
RESEARCH HYPOTHESIS AND OBJECTIVES

1.1 HYPOTHESIS

Conjugation of folate as a targeting ligand to chitosan via a poly(ethylene glycol) spacer molecule will improve the transfection potential of modified chitosan/alginate particles, particularly in cancer cell lines known to express the folate receptor.

1.2 OBJECTIVES OF THE PROJECT

In order to evaluate the transfection potential of this modified chitosan/alginate carrier system, the objectives of this Master's project were:

1. Synthesis of modified chitosan-PEG-folate polymer.
   - Confirmation of successful synthesis will be determined by ^{1}H NMR analysis and UV spectrophotometry.
2. Preparation and characterization of modified chitosan/ alginate particles.
   - Preparation conditions are to be optimized for particles in the nano-scale size range, with an overall positive surface charge.
3. Assessment of transfection ability of chitosan/alginate particles.
   - Transfection is to be assessed and optimized in the non-cancerous HEK 293T cell line before comparison with cells known to overexpress the folate receptor. Transfection efficiency will be compared to unmodified chitosan/alginate particles as well as the commercially available liposomal vector Lipofectamine.

CHAPTER 2
INTRODUCTION

2.1 GENE THERAPY

Gene therapy refers to the transfer of genetic material into targeted cells or organs with the aim of preventing, treating, or curing disease. There have been over 1400 clinical trials approved worldwide since 1989, treating a wide range of monogenic and multigenic diseases, including cancer, SCID, hemophilia and multiple sclerosis, although none have yet been approved for general use (John Wiley and Sons Ltd., 2009).

2.1.1 Viral gene therapy

In the past, the most promising approaches to gene therapy have been through the use of viral vectors, which consist of genetic material (either RNA or DNA) contained within genetically engineered replication-defective viruses, including, but not limited to: adeno-associated viruses, adenoviruses, herpes simplex viruses and retroviruses (Rubanyi, 2001). Due to their innate ability to carry and deliver genetic material into cells, viral vectors have shown high transfection ability and therefore have been very promising in terms of gene therapy. In fact, approximately 70% of clinical trials currently underway involve some form of viral vector. Despite the potential of viral vectors, major disadvantages also exist, including issues of oncogenicity due to random chromosomal integration, potential for mutation, issues related to targeting, and prevention of repeated dosages due to immunogenicity from viral proteins. Viral vectors are also limited by the size of plasmid that can be carried, which can be an issue in targeting multigenic diseases.

The first and most prominent example of the potentially deadly risks of viral gene therapy can be found in the death of Jesse Gelsinger, an 18-year old who participated in a clinical trial taking place at the University of Pennsylvania's Institute of Human Gene Therapy in September of 1999. Gelsinger died 4 days after high dose adenoviral gene therapy to treat ornithine transcarbamylase, a rare form of liver disease. His death initiated a flurry of investigations into the risks involved with viral gene therapy, as well as the shutdown of that particular clinical trial by the FDA. Since then, in a French clinical trial to treat X-linked severe combined immunodeficiency disease (SCID), 3 children were reported

to have developed leukemia after gene therapy (Couzin & Kaiser, 2006). Due to the risks associated with viral vectors, brought to the forefront of public attention by Gelsinger's death, many researchers are now looking towards alternative forms of gene therapy.

2.1.2 Non-viral gene therapy

Non-viral vectors currently studied for gene therapy include naked DNA/RNA delivery methods, as well as liposomal and polymeric vehicles. These non-viral options are attractive due to relatively simpler production of large amounts of vector, increased options for tissue targeting, and potential lack of immunogenicity depending on vehicle design.

2.1.3 Naked DNA/RNA delivery

Gene delivery without the use of a vector is being researched in approximately 18.3% of clinical trials worldwide. These methods generally depend on physical methods such as microinjection, the use of the gene gun, or electroporation to achieve entry of genetic material into cells. The gene gun functions by particle bombardment of DNA deposited onto the surface of gold particles, which are accelerated by pressurized gas onto exposed tissues such as skin, mucosa, or areas that have been surgically exposed. The force of acceleration serves to drive the gold-DNA particles a few millimeters deep into tissue, driving DNA into the cells in its path. This method does indeed achieve effective delivery of genetic material but is limited by potential sites of application, capacity of carried genetic materials to be delivered, and lack of precise cell targeting. Electroporation involves injection of DNA into tissues into which electrodes have been inserted. By generating a current through the electrodes, cell membranes in the area are disrupted, causing small openings through which injected DNA can enter cells. This method is limited by the necessity for a surgical procedure, the use of high voltages risking irreversible tissue damage as well as instability to DNA, and its potential to be applied to large tissues, as the effective range of electrodes is generally limited to 1 cm. While these methods are relatively simple and exhibit low levels of toxicity, these methods often involve injuries or defects to cell membranes in order to achieve their goal and are limited by where they can be applied *in vivo* as well as a general lack of precise targetability (Gao, Kim, & Liu, 2007).

2.1.4 Liposomes for gene delivery

Approximately 7.1% of current clinical trials approved involve the use of lipid vectors. Liposomes are formed as layered complexes made up of amphipathic phospholipids. These complexes can be multilamellar (having many layers, generally between 100 nm-20 mm), small unilamellar (having one layer in the size range between 10 to 50 nm) or large unilamellar (between 50 to 1000 nm in size) (Chrai, Murari, & Ahmad, 2001). They can therefore encapsulate materials of varying sizes, and these materials include both hydrophilic and hydrophobic compounds, due to the amphipathic nature of the liposomal layers. Commercial gene carriers employing liposomes include Transfectam and Lipofectamine, but are limited by toxicity, potential complement activation, and liver and lung tropism (Li & Huang, 2000).

2.1.5 Polymers for gene delivery:

Due to the wide range of polymers available, with an equally wide range of physical and chemical properties, polymeric vehicles have also been studied for gene therapy. They offer the further advantage of being able to contain multiple or larger plasmids for transfection, which may be important in the treatment of multigenic diseases such as cancer or AIDS. These include neutral polymers, which interact with DNA via hydrogen bonding, including poly(vinylpyrolidone) and poly(vinylalcohol).

More promising alternatives are cationic polymers, which are favored in gene therapy research due to advantageous electrostatically driven interactions with DNA, including poly(L-lysine) (PLL), poly(ethyleneimine) (PEI), gelatin and chitosan (Godbey & Mikos, 2001; Leong et al., 1998; Liu & De Yao, 2002). While complexes formed using PLL and PEI have demonstrated encouraging results, they also mediate significant cellular toxicity. Among cationic polymeric materials, PEI generally achieves the highest transfection efficiencies, due to the "proton sponge" effect. Unfortunately, PEI-based complexes generally exhibit dose-dependent cytotoxicity, due to interaction with negatively charged cell membranes.

Polyplexes are complexes formed from oppositely charged components, whether made up of oppositely charged polymers or with negatively charged plasmid DNA (pDNA). Polyplexes containing pDNA with a net positive charge offer protection from degradation

by nuclease activity as well as non-specific interaction with the negatively charged cell membrane. The polymer-DNA interactions vary depending on salt concentration, pH, charge density, MW, tertiary structure and polymer to DNA charge ratio (N/P) (Boussif et al., 1995; Kabanov & Kabanov, 1995).

2.2 TARGETING FOR IMPROVED CELL UPTAKE

Targeting strategies for gene and drug delivery have been shown to enhance cellular uptake and increase the effectiveness of encapsulated materials. These targeting strategies have the obvious advantages of reduced systemic toxicity, both from the carrier itself or from the carried material, while increased effectiveness at the site of interest offers the potential for lower dose administration, longer term effectiveness, and lowers the risk of systemic multidrug resistances. Targeting strategies can be categorized as either passive or active, where active targeting increases the affinity of the vector for a target and passive targeting generally acts to minimize non-specific interaction of the vector with non-targeted sites as well as cells of the reticuloendothelial system (RES).

Passive targeting can be achieved by incorporation of hydrophilic coatings on particles, whether associated through covalent bonding or by adsorption on surfaces. This includes the use of poly (ethylene glycol) (PEG), poloxamers, and poloamines. Hydrophilic coatings form a cloud of hydrophilic and neutral chains at the surface of particles (Jeon, Lee, Andrade, & Degennes, 1991), providing a shield against binding to plasma proteins, blood cells, and each other and can therefore provide longer circulation times (Rubanyi, 2001). Poloxamer 407 and Poloxamine 908 coatings on poly (methylmethacrylate) nanoparticles prolonged the half-life of particles in solution when adsorbed to the surface (Lode et al., 2001). Adsorption of hydrophilic polymers on particle surfaces does risk desorption of the coating in the circulation and so covalent bonding of hydrophilic polymers to surfaces have been more widely studied. Modification of the vector may also be used to achieve passive targeting, such as increasing hydrophobicity through the conjugation of deoxycholic acid and trimethylation of acetyl groups of chitosan.

Active targeting often includes the association of a targeting ligand with high affinity for a receptor. Targeting ligands that have been studied include monoclonal antibodies, viral

protein fragments, sugar molecules, and small molecules that have an associated cell surface receptor, such as transferrin or folate.

2.3 BARRIERS TO GENE THERAPY

Physical barriers to gene transfer include those first encountered upon introduction to the body, including the blood, interstitial matrices, mucus lining, and epithelial tight junctions between cells, as well as the physical barrier of the plasma membrane of targeted cell itself. For effective gene delivery, genetic material must be released by its vehicle and effectively cross the nuclear membrane of the cell into the nucleus. Biochemical barriers include potential DNA degradation by nucleases in the body as well as the acidic environment presented by endosomes and lysosomes as transport vesicles into the cell.

Opsonizaton, or clearance of nanoparticles by the mononuclear phagocytotic system (MPS), is a major barrier to the delivery of therapeutic agents in the body. Particles and their contents are therefore removed from circulation but also accumulate preferentially at MPS organs (the liver, lung, spleen and in bone marrow) (Brigger, Dubernet, & Couvreur, 2002). This effect may be an advantage in targeting those particular organs, but otherwise, this is a disadvantage of conventional nanoparticle delivery.

CHAPTER 3
RATIONALE AND MATERIALS

3.1 RATIONALE

An ideal DNA carrier is not only biocompatible, and nontoxic, but can also protect genetic material from degradation and clearance in the host circulation, is able to carry large or multiple plasmids, and, most importantly, yields a high transfection efficiency. This ideal DNA carrier should additionally be easily produced in mild conditions that do not degrade complexed genetic material, and be easily modified to include targeting moieties.

While non-viral vectors have shown promise in being able to meet most of these requirements, the main impasse is met at transfection efficiency. Of the non-viral vectors discussed, liposomal vehicles have shown the highest transfection efficiencies but suffer from issues of toxicity. Conversely, polymeric vehicles, and particularly biopolymers, have shown great biocompatibility and lack of toxicity but transfection efficiencies have not matched those of liposomal vectors, to say nothing of viral vectors. Thus, in designing an improved non-viral carrier, one can either attempt to moderate the immunogenic and toxic effects of vehicles that display high transfection efficiency or focus on enhancing transfection in more biocompatible vehicles.

In this work, we have chosen the latter approach, using a polymeric vehicle composed of chitosan and alginate, which are already biocompatible, show little toxicity *in vitro* and *in vivo,* have previously demonstrated transfection ability, and most importantly, are amenable to conjugation and complexation with other molecules, such as folate, that can improve and enhance transfection (Richardson, Kolbe, & Duncan, 1999; MacLaughlin et al., 1998; Erbacher, Zou, Bettinger, Steffan, & Remy, 1998; Mansouri et al., 2004; Mansouri et al., 2006; Douglas & Tabrizian, 2005; Douglas, 2006; Anderson & Akkina, 2005; Koping-Hoggard et al., 2001; Murata, Ohya, & Ouchi, 1997b; Corsi, Chellat, Yahia, & Fernandes, 2003; Muzzarelli, 1993; Illum, Farraj, & Davis, 1994).

3.2 CHITOSAN

Chitosan is a cationic polysaccharide derived from chitin, which makes up the shells of crustaceans and some insects, and is also present in some forms of fungi. It is made up of D-glucosamine and N-acetyl-D-glucosamine subunits linked by β(1, 4) glycosidic bonds (see Figure 1). Two of the most important characteristics of this material, are its molecular weight and degree of deacetylation (DDA). The DDA of chitosan measures the average content of glucosamine units in the polymer chain and is used to approximate potentially reactive cationic amino groups. These amino groups have an intrinsic pK_a of 6.5, thus indicating that chitosan behaves as a polycation at low pH (MacLaughlin et al., 1998). Chitosan with higher degrees of deacetylation have been found to be more biologically active than chitin and less deacetylated forms (Howling et al., 2001). Although chitosan biocompatibility has been demonstrated in various cell lines, several studies suggest that shorter chain length polymers may have lower cytotoxicity (Richardson et al., 1999; Mao et al., 2004; CarrenoGomez & Duncan, 1997).

In vivo, chitosan is mainly biodegraded by lysozymes, as well as other enzymes such as N-acetylglycosaminidase and chitinase, to N-acetyl glucosamine, which enters the synthetic pathway of glycoproteins, to be excreted eventually as carbon dioxide (Chandy & Sharma, 1990). These degradation products are thus nontoxic, nonimmunogenic and noncarcinogenic (Muzzarelli, 1997; Kim et al., 2008) and therefore chitosan can be safely used in the body. The rate of this degradation is inversely proportional to its degree of crystallinity and DDA (Hirano, Tsuchida, & Nagao, 1989).

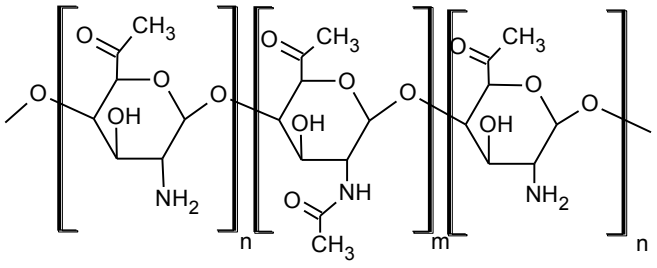

Figure 1 Chemical structure of chitosan

As a polycation, chitosan can form polyelectrolyte complexes with anionic materials through electrostatic interactions. Chitosan polyelectrolyte complexes have been formed with a variety of polyanions and as well as negatively charged DNA (MacLaughlin et al., 1998). Characteristics of these polyelectrolyte complexes depend on the properties of the

polymers involved as well as reaction conditions, such as pH, ionic strength, concentration, ratio of polymers and temperature of formation. Chitosan complexes are generally hydrophilic and tend to swell in solution (Muzzarelli & Muzzarelli, 2005).

Chitosan-DNA uptake in cells has been shown to occur through endocytosis (Erbacher et al., 1998) followed by endosomal escape and then subsequent nuclear accumulation (Ishii, Okahata, & Sato, 2001). Since transfection efficiencies of chitosan-DNA nanoparticles have been found to be lower than those achievable by commercial liposomal vectors (Roy, Mao, Huang, & Leong, 1999), many groups have explored different strategies for improving chitosan-based transfection..

A few groups have studied the effect of molecular weight fractions on chitosan transfection efficiency. Richardson *et al.* found that lower MW oligomers demonstrated slower clearance from the circulation, lower particle accumulation in the liver, and were neither haemolytic or cytotoxic, with better DNA binding as compared to higher molecular weight fractions and PLL. Low MW oligomers also protected DNA from degradation by DNAse, potentially due to changes in tertiary structure due to steric hindrance after polymer complexation (Richardson et al., 1999), as seen in previous SEM studies which demonstrated changes in the tertiary conformation of DNA when complexed with PLL (Wagner, Cotten, Mechtler, Kirlappos, & Birnstiel, 1991). MacLaughlin *et al.* similarly studied various MW chitosan oligomers, from 7 to 540 kDa, finding that the size of complexes decreased with MW and charge ratio. *In vitro* transfection of Cos-1 cells demonstrated that the highest transfection efficiency was obtained using chitosan of 102 kDa MW in the absence of serum, though at 250-fold lower efficiencies as compared to Lipofectamine. However, strong complex stability was associated with low *in vivo* expression, suggesting uptake and de-complexation but not endosomal release may be the critical rate limiting steps in uptake (MacLaughlin et al., 1998). Meanwhile, Kőping-Hőggård *et al.,* analyzing chitosan ranging from 1.2 to 10 kDa, showed increased transfection in HEK293 cells *in vitro* as well as in the lung *in vivo* when compared to chitosan of higher molecular weights (Koping-Hoggard et al., 2004).

Although tailoring molecular weight can lead to some improvements in transfection levels, transfection efficiencies obtained by chitosan alone remain lower than those

achieved by other polymers, such as PEI, or liposomal vectors, such as Lipofectamine. Thus, other approaches to increasing chitosan-based transfection efficiency have included modificiation of the chitosan molecule, association of a secondary anionic polymer, such as hyaluronic acid, tripolyphosphate, numerous dextrans and alginate (Borchard, 2001; De & Robinson, 2003; Douglas, 2006; Zhang, Guo, Peng, & Jin, 2004), or conjugation to targeting molecules.

Chitosan has also proven to be amenable to modification and conjugation without losing its advantageous materials properties. Attempted modifications include those that increase stability and water solubility of particles through glycosylation and PEGylation. Trimethylation of chitosan, thereby increasing the degree of quaternization of the polymer, was used to enhance its cationic nature and therefore its DNA condensing abilities. Quaternized chitosan complexes were found to transfect COS-1 cells with higher efficiencies as compared to un-modified chitosan but displayed no transfection of Caco-2 cells (Thanou, Florea, Geldof, Junginger, & Borchard, 2002). Chitosan has additionally been modified with sugar molecules for the purposes of targeting. Fucose-branched-chitosan derivatives were found to interact with specificity on corresponding lectins in *Pseudomonas aeruginosa* (Morimoto et al., 2001; Li et al., 2000). Lactosaminated N-succinyl chitosan was formed for liver specificity and mediated transfection efficiencies in HeLa cells comparable to those by PEI, but did not successfully transfect BNL CL.2 and HepG2 cells (Erbacher et al., 1998). Chitosan has been further examined as comjugated to galactose, for hepatocyte targeting (Murata, Ohya, & Ouchi, 1997a), showing increased transfection efficiency in HepG2 hepatoblastoma cells expressing the asialoglycoprotein receptor as compared to non-expressing HeLa cells (Kim, Park, Nah, Choi, & Cho, 2004). Galactosylated chitosan-graft-dextran-DNA complexes were also found to efficiently transfect Chang liver cells (Park et al., 2000). Sialic residues have also been conjugated to chitosan to target mammalian cell surface glycolipids and proteins (Sashiwa, Shigemasa, & Roy, 2001).

Targeting strategies using chitosan-based vectors have further been examined using viral proteins as well as small ligands such as transferrin and folate. Chitosan-DNA nanoparticles were conjugated to KNOB proteins (the C-terminal domain of the fiber protein of adenoviruses), resulting in a 130-fold increase in efficiency. Meanwhile

chitosan conjugated to transferrin as a targeting molecule was found to mediate only low levels of transfection in HEK 293 and HeLa cells (Mao et al., 2001).

3.3 ALGINATE

Alginate is a linear block polyanion consisting of alternating β-D-mannuronic acid (M) and α-L-guluronic acid (G) residues, produced from certain forms of brown algae. The proportion of M to G blocks in the polymer, whose structures appear as Figure 2 and Figure 3, respectively, determine the polymer's ultimate gelling properties. Due to its anionic nature, alginate can be used to form polyelectrolyte complexes with cationic materials, such as chitosan. Alginate can be included in the formulation of chitosan particles to reduce the strength of binding of chitosan to DNA, thereby increasing the availability of DNA for transfection. Alginate-chitosan nanoparticles have been successfully formed, shown to complex DNA, and have demonstrated the ability to protect plasmids from degradation *in vivo* (Richardson et al., 1999).

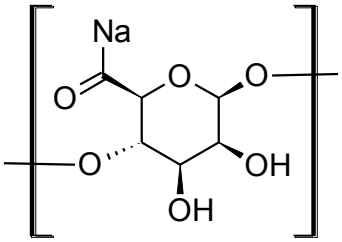

Figure 2 Sodium mannuronic acid block of alginate.

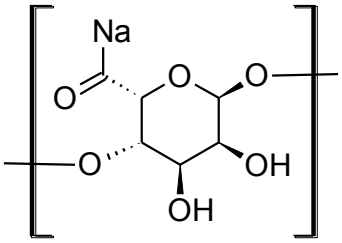

Figure 3 Sodium guluronic acid block of alginate.

Chitosan complexes have been found to compact DNA into globular shapes. Ethidium bromide fluorimetric titration compared the DNA complexation ability of chitosan with that of PLL, along with the polyanions alginate, and xanthan, finding that both

polycations were equally effective at compacting DNA. When the polyanions were added to complexes, results indicated competition between DNA and the added polyanion with respect to polycation binding, confirming that association with a polyanion can decrease the strength of binding between chitosan and DNA. Competitive binding studies revealed that the affinity between chitosan and polyanions was the same as for chitosan and DNA (Danielsen, Maurstad, & Stokke, 2005). Chitosan/alginate complexes have been produced previously, though generally as microparticles for the delivery of larger protein drugs. Microparticles previously formed with chitosan alone mediated transfection of HEK 293T cells, though to a lesser degree than liposomal vectors. Transfection of HeLa and 3T3 cells was not successful and it was theorized that this was due to the strong interaction between chitosan and DNA, impeding gene transport into the nucleus (Dastan & Turan, 2004). Chitosan/alginate core shell nanoparticles formed through reverse microemulsion with sizes less than 100 nm were found to mediate EGFP transfection of NIH 3T3 fibroblasts at a level comparable to that obtained by PEI 48 hours post-transfection (You, Liu, & Peng, 2006).

Previous work by our group demonstrated the formation and optimization of a novel nano-scale polymeric polyelectrolyte system formed by low molecular weight chitosan and alginate (Douglas et al., 2005). It was demonstrated, via competitive binding assays, that the interaction between chitosan and alginate did indeed decrease the strength of interaction between chitosan and DNA, making the DNA more readily available to cells for transfection. Chitosan-alginate-plasmid complexes were found to be non-toxic, and both transfection efficiency and cellular uptake mechanisms were found to be highly cell line dependent, with differences evident for HEK293, COS7, and CHO cells (Douglas, 2006). Transfection efficiency of HEK 293 cells with chitosan/alginate nanoparticles was improved over chitosan or plasmid DNA alone. These results indicate that the inclusion of the secondary polyanion, alginate, is a promising strategy for enhancing transfection efficiency. In order to further improve this system, active targeting of cells will be evaluated by inclusion of a targeting ligand with a high affinity for its associated cell surface receptor, folate, as conjugated through a PEG spacer molecule that acts to both shield the complex from clearance by the RES as well as decreasing steric hindrance of the targeting ligand to the cell surface.

3.4 FOLATE

Folate (Figure 4) is a small ligand (441 Da) with a high affinity for its cell surface receptor ($K_d = 10^{-10}$ M), a 38-44 kDa membrane-associated folate-binding protein. The folate receptor is expressed in a variety of tissues, including the lung, thyroid, kidney, placenta, choroid plexus, and at the blood-brain barrier, and, more importantly, is overexpressed in many malignant tumor cells, including ovarian, endometrial, colorectal, breast, lung, renal cell carcinomas and brain tumors derived from epithelial cancer cells (Beduneau, Saulnier, & Benoit, 2007; Hattori & Maitani, 2005; Weitman et al., 1992a; Weitman et al., 1992b; Antony, 1996; Leamon & Low, 1994). The folate receptor is also known to be internalized after binding with its ligand folate (Rothberg, Ying, Kolhouse, Kamen, & Anderson, 1990), which presents an advantage over targeting strategies that employ cell membrane markers that are not internalized.

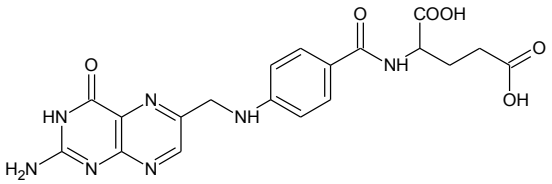

Figure 4 Molecular structure of folic acid.

Folate is transported across the cell membrane by at least 3 mechanisms: 1) via the reduced folate carrier, 2) through the folate export pump and, 3) by folate receptor-mediated endocytosis (Beduneau et al., 2007; Antony, 1996). The reduced folate carrier has low affinity (Kd ~ 1 μM) but high capacity for uptake of reduced folates into cancer cells at micromolar extracellular folate concentrations. While this reduced folate carrier has specificity for only reduced folates, the folate-receptor can transport folic acid as well as any conjugated molecules. Targeting strategies aimed at the folate receptor generally fall into one of two categories: the use of monoclonal antibodies against the receptor or the use of folate as a targeting ligand. Monoclonal antibody targeting has been successfully applied in medical imaging and immunotherapy. The second method of targeting is becoming increasingly attractive due to the smaller relative size of the folate molecule, the lower cost as compared to monoclonal antibodies, low risk of denaturation,

lowered potential for immunogenic reaction, as well as the fact that the antibodies used may target only one isoform of the receptor (Sudimack & Lee, 2000).

The folate receptor has three isoforms; α, β, and γ, the first two of which are attached to the cell membrane by glycosylphosphatidylinositol-anchors (GPI), while the last is secreted (Hattori et al., 2005). The α isoform is found in the caveolae of the cell membrane, thus suggesting a caveolin-coated endocytosis (potocytosis) model of receptor internalization. The α isoform is expressed in most normal and malignant epithelial tissues, while the β isoform is often overexpressed in non-epithelial tumors, and finally, the γ isoform has been found extensively in malignant hematopoetic cells. The α and β forms of the folate receptor show different relative affinities for folate and isomers of various folates, indicating that response to folate depends on the relative expression of one folate receptor over another (Antony, 1996). After uptake into cells, acidification in endocytotic vesicles results in release of the carried molecules into the cytoplasm, while the folate receptor is recycled back to the cell membrane. Receptor recycling in various cancer cells varies between 4 to 12 hours per cycle *in vivo* (Hilgenbrink & Low, 2005). As a result of receptor recycling, folate-conjugated materials can accumulate in cells, which may be advantageous for tumor treatment strategies (Hattori et al., 2005). Folate conjugates are rarely found in lysosomes, decreasing the chance of destruction by the acidic environment for hydrolytically sensitive materials (Hilgenbrink et al., 2005). Folate-conjugated proteins were found to maintain function after uptake via folate receptors (Leamon, Low, & Turek, 1992). While the folate receptor is expressed in certain non-cancerous cells, they would generally not be in contact with folate-conjugated therapies administered through the blood, as the folate receptor has been found mostly on the far side of polarized membranes (Hilgenbrink et al., 2005). In addition to being overexpressed in certain types of cancer cells, there is evidence to suggest that the expression of FR increases with increasing severity of cancer while chemotherapy-resistant tumors seem to express higher levels of the receptor (Zhang et al., 2006). Due to its relatively small size, folate may also achieve further penetration into tumors in comparison to normal antibodies (Zhao, Yue, & Yung, 2008). The potential of folate as a targeting ligand to cancerous tissues was demonstrated by early work with chimeric mouse-human antifolate receptor antibodies, used to mediate death of ovarian carcinoma

cells *in vitro,* showing its potential to be used as a so-called Trojan horse, carrying therapeutic materials into cells in a stealth-like manner (Coney et al., 1994). Thus, folate-mediated drug and gene delivery can be used as a targeting strategy to treat various cancers.

Folate receptor expression on several non-cancerous tissues and carcinomas were assessed by quantitative radioligand binding assay. Tissues expressing more than 6, between 2.5 to 6, and under 2.5 pmol/mg protein were labeled highly positive, low positive, and negligibly positive, respectively. Results indicated that tissues of ovarian origin most frequently expressed high levels of the folate receptor (up to 34.31 pmol FR/mg protein), with renal, endometrial and lung tissues following. Cell lines generally labeled as highly positive for the folate receptor, including L1210, KB, M109, and HeLa cells, were also assessed (Parker et al., 2005). The folate receptor is known to be overexpressed in approximately 90% of human epithelial ovarian cancer cells (Parker et al., 2005; Toffoli et al., 1997; Zhang et al., 2006). KB, Hela and 2008 cells were found to associate with large quantities of folate-protein conjugates (> 72 pmol/mg protein), while XC, SKOV3, Caco-2, Caov-3 and OVCAR3 cells were associated with lower quantities (< 6 pmol/mg cell protein) (Leamon, Pastan, & Low, 1993). Although KB and HeLa are generally studied in literature for the evaluation of folate binding, they have been designated as biosafety level 2 cells. Some concerns have been raised regarding contamination of KB human pharyngeal cancer cells with the HeLa cervical cancer cell line (Bae et al., 2005).

Conjugation of folate to another molecule does not hinder its specificity or affinity for the cell surface receptor, but may in fact increase multivalent interaction. Specific affinity of folate bound to poly[aminopoly(ethylene glycol) cyanoacrylate-co-hexadecyl cyanoacrylate] [poly(H_2NPEGCA-coHDCA)] nanoparticles via PEG terminal amino groups was assessed by surface plasmon resonance (SPR). Folate bound to nanoparticles was found to have stronger association with the FR, necessitating a 108-fold greater molar concentration of free folate to inhibit interaction of folate-bound nanoparticles to the receptor. SPR analysis showed that association of nanoparticles to the receptor occurred through two-step binding; a fast step comparable to that of free folate, followed by a slow isomerization step. As folate bound to nanoparticles have multivalent affinity

for the folate receptor, which are often found in clusters, this slow isomerization step was found to correspond to the clustering of the FR (Stella et al., 2000).

Folate-targeted delivery has been employed in the delivery of antibodies, proteins, anticancer drugs and genes. Folate has been covalently bound to penicillin-G-amidase (PGA) enzyme, for folate-directed enzyme prodrug therapy, whereby the folate-bound enzyme is first introduced to the body and allowed sufficient time to bind to target tissues. This is followed by introduction of a chemotherapeutic prodrug, whose activation by folate-bound enzyme will allow targeted delivery of the anticancer drug while avoiding systemic toxicity and development of drug resistance. This approach was evaluated using folate-PGA and N-(phenylacetyl) Doxorubicin as a prodrug. Results found increased sensitivity of FR+ SKOV3 and HeLa cells to Doxorubicin with no increase in cytotoxicity as compared to the untargeted enzyme. Biodistribution studies confirmed localization of the folate-bound enzyme in subcutaneously implanted SKOV3 tumors in BALB/c mice while pharmacokinetic studies showed that the conjugates were cleared from the blood circulation 24 hours post-administration (Zhang et al., 2006).

Folate targeting strategies using liposomes as well as polymeric micelles and nanoparticles, among others, have been reported previously. Folate conjugated to liposomes via a PEG spacer (Leamon et al., 1994), mediated multiple folate-PEG surface attachments to cell folate receptors per liposome. This was found to subsequently increase binding affinity to the folate receptor by six orders of magnitude. Additionally, for the delivery of Doxorubicin, folate-PEG-liposomes were found to selectively target and kill only cancerous cells (Li, Sun, & Antony, 1996). Furthermore, folate-PEG-liposomes were also used to evaluate liposome-induced apoptosis, inducing dose-dependent apoptosis in FR+ KB cells but not in FR- WI-38 cells (Yoshida et al., 2006). Preferential binding of folate-PEG-liposomes has been shown *in vitro* and *in vivo* in cancer cells with high numbers of folate receptors, including in mouse lung carcinoma, human epidermal carcinoma and lymphoma (Shmeeda et al., 2006; Gabizon, Shmeeda, Horowitz, & Zalipsky, 2004; Gabizon et al., 1999).

Micelles formed by amphiphilic copolymers, having both a hydrophobic core and hydrophilic surfaces, have also been used to achieve folate-targeted therapy. Micelles

formed by folate-PEG-PLGA and loaded with Doxorubicin showed accumulation in tumoral tissues in mice. Many tumor cells are resistant to Doxorubicin and therefore targeted delivery strategies that can bring the drug into the cell, past the plasma membrane, are sought after (Yoo & Park, 2004). Folate bound to PCL/methoxyPEG micelles and loaded with Paclitaxel, a chemotherapeutic agent, were found to have an increased cytotoxic effect on MCF-7 and HeLa cells (Park, Kim, Lee, & Lee, 2005). Another strategy involved the use of micelles formed by folate-PEG-poly(aspartate hydrazone adriamycin), carrying the anticancer drug adriamycin into cells via an acid-sensitive hydrazone bond. This strategy inhibited viability of FR+ KB cells and SPR analysis of folate binding confirmed selectivity of folate receptors for modified liposomes (Bae et al., 2005).

Nanoparticles formed by folate bound through a PEG spacer to PLL, poly(dimethylaminomethyl methacrylate) and poly(ethylamine) provided longer circulation times and targeted gene delivery (Zhao & Lee, 2004). In regards to folate conjugated to chitosan, Mansouri *et al.* have demonstrated DNA complexation, positive zeta potentials and low HEK293 cell cytotoxicity for folate-chitosan-DNA nanoparticles (Mansouri et al., 2006). Chan *et al.* synthesized folate-PEG-chitosan for targeted gene delivery, showing increased water solubility due to PEGylation, with a slight decrease with subsequent folate addition (Chan, Kurisawa, Chung, & Yang, 2006). DNA complexation was demonstrated by gel electrophoresis and no cytotoxicity was shown in HEK 293 cells.

3.5 POLY(ETHYLENE GLYCOL)

The attachment of poly(ethylene glycol) (PEG, Figure 5) to the surface of chitosan-alginate nanoparticles has been shown to increase the stability of complexes to lyophilization by increasing hydrophilicity and therefore lowering surface free energy and decreasing opsonization by macrophages of the MPS (Storm, Belliot, Daemen, & Lasic, 1995). PEG-treated chitosan nanospheres did not aggregate in suspension and were able to achieve transfection after one month of storage post-lyophilization (Mao et al., 2001; Leong et al., 1998). PEG can also be used to "shield" particles from binding to

plasma proteins, blood cells, or each other and can therefore allow longer circulation times and more efficient uptake *in vivo* (Rubanyi, 2001). The addition of a PEG linker can also reduce steric hindrance of a ligand to the targeted cells.

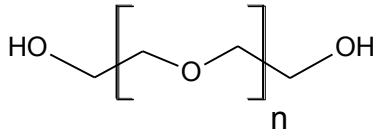

Figure 5 Structure of poly (ethylene glycol).

In regards to the effect of degree of PEG substitution, chitosan nanocapsules were modified with PEG at 0.5 and 1.0% degrees of substitution and were found to increase stability of nanocapsules in simulated gastrointestinal fluids while furthermore, reducing cytotoxicity in Caco-2 cells. In simulated intestinal fluids, capsules having a PEGylation degree of 1.0 % were stable, while 0.5% PEGylated samples resulted in some aggregation (Prego et al., 2006). For the purposes of gene delivery, chitosan-PEG/DNA nanoparticles mediated comparable levels of transfection as un-modified chitosan in HepG2 cells. Under challenge by serum and bile, chitosan-PEG/DNA complexes remained stable for up to 30 minutes and prevented DNA degradation, in contrast to un-PEGylated samples (Jiang et al., 2006).

As one of the motivations for PEG inclusion into nanoparticle formulations is the reduction in non-specific uptake by the RES, folate-bound liposomes were coated with PEG, however the coating was found to interfere with folate binding to its cell surface receptor. Therefore, PEG was used as a spacer molecule, tethered between liposomes and folate, and, and thereby increasing the availability of folate for the folate receptor. The presence of 0.03% folate-bound-PEG-liposomes was sufficient to achieve optimal binding and the folate-PEG-liposomes were able to reduce non-specific gene transfer by 50- to 100-fold. Specificity for targeted tissues increased up to 3 mol% of folate-targeted liposomes (Reddy et al., 2002; Hofland et al., 2002). *In vivo* analysis of folate-PEG-liposomes using the interperitoneal L1210A tumor model demonstrated that low amounts (0.01 mol%) of the modified liposomes were able to mediate the highest transfection confirming *in vitro* results in M109 cells. It was also found that higher amounts (> 0.5%) of the folate-PEG-liposomes were found to decrease cellular binding. (Reddy et al.,

2002). These folate-bound liposomes were able to mediate an 8- to 10-fold higher level of luciferase expression as compared to non-targeted lipid formulations. Nanoparticles formed by folate-PEG-poly[H_2NPEGCA-co-HDCA] were found to exhibit a more hydrophilic surface as compared to free polymer. Conjugation of 15% folate to PEG was found to be enough for efficient recognition of nanoparticles by the FR (Stella et al., 2000).

CHAPTER 4
CRITERIA AND ANALYSIS

In order to evaluate success in meeting our project objectives, it is important to understand why the criteria of complex size and surface charge were chosen, as well as the implications of the methods chosen to evaluate each criterion.

4.1 IMPORTANCE OF SIZE

It has been reported that nano-sized carriers have a better capacity to enter cellular internalization pathways and may also avoid clearance by the reticuloendothelial system (RES), thus providing longer circulation times *in vivo* and increasing the potential for therapeutic effects (Garnett & Kallinteri, 2006). The size beyond which nanoparticles may risk clearance by phagocytotic cells is not concrete, but particles around 100 nm in size have shown promising results (Storm et al., 1995).

In cancer cells, nano-sized carriers can take advantage of the enhanced permeation and retention (EPR) effect, whereby small carriers are able to accumulate within tumor tissues that have developed disorganized and defective vascular networks. While these networks allow increased blood flow into tumor cells, they also allow entry of larger macromolecules, while limiting lymphatic drainage from the site. This combined effect results in particles accumulating within tumor cells but not being cleared effectively, achieving a form of passive tumor targeting that maintains the therapeutic agent of interest at the tumor site while reducing its effect on surrounding non-malignant tissues (Brigger et al., 2002; Gaumet, Vargas, Gurny, & Delie, 2008; Park et al., 2008). While these tumor pore sizes can be as large as 200 nm to 2 μm (Hwang, Kim, Kwon, & Kim, 2008; Min et al., 2008), developing nanoparticles at the lower end of that range can increase the likelihood that they will accumulate within tumor tissues.

4.1.1 Dynamic light scattering

Particle size is commonly examined by dynamic light scattering (DLS), whereby the light scattered off a material due to Brownian motion is analyzed. This method of analysis is

also referred to as photon correlation spectroscopy (PCS) or quasi-elastic light scattering (QELS). As focused light, such as a laser, hits a particle, light will scatter in all directions. Propagated waves of light from this scattering are read by a detector. While some waves will be cancelled out through destructive interference, other waves having the same phase will interact constructively. Additionally, particles in solution are constantly moving as a result of random Brownian motion, with this movement depending on the size of the particle. The Stokes-Einstein equation relates the speed of movement of particles to their size. The moving particles will cause the pattern of constructive and destructive wave interference to fluctuate as the particles move about and the rate of this fluctuation is used by DLS software to calculate the size of particles in solution. Essentially, larger particles will move more slowly and therefore cause slower fluctuations in intensity while smaller particles move faster and cause faster fluctuations in intensity.

Size can also be confirmed through various microscopy methods, however it should be noted that the size of particles found through microscopic imaging will often not coincide with those measured by dynamic light scattering, particularly for those with polydispersity indices above 0.5. Since most microscopic methods involve the use of dry samples, particle size and shape can change. Most often, this results in smaller particles sizes than those measured in solution, due to shrinking of the particle as well as the lack of a surrounding hydrodynamic solvent layer. For use in biological systems, we are most concerned with size of the particles in solution, as this is how they will be introduced to living cells and thus for the purposes of this work, size determination was carried out by DLS analysis.

4.2 IMPORTANCE OF SURFACE CHARGE

Gene delivery carrier materials are developed with the aim of having an overall positive charge in order to promote electrostatic interactions with the negatively charged phosphate groups present on the DNA backbone. An overall positive charge is also useful in encouraging particle association with negatively charged cell membranes. In reference to the nanoparticles designed in this work, chitosan carries positively charged reactive

amino groups while alginate carries negatively charged carboxyl groups. In general, complexes formed with an excess of chitosan should carry a positive charge.

4.2.1 Zeta potential analysis

Surface charge is measured by zeta potential analysis. Charged particles in a solution will move in response to an applied electric field. This movement is detected as a Doppler shift in the frequency of laser light scattered from the particles. The direction of motion of the particles give an indication of whether the particles are positively or negatively charged, while the speed of movement can be interpreted to obtain the magnitude of the charge. Zeta potential (ζ) is expressed in mV and it should be noted that measurements are sensitive to solution conditions, such as pH and ionic strength.

4.3 TRANSFECTION EFFICIENCY

4.3.1 Flow cytometry analysis

A brief overview of how data is collected and analyzed by flow cytometry will be provided. Briefly, a laser beam at a specific wavelength (in this case, at 488 nm) is directed into a hydrodynamically focused stream of fluid containing the sample, where cells pass through in single file. Forward scatter (FSC) detectors determine volume and size, side scatter (SSC) provides data concerning the internal structure of each cell, and fluorescence detectors are filtered to measure fluorescence within a certain range of wavelengths. Cells that are similar in size, shape and other characteristics will be detected similarly by FSC and SSC and therefore this is used to differentiate between cell types in a mixed population as well as to separate viable cells from debris. Voltages applied to each detector enable them to effectively recognize each photon as it passes through the sample stream. A higher current output can be generated by increasing voltage to a particular detector and vice versa. Voltages can therefore be modified so that each cell type occupies a dense, discrete area of a two dimensional FSC vs. SSC plot. Information passing through fluorescence detectors should also be modified as data as collected, to ensure that each fluorochrome is detected as a signal of one. Since some fluorochromes fluoresce over a broad range, they may be detected more than once by fluorescence

detectors. The data from each fluorescence detector is therefore compensated to correct the overestimation. When applied correctly, flow cytometry analysis is a powerful quantitative tool to measure fluorescence.

After data collection, cell populations of interest are isolated by gating on the FSC vs SSC dot plot, eliminating any signals potentially generated by debris. This gate over viable cells can be quite generous or more narrow, which can affect data analysis, since a generous gate will more likely pick up cell debris that will be read as dead while a more narrow gate may eliminate some of the viable cell population. Since most information collected is reported as a percentage on live cells, the number of cells enclosed in this gate can also have a small effect on this value. For the purposes of this study, two fluorescent molecules were used, EGFP (enhanced fluorescent green protein) and PI (propidium idiode), and therefore the gated live population is then viewed as a two color dot plot with EGFP on the x-axis and PI on the y-axis. Any cells appearing to be double negative (GFP-/PI-) are live but not transfected, while single positive populations (GFP+/PI- and GFP-/PI+) indicate transfected cells and dead cells, respectively. Any cell population appearing to be double positive (GFP+/PI+) can be considered autofluorescent. These populations are isolated again by gating, and while generally these gates are generated on positive and negative controls and subsequently applied to all samples in the experiment, it should be noted that due to a shift in the live cell population with inclusion of PI, gates were shifted manually for those samples. For the purposes of this study, cells that were single positive for GFP (GFP+) are taken as a measure of transfection efficiency and reported as a percentage on live cells, which is the viable cell population excluding the PI+ population indicating cell death.

4.4 TERMINOLOGY AND SYNTAX

Throughout this document, synthesized chitosan will be referred to as chitosan-PEG-folate, chi-PEG-FA or simply CPF, due to spacing constraints. This may be followed by a sample designation (such as chi-PEG-FA1a or chi-PEG-FA2b). Chitosan to alginate charge ratios will be indicated, where applicable, after a dash (chi-PEG-FA1a-15).

CHAPTER 5
METHODS

5.1 SYNTHESIS OF CHITOSAN-PEG-FOLATE

The synthesis of chitosan-PEG-folate presented some difficulties in achieving our desired result, so two synthetic protocols were followed. The initial method is based on the published works of Chan *et al.* (Chan et al., 2006) and will be referred to in this document as chitosan-PEG-folate (Chan). Reasons for abandoning this method are listed in the discussion. The revised protocol, as designed by Xingping Qiu (Department of Chemistry, University of Montreal) is presented second and will be referenced for the purposes of this work as chitosan-PEG-folate (Qiu).

5.1.1 Chitosan-PEG-folate (Chan)

The synthetic route followed to produce chitosan-PEG-folate (Chan) is described in Scheme 1.

Materials:

Chitosan (Medipol M, DDA = 90%, MW = 97 kDa as determined by GPC; Medipol, Lausanne, Switzerland) and heterobifunctional PEG (NHS-PEG-maleimide, MW ~ 4800 Da; Rapp Polymere, Tübingen, Germany) were purchased and used as received. Anhydrous dimethylsulfoxide (DMSO, 99.7+ %, extra dry over molecular sieves, < 50ppm water), folic acid (FA), *N*,*N*′-dicyclohexylcarbodiimide (DCC), *N*-hydroxysuccinimide (NHS), 2-aminoethanethiol, and triethylamine (TEA) were obtained from Sigma-Aldrich Co., Oakville, Ontario. Pierce snakeskin dialysis membrane (MWCO 10 000 Da) was purchased from Fisher Scientific Inc. Ultrapure water was obtained using the Nanopure Diamond system (Barnstead, 18.2 MΩ-cm).

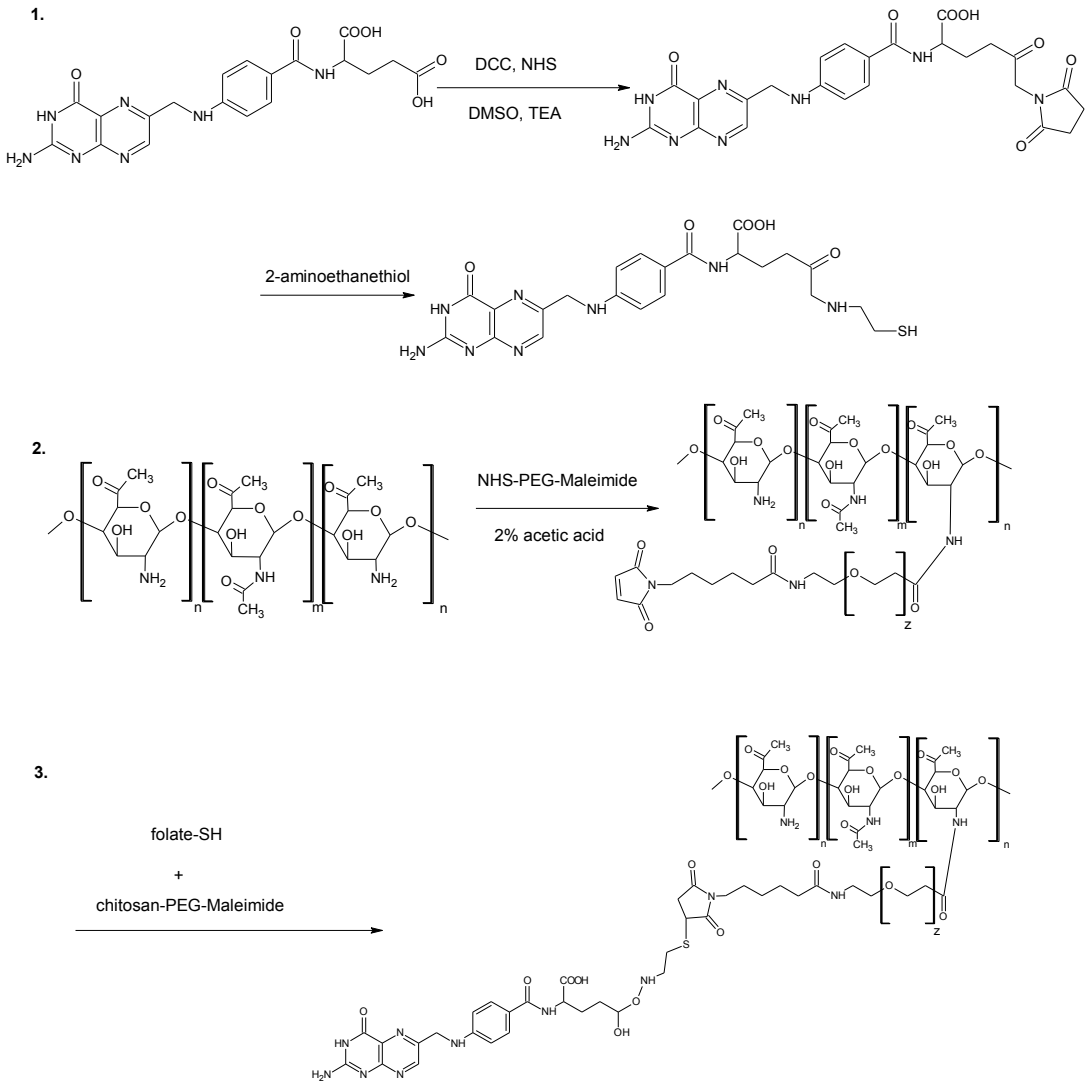

Scheme 1 Synthetic procedure for formation of chitosan-PEG-folate (Chan)

These steps involve 1) activation of folate using carbodiimide chemistry 2) conjugation of chitosan primary amino group to heterobifunctional PEG NHS ester 3) reaction of maleimide –PEG-chitosan to thiolated folate to form a stable thiol ether linkage.

Instruments and Equipment:

Vacuum evaporation was carried out using a Maxima C Plus vacuum pump (Model M2C, Fisher Scientific). The reaction volume was heated using a hemispherical heating mantle (Fisher Scientific) connected to a power regulator (MC228X1, Barnstead Electrothermal). Solution volumes were reduced on a Buchi Rotavapor R-200 and lyophilization carried out on a ModulyoD freeze dryer with a VLP200 vacuum pump (both ThermoSavant).

Solutions were pH adjusted using an Accumet basic pH meter (model AB15, Fisher Scientific).

Synthetic Methods:

In order to obtain a very dry environment, anhydrous DMSO was stored for a day in molecular sieves that had previously been rinsed in chloroform and dried in the oven overnight. All glassware was washed in 6N HCl, rinsed, and oven- dried overnight prior to synthesis. The synthesis is achieved in three steps; activation of folate to folate-thiol, conjugation of chitosan to heterobifunctional PEG to form chitosan-PEG-maleimide, and lastly the reaction of maleimide-PEG-chitosan with thiolated folate to form chitosan-PEG-folate through a thiol ether linkage.

Activation of folate: The reaction vessel (a Schlenk flask) was purged with nitrogen and a mixture of anhydrous DMSO (40 mL) and TEA (0.5 mL) added. Folic acid (1.0 g, 441 g/mol, 2.27 mmol) was added with stirring and allowed to dissolve overnight in the dark under nitrogen gas. DCC (0.5 g, 206 g/mol, 2.43 mmol) and NHS (0.52 g, 115 g/mol, 4.52 mmol) were added and stirred in the dark for a further 18 hours. The white crystalline solid precipitate (dicyclourea, DCU) was removed by vacuum filtration and discarded. The yellow liquid remaining was transferred into a round bottom flask with a stir bar for vacuum evaporation.

To remove DMSO, the reaction vessel was placed on a heating mantle, attached to a condenser, through two solvent traps, to the vacuum pump. Vacuum was applied to the mixture for 15-25 minutes before slowly increasing the heat applied through the heating mantle. The boiling point of DMSO is 189^{o}C and under vacuum, the solvent should be removed at lower temperatures. It should be noted that there was difficulty in removing the DMSO (as discussed further in later sections) and for some attempts, a mixture of solvents was used in order to remove more of the DMSO at a lower temperature. Both a 5:1 and 2:1 ratio of DMSO/ethanol were attempted, but while liquid began to separate at lower temperatures, the time and temperature required to remove the last vestiges of solvent were not very much improved.

After DMSO removal, the residue was re-dissolved in a 2:1 volumetric mixture of DMSO/TEA (3 mL). An equal molar quantity of 2-aminoethanethiol (77 g/mol) was added and allowed to stir overnight in the dark under nitrogen.

Conjugation of chitosan to NHS-PEG-maleimide: Chitosan (100 mg, ~97 kDa) was dissolved in a 2% acetic acid solution (50 mL) and the solution was adjusted to pH 6.0. Heterobifunctional NHS-PEG-maleimide was added to the solution under stirring for 3 hours then pH adjusted to 7.0. This mixture was left overnight in the dark under nitrogen.

Formation of chitosan-PEG-folate: The folate-thiol mixture was added dropwise to the chitosan solution with stirring, then adjusted to between pH 6.5 to 7.5. The reaction mixture was either vacuum filtered or centrifuged isolate the dark yellow liquid, which was subsequently purified by dialysis against ultrapure water for 48 hours (Pierce snakeskin dialysis tubing, MWCO 10 000). The volume of the sample was reduced on a Rotavap and lyophilized to obtain the final solid product.

5.1.2 Chitosan-PEG

Chitosan-PEG was also synthesized in order to attempt comparison with un-modified chitosan and chitosan-PEG-folate. Based on reported synthesis by Chan *et al.*, chitosan (100 mg) was dissolved in 2% acetic acid solution (50 mL) and adjusted to a pH of 6.0 using sodium hydroxide. An equal molar amount of methoxy-PEG-NHS ester (MW ~ 4870 Da; Rapp Polymere, Tübingen, Germany) was added to the solution with stirring and allowed to react for 24 hours at room temperature. The synthesized product was reduced in volume using the Rota-Vap, purified by dialysis (Pierce, MWCO 10 000), and lyophilized.

5.1.3 Chitosan-PEG-folate (Qiu)

The revised synthetic protocol was designed by Xingping Qiu, based on work published by Cho *et al.* (Cho et al., 2005). Synthesis, NMR, GPC and UV characterization were performed on site in the Chemistry Department at the University of Montreal, thanks to generous help from Francoise Winnik and her lab. The procedure followed is described in Scheme 2.

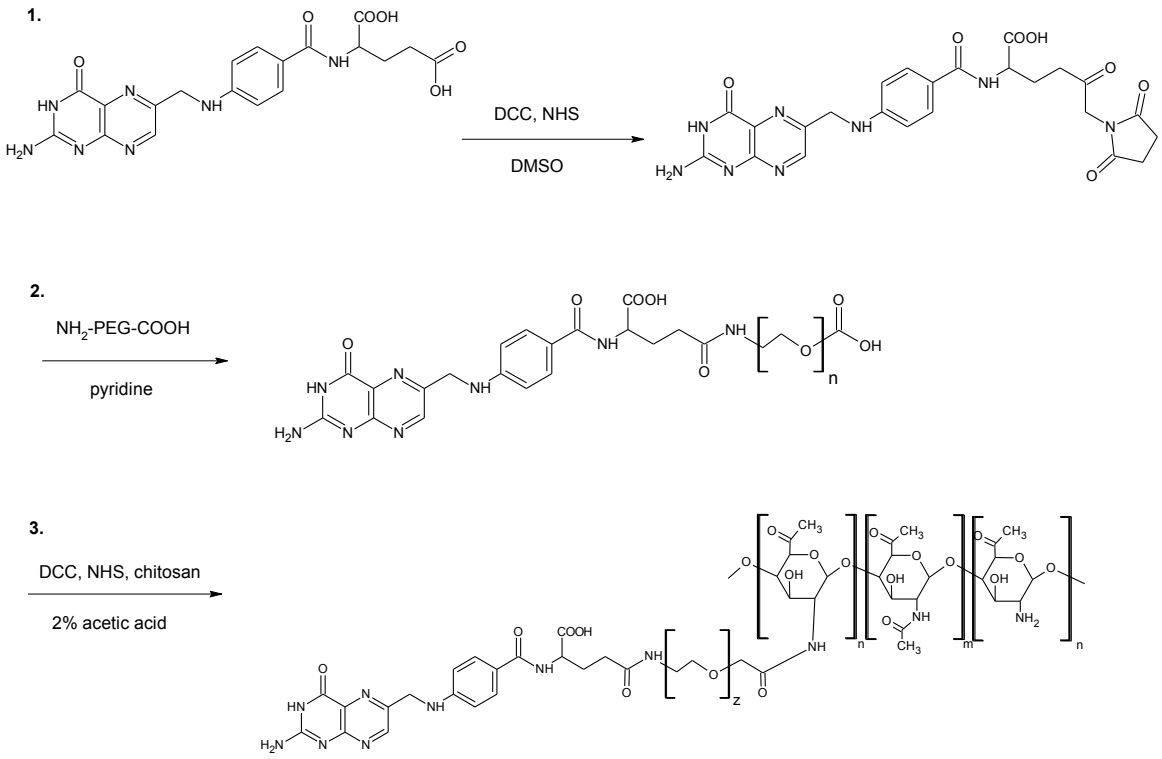

Scheme 2 Synthetic procedure for formation of chitosan-PEG-folate (Qiu)

based on work by Cho *et al*., in three steps: 1) carbodiimide activation of folate to folate-NHS ester 2) conjugation to primary amine on PEG to produce folate-PEG-COOH 3) carbodiimide activation to folate-PEG-NHS ester with subsequent conjugation to primary amine groups on chitosan to form folate-PEG-chitosan.

Materials:

Chitosan, as purchased previously (Medipol M, Lausanne, Switzerland), was used again for this protocol. Heterobifunctional PEG was once again purchased from Rapp Polymere of Germany, though having different reactive end groups (NH_2-PEG-O-C_3H_6- COOH HCl, MW ~ 3274 Da; Rapp Polymere, Tübingen, Germany). Folic acid (FA), *N*-(3-dimethylaminopropyl)-*N′*-ethylcarbodiimide hydrochloride (EDC), DCC, NHS, and glacial acetic acid (HAc) were obtained from Sigma-Aldrich Co., Oakville, Ontario. Spectrum Laboratories Spectra/Por dialysis membranes (MWCO 1000 Da and 12 000 – 14 000 Da) and powdered sodium bicarbonate were purchased from Fisher Scientific Inc. Deionized water was obtained from a Milli-Q water purification system. Solvents including DMSO, pyridine, acetone and ether, were of reagent grade and used as received.

Synthetic Methods:

The synthesis of chitosan-PEG- folate was achieved in three steps: 1) activation of the folate to form a folate-NHS ester; 2) reaction with heterobifunctional PEG (NH_2-PEG-O-C_3H_6-COOH) to form folate-PEG-COOH; and 3) activation of folate-PEG to form folate-PEG-NHS and reaction with chitosan to form chitosan-PEG-folate. This procedure was adapted from a previously reported work by Cho *et al.*, as modified by Xingping Qiu.

Folate NHS ester was prepared as follows: folic acid (300 mg, 441 g/mol, 0.680 mmol) was dissolved in 12 mL of anhydrous DMSO. DCC (93 mg, 206 g/mol, 0.45 mmol) and NHS (77 mg, 115 g/mol, 0.67 mmol) were added to the solution and the mixture was allowed to react at room temperature for 6 hours with stirring. The side product DCU was removed as a white precipitate by filtration. The yellow filtrate was added to 100 mL of a mixture of acetone/ether (30% v/v) with stirring, causing a yellow solid to precipitate from solution. This precipitate was filtered through sintered glass and further washed with 100 mL of 30%v/v acetone/ether. The yellow solid was dried overnight in a dessicator and weighed to determine yield. The full amount produced was used in the next synthetic step.

Based on the mass of folate-NHS-ester obtained in the previous step, NH_2-PEG-O-C_3H_6-COOH HCl (MW = 3274 Da, Rapp Polymere) was added to 100 mL of dry pyridine and allowed to dissolve completely. In order to determine the amount of PEG to add, a success rate of approximately 66% was assumed for the activation of folate. Based on estimated molar amount of activated folate, 3-fold less PEG was measured out, to ensure reaction only on the distal end of the molecule.

The dried folate-NHS ester produced earlier was dissolved in another 12 mL of dry DMSO, with stirring and sonication to ensure complete dissolution. This folate-NHS ester in DMSO was added to the pyridine solution and the reaction mixture was stirred overnight in the dark at room temperature. The following day, pyridine was evaporated *in vacuo*, leaving most of the DMSO and the product. To this flask, 20 mL of deionized water was added and the entire mixture purified by dialysis (MWCO 1000 Da) against saturated sodium bicarbonate in deionized water (to obtain a pH between 7.0 and 8.0) for

one day and for a further two days against deionized water to remove any un-reacted folate. The product was recovered by freeze drying and weighed to determine yield.

Folate-PEG-COOH was dissolved in 5 mL of dry DMSO and activated using EDC (~2.5 mg, 15 μmol) and NHS (~5.8 mg, 25 μmol) with stirring for 4 hours at room temperature. Chitosan (200 mg, ~1.2 mmol amino groups) was dissolved in 20 mL of 2% v/v acetic acid solution. The activated folate-PEG-NHS was added to chitosan dropwise and allowed to stir in the dark at room temperature for 20 hours. The final mixture was purified by dialysis (MWCO 12-14 kDa) against deionized water over 3 days to remove un-reacted folate-PEG-NHS and recovered by freeze drying.

Control experiment: Removal of un-reacted folate-PEG by dialysis was followed by a control experiment whereby folate-PEG was dissolved in DMSO and added to chitosan in 2% v/v acetic acid solution (amounts determined for 1 mol% PEG on chitosan amino groups). The mixture was dialysed against deionized water for 3 days, with samples taken from within the dialysis tubing to determine presence of folate.

5.2 ANALYSIS OF SYNTHETIC PRODUCT

5.2.1 Proton nuclear magnetic resonance spectroscopy (^{1}H NMR)

For the initial synthesis, ^{1}H NMR analysis was performed on a Varian INOVA 500 MHz spectrometer in the Québec/Eastern Canada High Field NMR Facility. Solvents used for analysis include DCl, D_2O and deuterated DMSO.

Meanwhile, the revised synthesis was analyzed on a Bruker ARX-400 400 MHz spectrometer at the University of Montreal. The solvent used for analysis of chitosan samples was a mixture of DCl / D_2O(1 % v/v) while deuterated DMSO was used to solubilize folate-PEG-COOH samples.

Data from both synthetic procedures was analyzed using MestReNova software (Mestrelab Research SL, Spain). Samples were diluted to an approximate concentration of 10 mg /mL of solvent and filtered prior to analysis. Relevant deuterated solvent peaks appear at the following locations in parts per million (ppm), with multiplets indicated in

brackets where applicable: DMSO at 2.5 ppm (5), acetic acid at both 11.5 ppm (1) and 2.04 ppm (5), and D_2O at 4.7 ppm (1) (Cambridge Isotope Laboratories, 2009).

NMR signals correspond to protons on the chitosan glucosamine backbone. A signal near 2.0 ppm is associated with acetyl protons, of which there are three per monomer unit. The signal at 3.0 ppm is associated with H-2 while signals between 3.3 to 4.0 ppm originate from H-3 to H-6. The proton H-1 appears around 4.6 ppm for acetylated residues and around 5.0 ppm for deacetylated residues. The molecular structure of an acetylated chitosan monomer is displayed as Figure 6, with associated carbon labels.

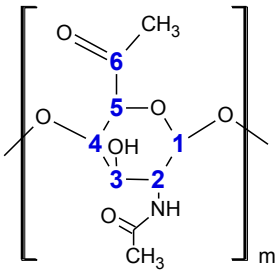

Figure 6 The chitosan monomer unit (acetylated).

.

The degree of deacetylation of chitosan can be calculated using Equation 1. The signal at 3.0 ppm represents H-2 and is therefore a measure of one chitosan unit. The signal at 2.0 ppm is divided by three since it represents three acetyl protons.

$$DDA = \left[1 - \frac{{}^{1}/_{3}\, H_{2.0\ ppm}}{H_{3.0\ ppm}}\right] \times 100\%$$

Equation 1 Degree of deacetylation of chitosan, expressed as a percentage.

Degree of substitution of PEG was calculated using Equation 2, modified from Sugimoto *et al.*(Sugimoto, Morimoto, Sashiwa, Saimoto, & Shigemasa, 1998), where 6 is the total number of protons including H-2, H-3, H-4, H-5 and two protons H-6.

$$DS\ PEG = \frac{\left[\frac{H_{3.3-4.0\ ppm}}{H_{3.0\ ppm}}\right] - 6}{\#\ protons/PEGchain} \times 100\%$$

Equation 2 Degree of substitution of PEG, expressed as a percentage.

Where

$$\#protons/_{PEGchain} = \frac{average\ chain\ MW\ PEG}{MW\ of\ one\ PEG\ unit} \times 4$$

5.2.2 UV spectrophotometry

UV/vis spectrophotometry was performed on a Hewlett-Packard 8452A photodiode array spectrometer in a 2% v/v acetic acid aqueous solution. Chitosan-PEG-folate samples were analyzed by UV spectrophotometry to determine amount of folate with respect to chitosan amino groups, using a molar extinction coefficient of folate at λ_{323nm} of 6165 $M^{-1}cm^{-1}$.

Based on the Beer-Lambert equation, as noted by Equation 3, synthesized chitosan-PEG-folate samples were diluted to a concentration intended to achieve an absorbance around 0.5, in order to be read on the apparatus. A 1:1 ratio of PEG substitution on folate was assumed for the purposes of this calculation and optical pathlength through the cavetto is 1 cm. Absorbance was measured at 323 nm.

$$A = \varepsilon \times c \times L$$

Equation 3 Beer Lambert equation.

As a guideline, for A = 0.5,

$$c_{folate} = \frac{A}{\varepsilon L} = \frac{0.5}{(6165\ M^{-1}cm^{-1})(1\ cm)} = 8.11\ x\ 10^{-5}\ mol/_{L} = 8.11\ x\ 10^{-8}\ mol/_{mL}$$

For samples intended to have a 1% degree of substitution of PEG (and therefore folate), chitosan would be present in 100 x this amount, at 8.11 x 10^{-6} M. Assuming an average glucosamine unit molecular mass of 167 g/mol, the concentration of solution needed is

$$c_{sample} = 8.11\ x\ 10^{-6}\ mol/_{L} \times 167\ g/_{mol} = 1.35\ x\ 10^{-3}\ \frac{g}{mL}$$

In 4 mL of solution, the amount of sample to be weighed out is

$$mass_{sample} = 1.35\ x\ 10^{-3}\ \frac{g}{mL} \times 4\ mL = 5.41\ x\ 10^{-3} g = 5.41\ mg$$

The amount of sample needed for UV analysis was calculated for each sample based on this method.

5.2.3 Gel permeation chromatography (GPC)

Gel permeation chromatography to determine weight average molecular mass of chitosan samples was carried out using an Agilent 1100 isocratic pump, with a Dawn EOS multi-angle laser light scattering detector (Wyatt Technology Co.), an Optilab DSP interferometric refractometer (Wyatt Technology Co.) and a TSK-GEL $GMPW_xL$ column (Tosoh Biosep). Acetate buffer was used as a mobile phase (0.3 M acetic acid 0.2 M sodium acetate, pH 4.5) with a flow rate of 0.8 mL min^{-1} and a d*n*/d*c* value of 0.192. Samples were prepared at a concentration of 5 mg/mL and analyzed by Zhimei Miao and Satu Strandman (Department of Chemistry, University of Montreal).

Osmometric data is collected by the refractive index detector, which measures the refractive index of the sample as its concentration in solution changes. This data yields information regarding number average molecular weight (M_N). Light scattering detectors can provide information regarding weight average molecular weight (M_W). The ratio of M_W to M_N is referred to as the polydispersity index (PDI) or molecular weight distribution (MWD) of the material.

5.3 NANOPARTICLE FORMATION

Chitosan/alginate nanoparticles were formed using both un-modified chitosan and modified chitosan. Stock solutions of chitosan and alginate were prepared and filtered through 0.22 μm syringe filters (Millipore Express PES syringe filters).

Chitosan was dissolved in 3 mL 1N HCl and ~5 mL ultrapure water and left to stir gently with heating overnight. Solutions were pH adjusted between 5.6 to 5.9 using sodium hydroxide added dropwise, filtered, and ultrapure water added up to a final volume of 10 mL.

Alginate (low viscosity sodium salt, Sigma Aldrich) was added to just less than 1000 mL of ultrapure water and allowed to dissolve overnight. The solution was adjusted to a pH between 5.6 and 5.8 and adjusted to a final volume of 1000 mL.

Initial particles were made using 1% chitosan (100 mg in 10 mL volume; 0.01 g/mL) and 0.005% alginate solutions (50 mg in 1000 mL volume; 5 x 10^5 g/mL). Later particles were made 10x less concentrated, using 0.1% chitosan and 0.0005% alginate solutions in order to conserve the synthesized product. Particles were formed either with magnetic stirring or with vortexing for 1 hour at room temperature (Vortex Genie 2T; speed 4, Scientific Industries). Nanoparticles were identified by their chitosan/ alginate charge ratio.

5.4 NANOPARTICLE CHARACTERIZATION

5.4.1 Particle size

Nanoparticles were analyzed using low angle dynamic light scattering (DLS) on a Malvern high performance particle sizer (HPPS, Malvern Instruments Ltd, MA, U.S.A.) and data collected on DTS software.

5.4.2 Surface charge

The surface charge of particles was assessed using zeta potential analysis (ZetaPlus, Brookhaven Instruments Corporation) using ZetaPALS (Phase Analysis Light Scattering) software. Reference solutions were prepared using Brookhaven BI-ZR3. When diluted properly in 1 mM KCl, reference solution should have a charge of +53 ± 4 mV.

5.4.3 Scanning electron microscopy (SEM)

An effort was made to image the nanoparticles by scanning electron microscopy (SEM) using a variety of preparation methods. These methods included drying particle solutions directly on bare silicium slides as well as on PLL-coated glass slides. Additionally, a portion of nanoparticle solution was freeze-dried and the resulting powder was analyzed. All samples were sputter coated with gold palladium prior to imaging. Images were obtained using a field emission gun SEM (FEG SEM, Hitachi S4700) operated at 2 kV and 10 μA.

5.5 IN VITRO ANALYSIS

The transfection ability of chitosan-PEG-folate/ alginate nanoparticles was assessed in comparison with un-modified chitosan/ alginate nanoparticles as well as the commercially available cationic liposomal vector, Lipofectamine^{TM} transfection reagent (Invitrogen, Ontario, Canada; 2 mg/mL stock concentration). Centrifugation was carried out on the Accuspin 400 (Fisher Scientific).

According to the recommended starting protocol given in the Lipofectamine reagent literature, the amount of Lipofectamine for use in each well of a 24-well plate ranges between 0.5 to 5 μL, using between 0.2 to 0.4 μg of DNA per well, with a plating volume of 500 μL. Due to the dilution of chitosan/alginate nanoparticles, a higher plating volume (1 mL) was chosen and also used for this positive control. Initial trials using recommended amounts of DNA and Lipofectamine yielded poor results. As recommended by a colleague, higher amounts of DNA were used (and improved transfection efficiency). DNA trials using varying amounts of DNA held the amount of Lipofectamine at 2 μL per well , in order to keep this variable constant.

5.5.1 Cell culture conditions

Nanoparticles were assessed in a human embryonic kidney cell line (HEK 293T) as well as screened in two cancer cell lines, one ovarian (Caov-3) and one breast cancer cell line (MDA-MB-231). Cells were maintained at 37 ^{o}C and 5% CO_2. Cell stocks were kept in aliquots between 1 to 3 x 10^6 cells per mL in 90% FBS/ 10% DMSO freeze media at -80 ^{o}C and thawed as needed.

HEK 293T cells were cultured in Dulbecco's Modified Eagle Media (DMEM; Gibco by Invitrogen 10569), supplemented by 10% fetal bovine serum (FBS; Gibco) and 1% penicillin/ streptomycin (pen/strep; Gibco 15140). In general, cell passages were performed every 2 days at a 1:8 ratio.

Caov-3 cells are an adherent, epithelial cell line derived from ovarian adenocarcinoma and were maintained in DMEM, with 10% FBS and 1% pen/strep and passaged 1:2 every 2 to 3 days. This cell type in particular was prone to lifting off the cell culture plate and had a slower growth rate as compared to the other cell types.

MDA-MB-231 cells are an adherent epithelial cell line, derived from breast adenocarcinoma. They were grown in DMEM, 10% FBS, 1% pen/strep, and supplemented additionally with 1% MEM non-essential amino acids (NEAA; Gibco 11140). The cells were passaged in a 1:4 ratio every 2 days.

5.5.2 pEGFP and propidium iodide

Cells were transfected using a 4.7 kb pDNA encoding enhanced green fluorescent protein (pEGFP- C3). The expressed protein has an excitation maximum of 488 nm and an emission maximum of 507 nm. From an initial glycerol stock of pDNA, pEGFP- C3 was amplified and isolated using a Maxi kit (Qiagen Inc., Ontario, Canada) and final concentrations of pDNA was assessed by UV spectrophotometry by measuring optical density at an absorbance of 260 nm.

The concentration of pDNA in ng/µL was calculated using the Beer-Lambert equation (Equation 3),

Since the extinction coefficient of double stranded DNA is 20 µL/µg/cm,

$$C_{DNA} = \frac{A_{260}}{20^{\mu L}/_{\mu g}} \times \frac{1000\ ng}{\mu g} = A_{260} \times 50 \frac{ng}{\mu L}$$

Samples were diluted prior to reading on the instrument and this dilution factor must be taken into account, therefore

$$C_{DNA} = A_{260} \times 50 \frac{ng}{\mu L} \times dilution\ factor$$

As a marker for cell death, cells were stained with a fluorescent molecule, propidium iodide (PI), which binds to DNA but is excluded from cell membranes, meaning that it will stain DNA that is outside of the cells and not DNA inside viable cells. It can be excited at a wavelength of 488 nm and detected in the range of 562 to 588 nm.

5.5.3 Transfection procedure

Transfection experiments were performed in 24-well cell culture-treated plates (surface area per well approximately 2.0 cm^2, nominal volume 3.5 mL, working volume up to 1.0 mL). One day prior, cells were seeded between 2.5 x 10^4 to 5.0 x 10^4 cells per well in 1 mL of full growth media, for confluence between 50 to 80% at the time of transfection.

Solutions were prepared for each well, with no binning of samples (meaning that for triplicate samples, three separate sets of tubes were prepared, as opposed to one set with 3x the amount needed).

For each sample, pDNA was diluted in the chosen transfection media in a microcentrifuge tube. The complexes (either the nanoparticles or liposomal positive control) were similarly diluted in chosen transfection media in a separate microcentrifuge tube, taking care that the volumes of each tube were equal (in most cases, each tube contained a total volume of 100 μL). The tubes were mixed gently and allowed to remain at room temperature for between 15 minutes to an hour. Complexes were then added to pDNA, mixed gently and allowed to incubate for between 20 to 40 minutes at room temperature (total volume per tube: 200 μL). Meanwhile, cells at the appropriate confluence were washed once in 500 μL of empty transfection media, then 800 μL of empty transfection media was placed in each well. The prepared samples were added to each well (for a total volume of 1 mL per well) and incubated at 37 ^{o}C and 5% CO_2.

After 4-hour incubation, transfection media was removed and replaced with 1 mL full media per well. Cells were screened quickly by fluorescent microscopy and then prepared for flow cytometry analysis, 48 hours post-transfection.

5.5.4 Amine/phosphate (N/P) ratio

The ratio of nanoparticles to pDNA used per well was identified as an N/P ratio, or a ratio of theoretical amino groups on chitosan (N) to theoretical phosphate groups on DNA (P). For every μg of DNA, there are 0.003 μmol of phosphate, and therefore the theoretical moles of phosphate can be approximated based on the amount of DNA used per well and represents the value of "P".

As for chitosan, the unit molecular weight of each chitosan monomer is approximately 167 g/mol and the degrees of deacetylation of both chitosan and modified chitosan were calculated from NMR spectra. Knowing the amount of chitosan used in each nanoparticle formation, as well as the degree of deacetylation, we can approximate the moles of reactive amino groups in that sample. Additionally, it is assumed that the negatively charged carboxyl groups of alginate interact stoichiometrically with the positively

charged amino groups of chitosan. Assuming that each mole of theoretical alginate carboxyl group neutralizes the charge from one mole of theoretical chitosan amino groups, we can subtract to obtain the theoretical moles of chitosan amine, or "N",that are available to interact with pDNA.

5.5.5 Fluorescence microscopy

Each experiment was screened under fluorescence microscopy (Nikon Eclipse TE2000-U inverted research microscope, Nikon Corporation, Japan) with ACT-1 software (Nikon Corporation), as a rapid measure of whether the experiment was successful. For experiments that were to be analyzed by flow cytometry, fluorescent images were not obtained, in order to lessen the effect of photobleaching, which could affect quantitative transfection results. For samples to be photographed, media was replaced with 500 μL of PBS to obtain clearer images.

5.5.6 Flow cytometry analysis

After screening under fluorescence microscopy, cells were harvested 48 hours post-transfection for flow cytometry analysis. Each well of the 24-well plate was rinsed in 500 μL phosphate buffered saline (1 x PBS, Gibco 70011) then 300 μL of trypsin-EDTA (0.05%, Gibco 25300) was added quickly. Cells were incubated for between 3 to 10 minutes to allow heat-activated trypsin to function, as monitored under light optical microscopy every few minutes. Between 500 μL to 1 mL of PBS supplemented with 2% FBS was then added to each well to inactivate trypsin activity. Samples were transferred into microcentrifuge tubes and spun down at 300 g for 5 minutes. At this point, all samples were kept on ice. Media was removed to the pellet and replaced with 300 μL of PBS with 2% PBS. Cells were resuspended and transferred into cell culture tubes for subsequent flow cytometry analysis. Before analysis, 3 μL of propidium iodide fluorescent dye was added to each sample tube (and relevant control tubes) in the dark.

The results of each transfection were analyzed using a BD FACSCalibur^{TM} multicolor flow cytometer (BD Biosciences, Mississauga, ON, Canada). Data was acquired using CellQuest Pro software (BD Biosciences). Both fluorescent markers of interest can be excited by the laser at 488 nm. Fluorescence signal generated by EGFP was collected on

FL1 (band pass filter: 530/30) while PI was collected on FL2 (band pass filter: 585/42). Data analysis was performed using FlowJo software (TreeStar Incorporated, Oregon, USA)

Using the BD Biosciences Fluorescence Spectrum Viewer (http://www.bdbiosciences.com/colors/fluorescence_spectrum_viewer//), the excitation and emission spectra for EGFP and PI are represented in Figure 7.

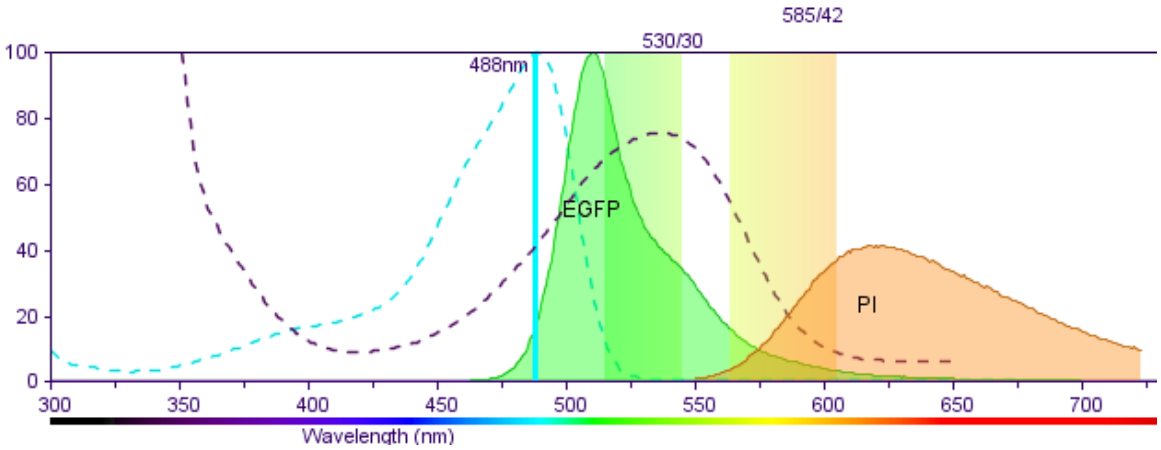

Figure 7 Excitation and emission spectra for EGFP and PI.

Spectra were produced by the BD Biosciences Fluorescence Spectrum Viewer, showing excitation in dotted lines while emission is shown as a filled solid line. Laser excitation wavelength at 488 nm and band pass filters used are represented by vertical bars.

Data obtained from the FACSCalibur was analyzed by Flowjo software. GFP positive gates were drawn around Lipofectamine positive controls, containing PI, while PI positive gates were drawn around negative controls, without PI. These gates were applied to the entire data set, however gates were modified around samples containing no PI (negative control with no PI and positive control with no PI) due to shifting of the live cell population.

5.6 STATISTICAL ANALYSIS

Where applicable, results are presented as the mean with standard deviation represented as error bars, however statistical analyses such as the Student's t-test or ANOVA could not be performed due to the nature of the results.

CHAPTER 6
RESULTS

The majority of results presented in this work refer only to those samples produced by the chitosan-PEG-folate (Qiu) synthetic protocol. Many additional experiments were performed with products produced from the alternative synthesis protocol developed by Chan *et al.*, however, due to reservations about the purity, activity and success of that reaction scheme, further highlighted by results from the initial nanoparticle characterization of these samples, these additional complexes were not extensively used in transfection. Unless otherwise noted, the following results are based upon the Qiu protocol for chitosan-PEG-folate synthesis.

6.1 ANALYSIS OF CHITOSAN-PEG-FOLATE

Six samples of chitosan-PEG-folate were synthesized according to the Qiu protocol, with different intended degrees of PEG and folate substitution.

Percentage yield from these syntheses are reported in Table 1.

Table 1 Percentage yield of chitosan-PEG-folate samples.

Sample ID	Final mass (mg)	Initial mass Chi + folate-PEG-COOH (mg)	Yield (%)
ChiPEGFA1a	162.1	239.8	67.6
ChiPEGFA1b	239.0	246.0	97.1
ChiPEGFA2a	232.1	280.2	82.8
ChiPEGFA2b	218.5	282.8	77.3
ChiPEGFA3	254.1	313.0	81.2
ChiPEGFA5	361.1	397.5	90.8

6.1.1 NMR

The ^{1}H NMR spectra of the un-modified chitosan starting material and one sample from the synthesized product, chitosan-PEG-folate1a, are presented in Figure 8 and Figure 9, respectively. Additional spectra for all chitosan-PEG-folate samples made through the Qiu protocol as well as representative NMR spectra from the synthesis of chitosan-PEG-folate by the Chan protocol are located in Appendix A. A sample spectra of folate is also found in Appendix A.

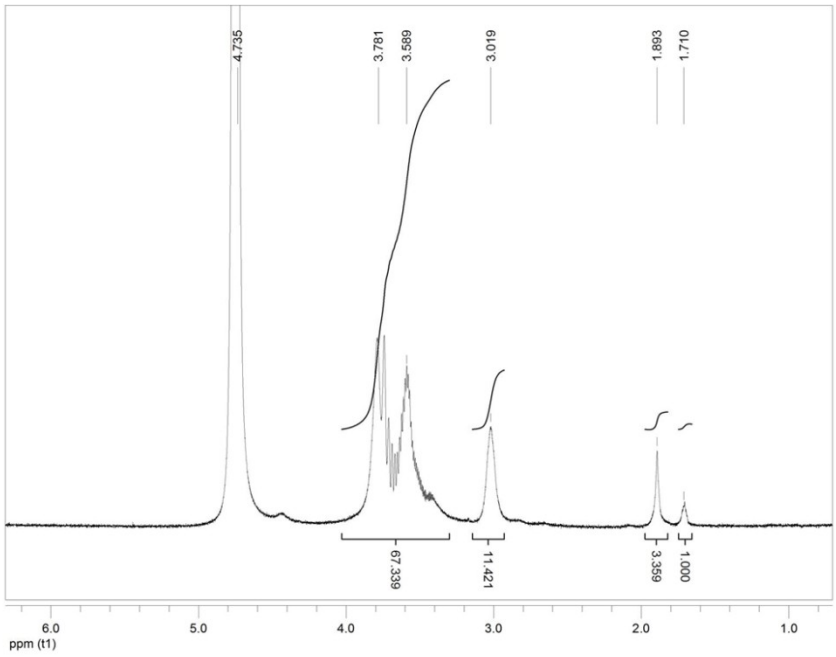

Figure 8 ^{1}H NMR spectrum of un-modified chitosan in 1% DCl in D_2O.

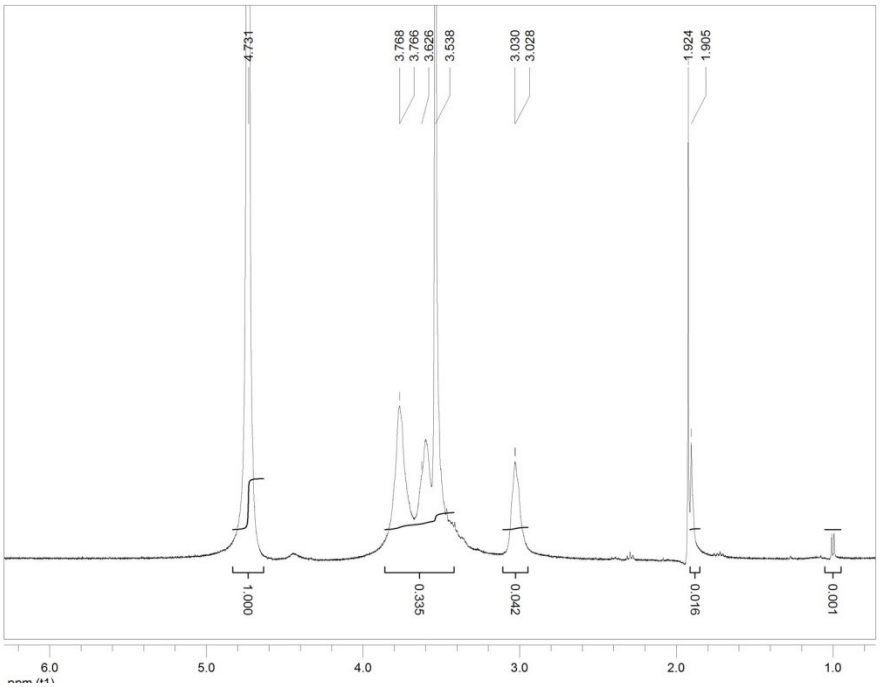

Figure 9 ^{1}H NMR spectrum of chitosan-PEG-FA1a in 1% DCl in D_2O.

A summary of the calculated degree of deacetylation and PEG substitution for each sample is presented in Table 2. These percentages are calculated based on peak assignments from NMR. Peak assignments relevant to these calculations are listed in Appendix A.

Table 2 Degree of deacetylation and degree of substitution of PEG for chitosan-PEG-folate samples, as calculated from NMR, reported as percentages.

Sample ID	DDA (%)	DS PEG (%)
chitosan	90.2	n/a
ChiPEGFA1a	87.3	0.72
ChiPEGFA1b	88.1	0.90
ChiPEGFA2a	85.4	3.48
ChiPEGFA2b	87.2	1.95
ChiPEGFA3	85.3	3.60
ChiPEGFA5	87.9	4.86

6.1.2 UV Spectrophotometry

Using the Beer Lambert equation and absorbances measured at 323 nm, the degree of folate substitution for chitosan-PEG-folate samples was calculated. A summary of percentage substitution of folate can be found in Table 3.

Table 3 Degree of folate substitution (DS FA%) from UV spectrophotometry. Results were calculated using a molar extinction coefficient of 6165 $M^{-1}cm^{-1}$ for folate at λ_{323nm}.

Sample ID	Intended degree of substitution (%)	Absorbance at $\lambda_{323\ nm}$	Mass sample (mg) in 4mL	DS FA (%)
Chi-PEG-FA1a	1	0.30751	5.75	0.58
Chi-PEG-FA1b	1	0.42717	5.54	0.84
Chi-PEG-FA2a	2	0.33358	2.98	1.21
Chi-PEG-FA2b	2	0.26588	2.38	1.21
Chi-PEG-FA3	3	0.341	2.4	1.54
Chi-PEG-FA5	5	0.23758	1.17	2.2

6.1.3 GPC

The molecular weights of synthesized chitosan-PEG-folate samples as well as un-modified chitosan were analyzed by GPC. Results are summarized in Table 4.

Table 4 GPC analysis, as interpreted on refractive index and light scattering detectors. Results are given as number- and weight- average molecular mass as well as polydispersity of chitosan samples.

Sample ID	M_N (g/mol)	M_W (g/mol)	PDI
Un-modified chitosan	75090	97350	1.30
Chi-PEG-FA1a	7409	100600	13.58
Chi-PEG-FA1b	5189	94150	18.14
Chi-PEG-FA2a	10950	94000	8.58
Chi-PEG-FA2b	8356	89540	10.72
Chi-PEG-FA3	5593	95000	16.99
Chi-PEG-FA5	3117	71440	22.92

Due to broad peaks and high PDI, data was analyzed again with integration on light scattering data only, presented in Table 5. It should be noted that although this analysis gave better polydispersity indices, light scattering measurements emphasize large scatter and disregard small peaks.

Table 5 GPC analysis, as integrated on light scattering detectors only. Results are given as number- and weight- average molecular mass as well as polydispersity of chitosan samples.

Sample ID	M_N (g/mol)	M_W (g/mol)	PDI
Chi-PEG-FA1a	32360	108100	3.34
Chi-PEG-FA1b	67940	115100	1.69
Chi-PEG-FA2a	59780	120900	2.02
Chi-PEG-FA2b	70820	122900	1.74
Chi-PEG-FA3	66840	139300	2.08
Chi-PEG-FA5	69710	129200	1.85

6.2 NANOPARTICLE CHARACTERIZATION

6.2.1 Particle size and zeta potential

An initial evaluation of the sizes and surface charges of nanoparticles formed by either un-modified chitosan or modified chitosan-PEG-folate with alginate was performed. A summary of the trends for both parameters can be seen in Figure 10 and Figure 11. Charge ratios are expressed as theoretical positive charges due to amine groups of chitosan divided by theoretical negative charges from carboxyl groups of alginate.

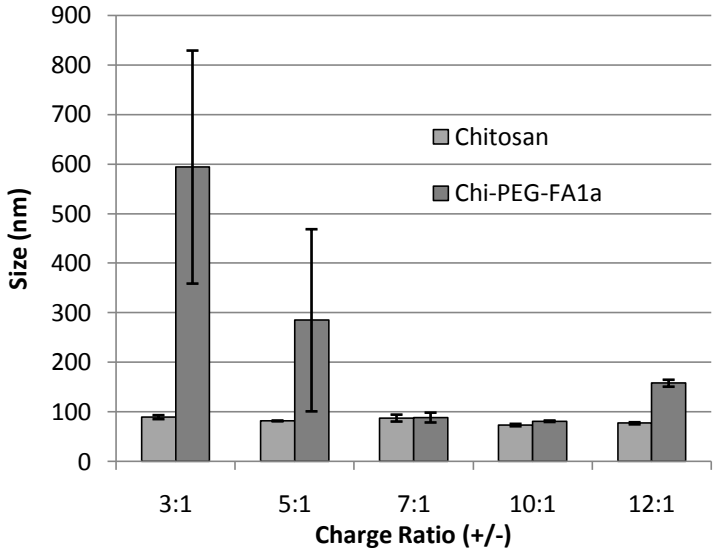

Figure 10 Particle sizes formed by chitosan and chi-PEG-FA1a at various charge ratios. Measurements were taken in triplicate and results are reported as mean with standard deviation.

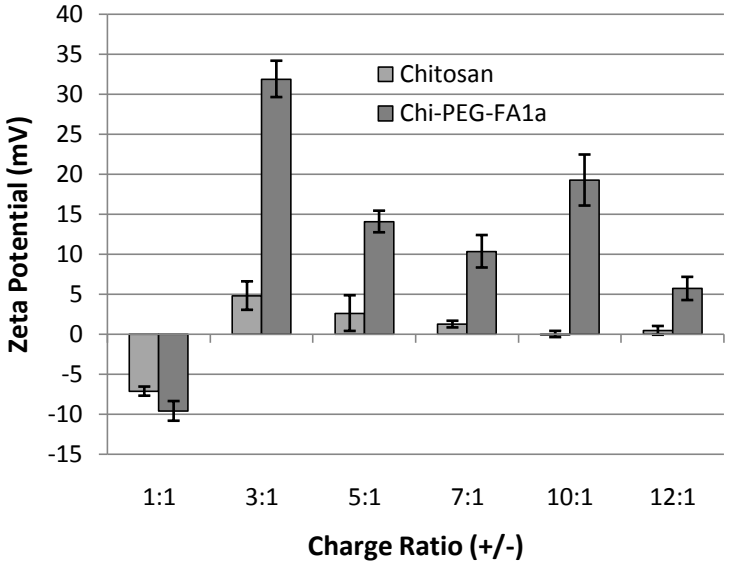

Figure 11 Surface charges of particles formed by chitosan and chi-PEG-FA1a at various charge ratios. Results are reported as mean of 5 runs with standard deviation.

6.2.2 Imaging by SEM

Sample images obtained after drying chitosan and chitosan-PEG-folate3 nanoparticle solutions prepared at a charge ratio of 15 on PLL-coated glass slides are shown below as Figure 12 and Figure 13, respectively. The sizes of chitosan-15 and chitosan-PEG-folate3-15 as measured by DLS, were 206.7 ± 0.58 and 162.3 ± 7.51 nm, respectively. Polydispersity indices were 0.395 ± 0.01 for chitosan15 and 0.456 ± 0.04 for chitosan-PEG-folate3-15, indicating fairly polydisperse samples. The apparent sizes observed via SEM seem to be much larger than DLS measurements for chitosan-15, between around 300-400 nm, and approximately the same size for chitosan-PEG-folate3 between 100 to 200nm. While the larger sizes of chitosan nanoparticles may be due to reorganization during drying, it is hard to make a statement about size from these images, due to issues related to drying of the sample (see Discussion section 7.3.2).

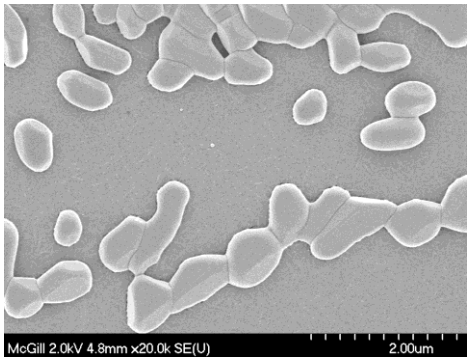

Figure 12 FEGSEM image of chitosan -15 nanoparticles dried on PLL-coated glass slides with 20 000x magnification.

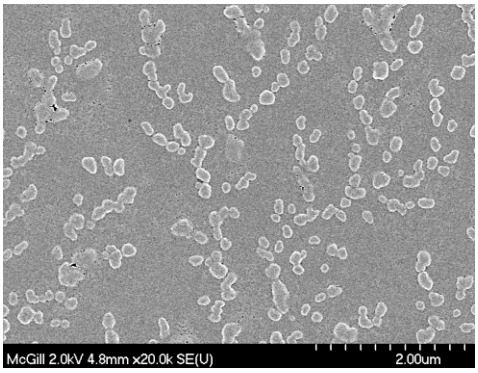

Figure 13 FEGSEM image of chi-PEG-FA3-15 nanoparticles dried on PLL-coated glass slides with 20 000x magnification.

6.3 IN VITRO ANALYSIS

We focused on evaluation of synthesized chitosan-PEG-folate1a, -2a, and -3 for transfection analysis, as these samples gave us a range of degree of folate and PEG substitution. In this document, cells exhibiting fluorescence due to GFP transfection are referred to as GFP+ while cells taking up propidium iodide as a marker for cell death are labeled PI+.

6.3.1 Flow cytometry analysis

Gates were drawn manually on GFP+ and PI+ populations and applied to the entire data set of each experiment, with the exceptions of PI- samples. An example of gating by experiment and the modification to the gates on samples with no PI can be seen in Figure 14. Due to a shift in the live cell population with inclusion of propidium iodide, any PI- samples display a shift that is corrected manually on these samples alone, to avoid overestimation of GFP+ cell populations. Figure 14 (a) represents the uncorrected gates and (b) is after correction.

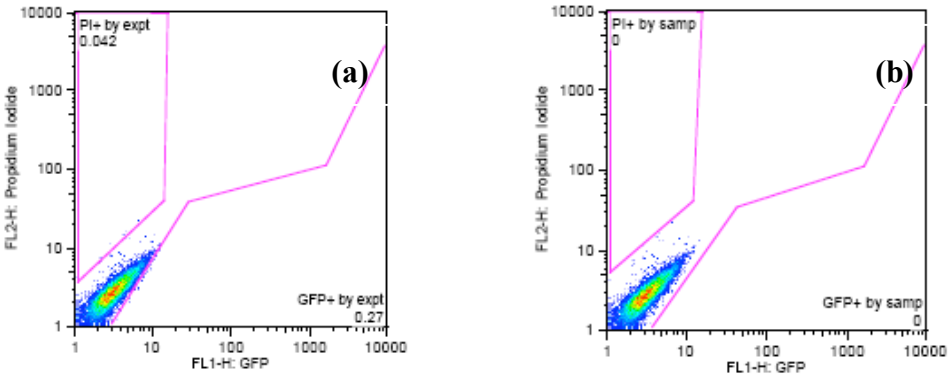

Figure 14 Flow cytometry analysis of HEK 293T negative controls gated (a) by experiment and (b) by sample to illustrate gating strategy. These represent untreated cells.

6.3.2.1 HEK 293T cells

In order to optimize transfection efficiency in HEK 293T cells, screening of various transfection media and various concentrations of DNA was undertaken.

Media trials

Six types of media were assessed: serum-free DMEM, DMEM with serum, and PBS solutions at pH 6.6, 7.0, 7.4 and 7.7. Un-modified chitosan as well as 3 modified chitosan-PEG-FA samples of different degrees of substitution were assessed in each

media, at a chitosan/ alginate charge ratio of 7. The N/P ratio used to form complexes was maintained at 1, using 7 μg of pDNA in each well of the 24-well plate. Total volume of transfection media was 1 mL. Control conditions included an untreated negative control, a positive control containing both pDNA and Lipofectamine transfection reagent, a third control condition containing Lipofectamine reagent alone and lastly, a condition using pDNA alone. These control conditions were performed in each individual media. Each experimental condition was assessed in triplicate. Positive and negative controls also included one well with no PI. The percentage of GFP+ cells was determined from the live population. Results are shown in Figure 15, with positive controls included.

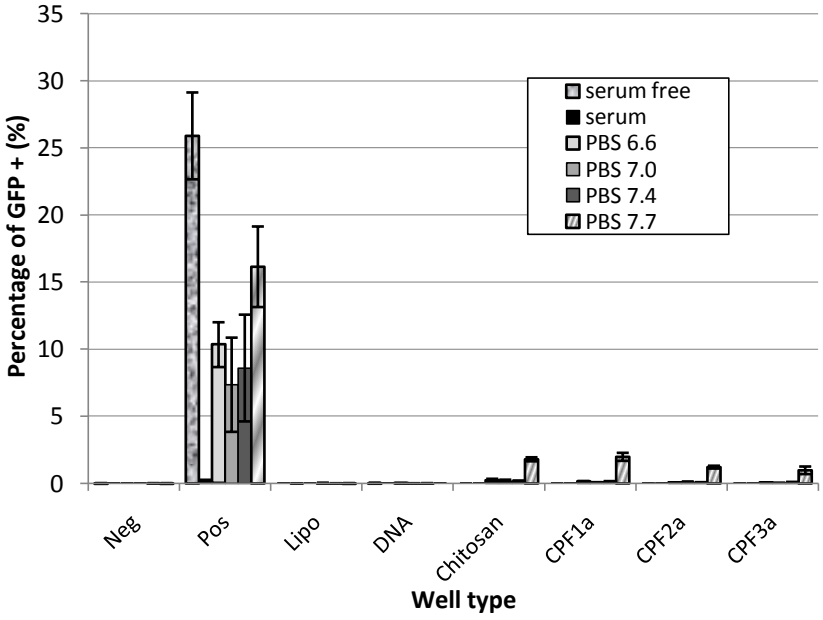

Figure 15 GFP+ HEK 293T cells in different media, including control conditions.
Percentage of GFP+ cells on live population is shown 48 hours post-transfection of cells incubated with 7μg of pEGFP-C3 for 4 hours in six types of media with various chitosan/alginate nanoparticle carriers. Each condition was performed in triplicate (n= 3) and error bars represent standard deviation of the mean.

Lipofectamine positive controls showed transfection in all media types except in full media containing serum and displayed highest efficiency in serum-free media, at 25.46 ± 4.38 % GFP+ on live cells. Data is presented again in Figure 16 without Lipofectamine control in order to better display transfection of chitosan and modified chitosan samples.

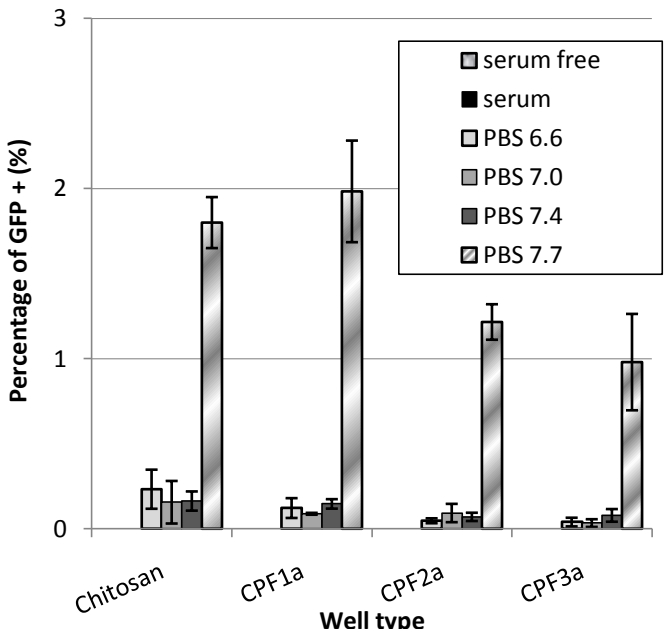

Figure 16 GFP+ HEK 293T cells in different media, without control conditions.
Percentage of GFP+ cells on live population is shown 48 hours post-transfection of cells incubated with 7μg of pEGFP-C3 for 4 hours in six types of media with various chitosan/alginate nanoparticle carriers. Error bars represent standard deviation of the mean and each condition was repeated in triplicate (n= 3). Control samples are not pictured.

Chitosan-PEG-folate and chitosan samples displayed no transfection in serum-free media or full media but showed increasing efficiency in PBS solutions, as pH increased. The highest efficiency was achieved in PBS at pH 7.7, with chitosan-PEG-folate1a, 2a and 3 showing 1.98 ± 0.30, 1.22 ± 0.1 and 0.98 ± 0.28 % GFP+ cells, respectively, as compared to un-modified chitosan with 1.80 ±0.15 % GFP+ on live cells.

Cell death was indicated by propidium iodide staining, as represented in Figure 17.

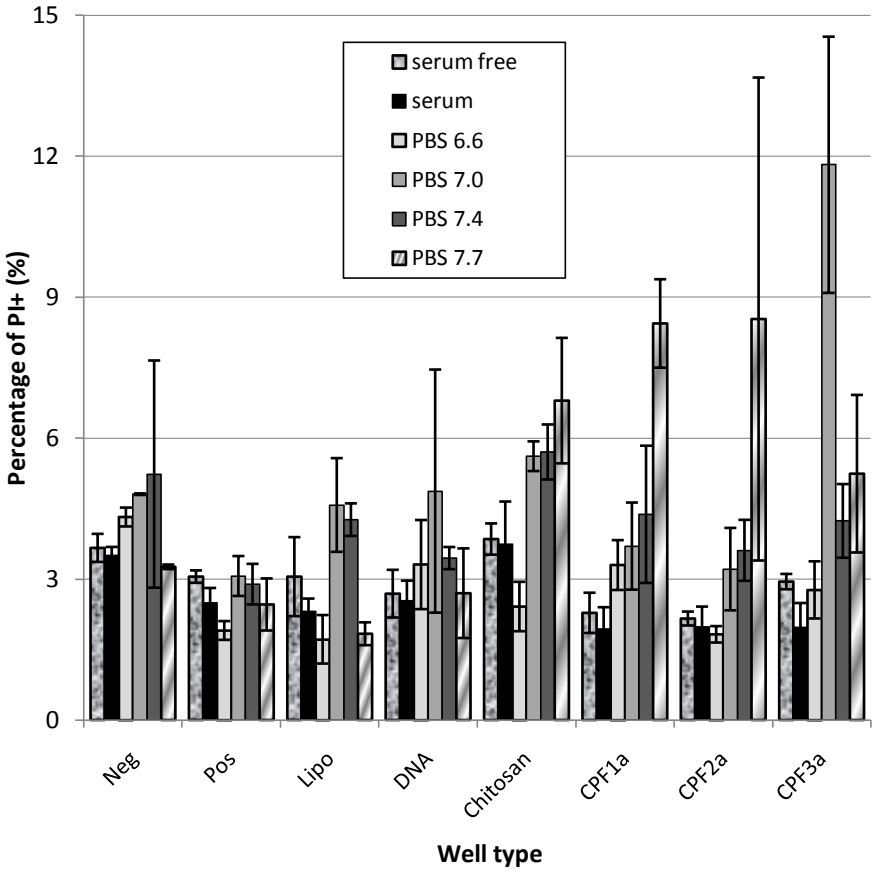

Figure 17 Percentage of PI+ cells for HEK 293T media trial.
Percentage of PI+ cells is shown 48 hours post-transfection of cells incubated with 7μg of pEGFP-C3 for 4 hours in six types of media with various chitosan/alginate nanoparticle carriers, with 3μL PI per sample. Error bars represent standard deviation of the mean and each condition was repeated in triplicate (n= 3).

The highest percentage of PI+ cells was 11.82 ±2.73 % for chitosan-PEG-folate3 in PBS at pH 7.0. In general, cells tranfected in full serum and serum free media displayed the lowest percentage of PI+ cells.

DNA trials

For DNA trials, the amount of pEGFP-C3 incubated per well was varied between 1 to 9 μg of DNA, per well of the 24-well plate, with a total volume of 1 mL. The amount of Lipofectamine reagent used was maintained at the equivalent of 2 μL per well, as mentioned previously, to keep the amount of DNA the only changing variable. The transfection media used was PBS at pH 7.7, while all nanoparticle formulations were made at a chitosan/alginate charge ratio of 7. Results of the DNA trial are depicted graphically in Figure 18.

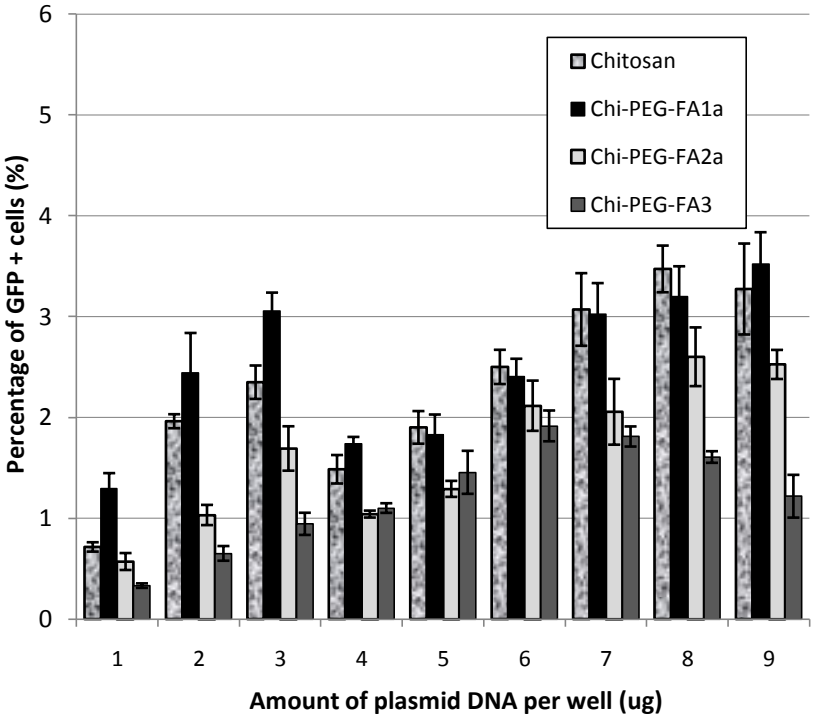

Figure 18 GFP+ cells from DNA trial in HEK 293T cells
pEGFP-C3 quantities ranging from 1 to 9 μg per well are evaluated. Transfection was assessed in un-modified chitosan and modified chitosan nanoparticles produced at a charge ratio of 7. Transfection media was PBS at pH 7.7 and incubation time was 4 hours. Error bars represent standard deviation of the mean, based on triplicate samples (n =3).

In general, higher transfection efficiency was achieved with higher amounts of pDNA, with some variance in this trend. Efficiencies above 3% were achieved with 7, 8, and 9 μg of pDNA per well in chitosan and chitosan-PEG-folate1a samples. For reference, positive controls using Lipofectamine with 2, 5 and 8 μg of pDNA are shown in Figure 19. Transfection in Lipofectamine positive controls also increased with increasing amounts of pDNA.

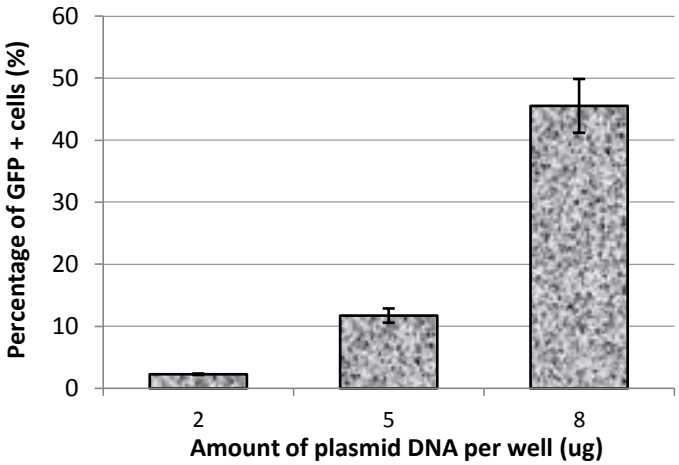

Figure 19 Positive control samples from DNA trial on HEK 293T cells using Lipofectamine reagent incubated with 2, 5 and 8 μg of pEGFP-C3 for 4 hours in PBS at pH 7.7. Conditions were repeated in triplicate (n= 3).

In order to determine whether increasing amounts of DNA also mediated increasing cell death, cells were stained with propidium iodide and data is presented in Figure 20.

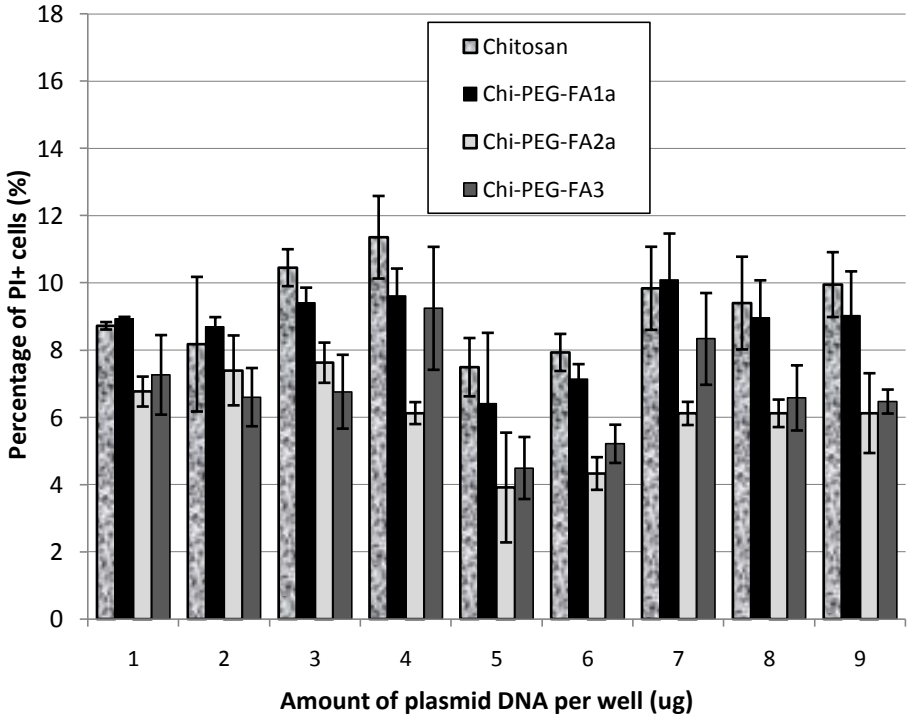

Figure 20 Cell death as measured by PI+ % for HEK293T DNA trial. pEGFP-C3 quantities ranging from 1 to 9 μg per well are evaluated. Transfection was assessed in un-modified chitosan and modified chitosan nanoparticles produced at a charge ratio of 7. Transfection media was PBS at pH 7.7 and incubation time was 4 hours, with 3μL PI per sample. Error bars represent standard deviation of the mean, based on triplicate samples (n =3).

Cell death did not increase much with increasing amounts of DNA. In general, cell death was highest in chitosan and chitosan-PEG-folate1a samples while chitosan-PEG-folate2a displayed the lowest percentage of cell death for each condition.

Optimized conditions

Using the results of the media and DNA trials, transfection experiments were performed for different chitosan-PEG-folate samples. Transfections were conducted with 7μg of pDNA per well of the 24-well plate for 4 hours in PBS at pH 7.7, while flow cytometry analysis was carried out 48 hours post-transfection. Some evidence has suggested that increasing the amount of plasmid DNA may also increase cell death and therefore a moderate value was chosen. Both un-modified and modified chitosan particles were prepared with chitosan/alginate charge ratios varying between 3 and 15, holding the N/P ratio constant at 0.26. The best transfection was achieved using chitosan-PEG-folate2a. Representative plots from these experiments are displayed in Figure 21.

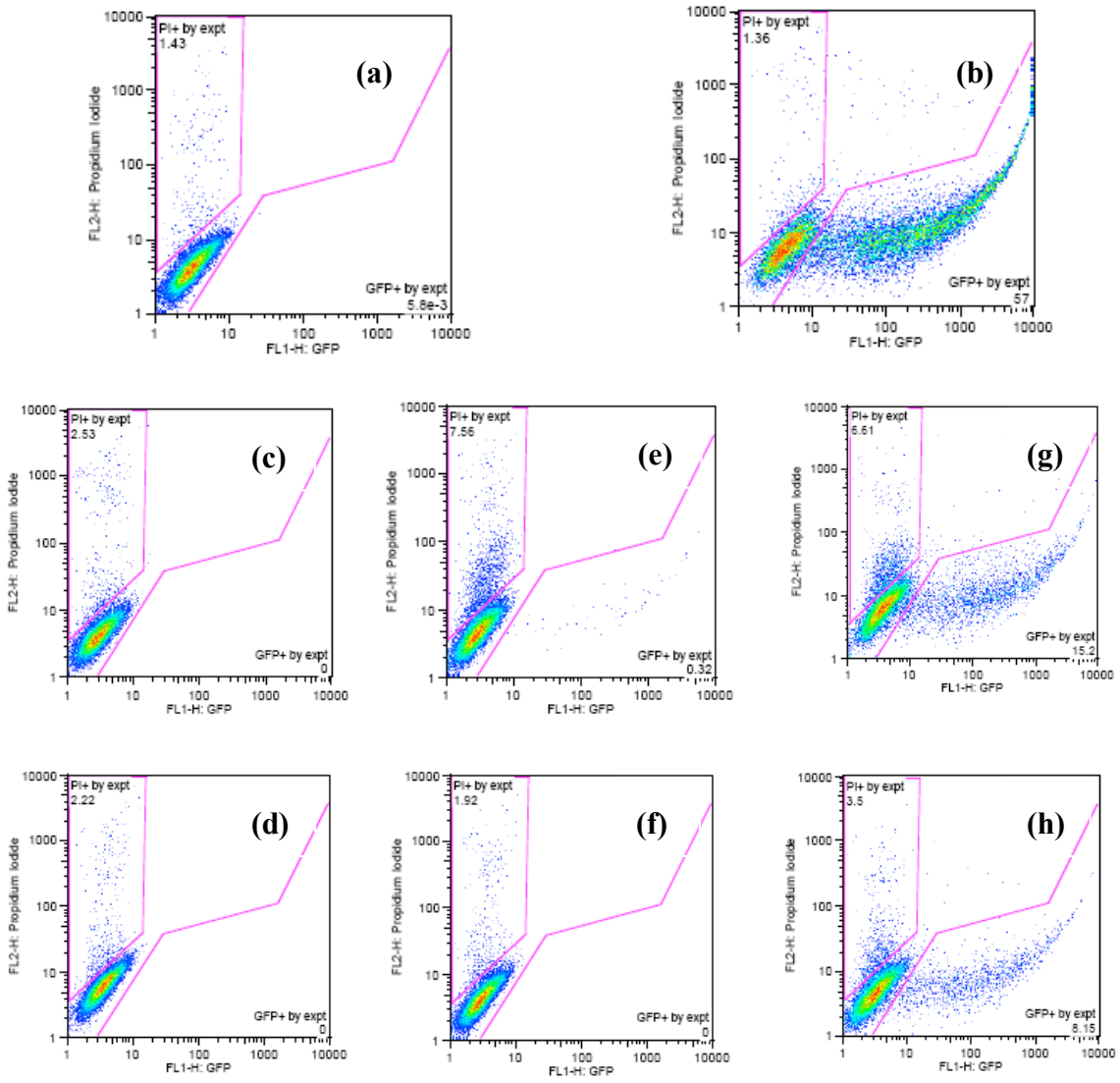

Figure 21 Flow cytometry analysis of HEK 293T transfection in PBS 7.7 incubated for 4 hours with 7 µg of pEGFP-C3 and nanoparticles, analyzed 48 hours post-transfection. Nanoparticles shown were formulated with charge ratios of 3 and 15. (a) negative control (b) Lipofectamine positive control (c)Lipofectamine alone (d) DNA alone (e) Chitosan -3 (f) Chi-PEG-FA-3 (g) Chitosan-15 (h) Chi-PEG-FA-15

The data from all wells was collected and analyzed on Flowjo, and a graphical summary is shown in Figure 22. Each sample condition was tested in triplicate.

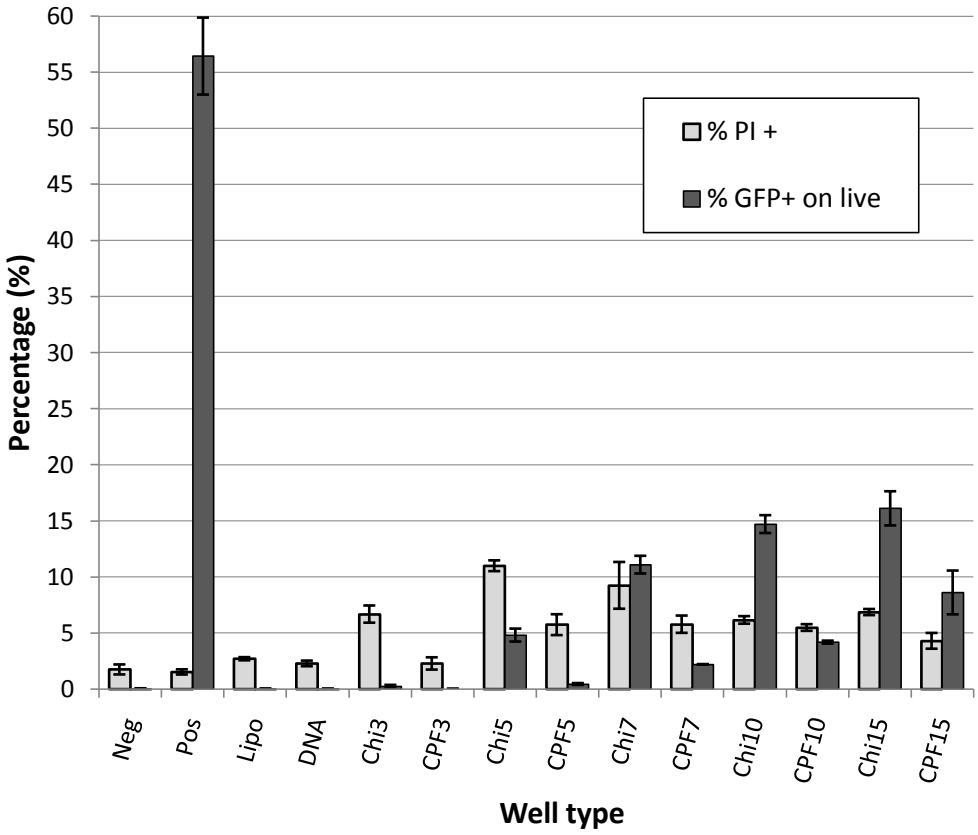

Figure 22 Summary of HEK 293T transfection at optimized conditions with 4 hour incubation of 7μg pEGFP-C3 pDNA using an N/P ratio of 0.26. Chitosan and chi-PEG-FA2a samples were formulated at chitosan/alginate charge ratios between 3 to 15. Data was collected in triplicate (n= 3). Percentage of GFP+ cells were calculated on the live population. Error bars represent standard deviation on the mean.

As the chitosan/alginate charge ratios increased, so did the transfection efficiency. The highest transfection efficiency was obtained with chitosan-PEG-folate2a at a charge ratio of 15, which yielded 8.6 ± 1.87 % GFP+ of live cells, as compared to chitosan-15 at 16.1 ± 1.52 % of live cells and lipofectamine controls at 55.1 ± 3.7 % of live cells. A clearer representation of chitosan and modified chitosan conjugates with increasing charge ratios is depicted in Figure 23 for GFP+ on live cell percentages while PI+ cell death is shown in Figure 24.

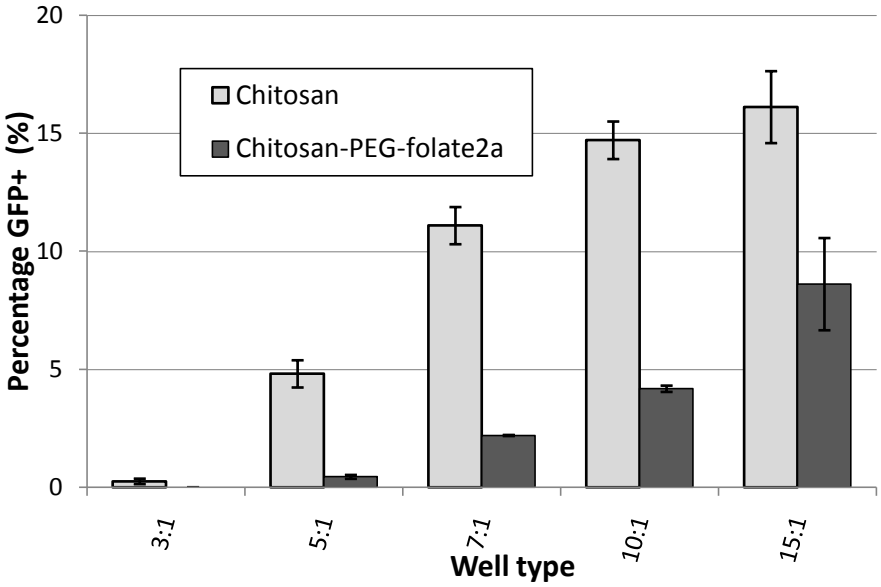

Figure 23 GFP+ cells from optimized transfection with chitosan and chi-PEG-FA2a representing transfection after 4 hour incubation with 7µg pEGFP-C3 pDNA using an N/P ratio of 0.26. Chitosan and chi-PEG-FA2a samples were formulated at indicated charge ratios. Data was collected in triplicate (n= 3). Percentage of GFP+ cells were calculated on the live population. Error bars represent standard deviation on the mean.

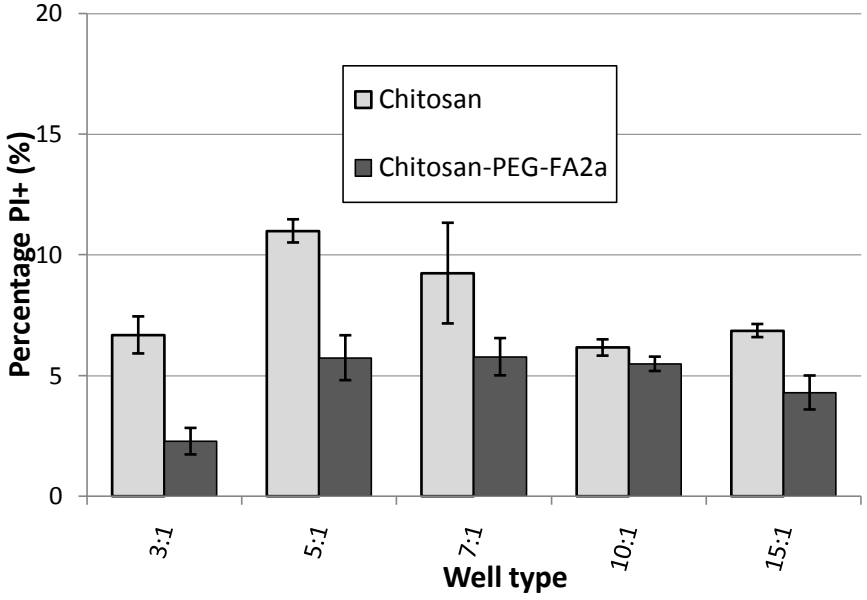

Figure 24 PI+ cells from optimized transfection with chitosan and chi-PEG-FA2a representing cell death after 4 hour incubation with 7µg pEGFP-C3 pDNA using an N/P ratio of 0.26. Chitosan and chi-PEG-FA2a samples were formulated at indicated charge ratios. Data was collected in triplicate (n= 3). Percentage of GFP+ cells were calculated on the live population. Error bars represent standard deviation on the mean.

Transfection of HEK 293T cells increased with increasing chitosan/alginate charge ratio for both un-modified and modified chitosan, reaching a maximum at 15.00 ± 1.45 % GFP+ for un-modified chitosan and 8.24 ±1.87 % GFP+ for chitosan-PEG-folate2a. At every charge ratio, un-modified complexes exhibited higher transfection efficiencies. Conversely, un-modified chitosan mediated higher cell death at each charge ratio, reaching a maximum at 10.98 ± 0.48 % PI+ for unmodified chitosan/alginate at a ratio of 5:1. Cell death also seemed to decrease with increasing charge ratio, with the exception of the chitosan/alginate ratio of 3:1, for which both cell death and transfection were at a minimum.

6.3.2.2 Fluorescence microscopy of HEK 293T cell transfection

Fluorescent images of the HEK 293T cells transfected with 7.0 μg of pEGFP-C3 in PBS at pH 7.7 using chitosan/alginate and chi-PEG-FA/alginate nanoparticles, are shown at 20x and 10x magnification in Figure 25 and Figure 26, respectively. Nanoparticles were formulated at chitosan/ alginate charge ratios of 10 and 15, as indicated, and the N/P ratio was 7.

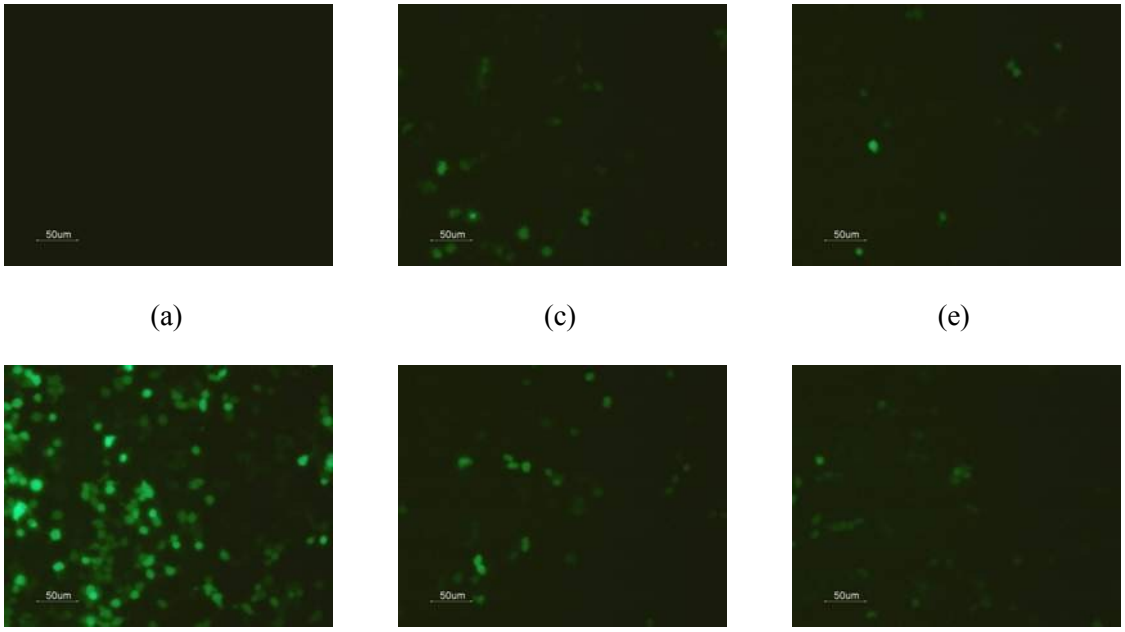

Figure 25 Fluorescence images of HEK 293T cells at 20X magnification.
Images represent 4 hour incubation of HEK 293T cells with 7μg of pEGFP and complexes. A) negative control B) positive Lipofectamine control C) Chitosan-10 D) Chitosan-15 E) Chi-PEG-FA-10 and F)Chi-PEG-FA-15.

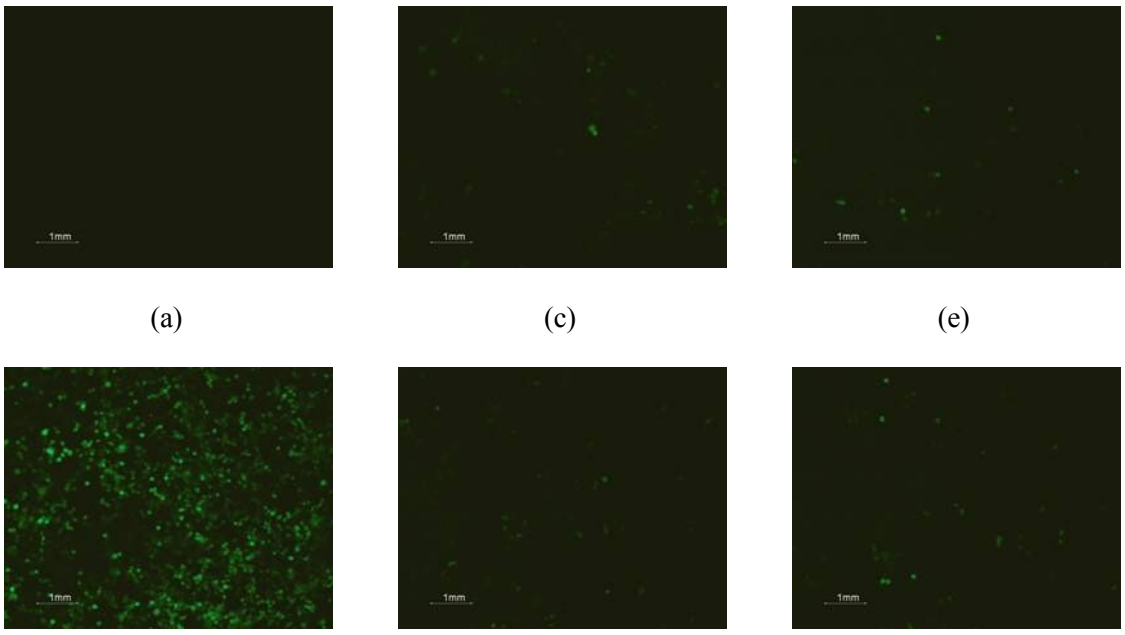

Figure 26 Fluorescence images of HEK 293T cells, 10X magnification.
Images represent 4 hour incubation with 7 μg of pEGFP and complexes. A) negative control B) positive Lipofectamine control C) Chitosan-10 D) Chitosan-15 E) Chi-PEG-FA-10 and F)Chi-PEG-FA-15.

6.3.2.3 Caov-3 cells

Using parameters optimized in HEK 293T cells, transfection trials were attempted in the Caov-3 cell line. Cells were incubated with nanoparticles, using 7 μg of pEGFP-C3 per well of the 24-well plate in PBS at pH 7.7 for a 4 hour transfection. Representative plots from these trials are shown in Figure 27.

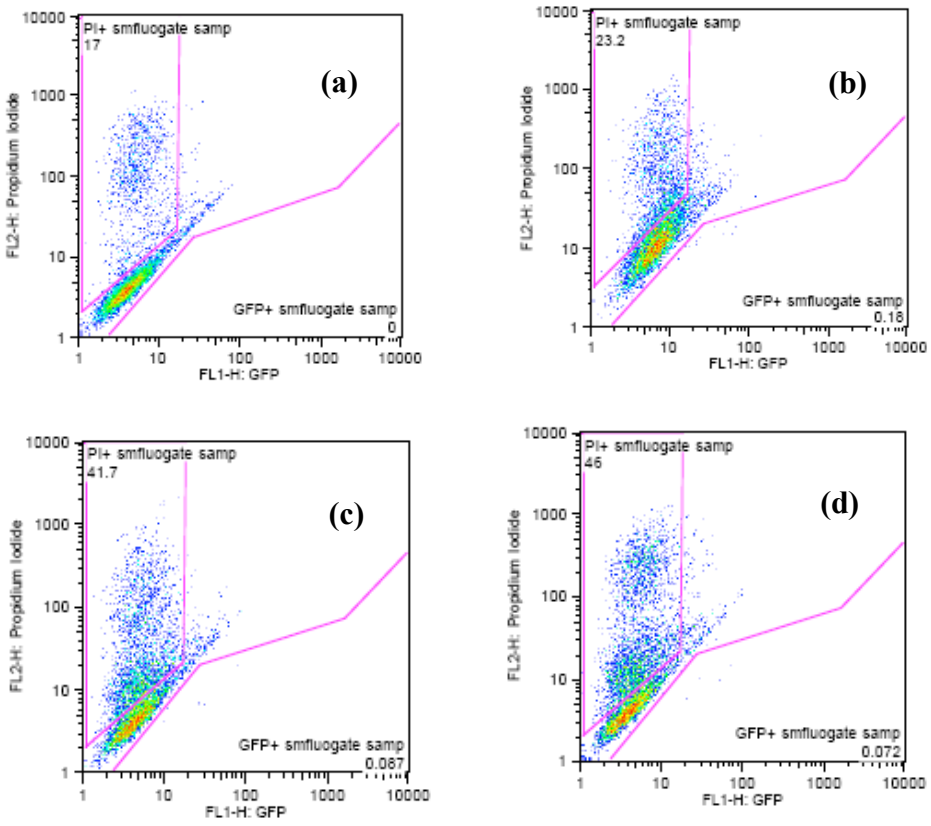

Figure 27 Flow cytometry analysis of Caov-3 cells post transfection with 7 µg of pEGFP and nanoparticles at varying chitosan/alginate charge ratios with 4 hour incubation. Transfection media used was PBS at pH 7.7 and data was analyzed by Flowjo software. (a) negative control (b) Lipofectamine positive control (c) Chitosan-10 (d) Chi-PEG-FA1a-10

GFP+ and PI+ cell data are summarized in Figure 28 and Figure 29, respectively.

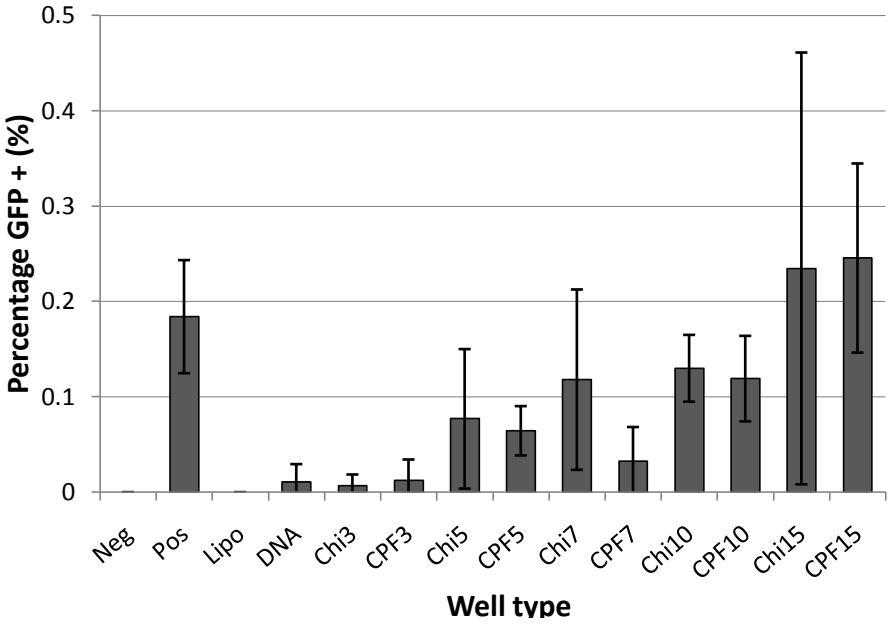

Figure 28 GFP+ percentages from transfection of Caov-3 cells in PBS pH 7.7 using 7 µg pEGFP-C3 with 4 hour incubation with chitosan and Chi-PEG-FA1a nanoparticles at various charge ratios. Data was collected in triplicate (n= 3). Percentage of GFP+ cells were calculated on the live population. Error bars represent standard deviation on the mean.

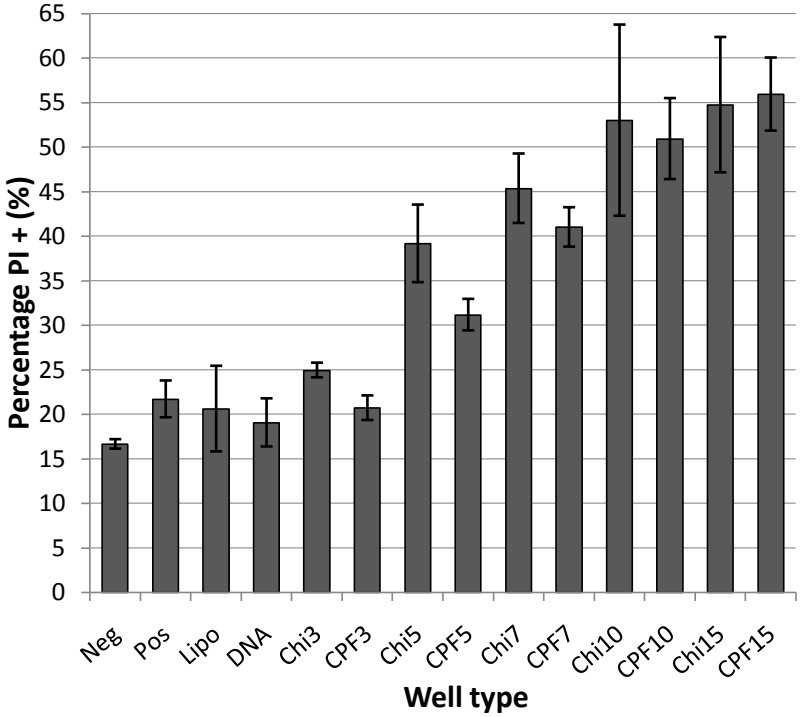

Figure 29 PI+ percentages from transfection of Caov-3 cells in PBS pH 7.7 using 7 µg pEGFP-C3 with 4 hour incubation with chitosan and Chi-PEG-FA1a nanoparticles at various charge ratios. Data was collected in triplicate (n= 3). Each well received 3µL PI. Error bars represent standard deviation on the mean.

Clearly, transfection in PBS at pH 7.7 was not successful, as even the Lipofectamine positive control mediated less than 0.2% GFP+ signal on live. Note that the vertical axis has a maximum of 0.5%. While samples with charge ratios of 15 achieved higher transfection in these cells as compared to Lipofectamine, these results cannot be appropriately compared at these low percentages and considering the high incidence of cell death. Increasing chitosan/ alginate charge ratios resulted in increased cell death as measured by the PI+ signal with a maximum of 55.9 ± 4.1 % PI+ cells using chitosan-PEG-folate1a-15. Cell death was lower or approximately equal to un-modified chitosan samples at the same charge ratios. Since transfection conditions were optimized for HEK 293T cells and not for Caov-3 cells, media screening was undertaken.

Media trials

The six media types used previously were assessed again for Caov-3 transfection: serum-free media, full media, and PBS solutions at pH 6.6, 7.0, 7.4 and 7.7. Results are shown in Figure 30. Note that the vertical axis extends only to 0.8%.

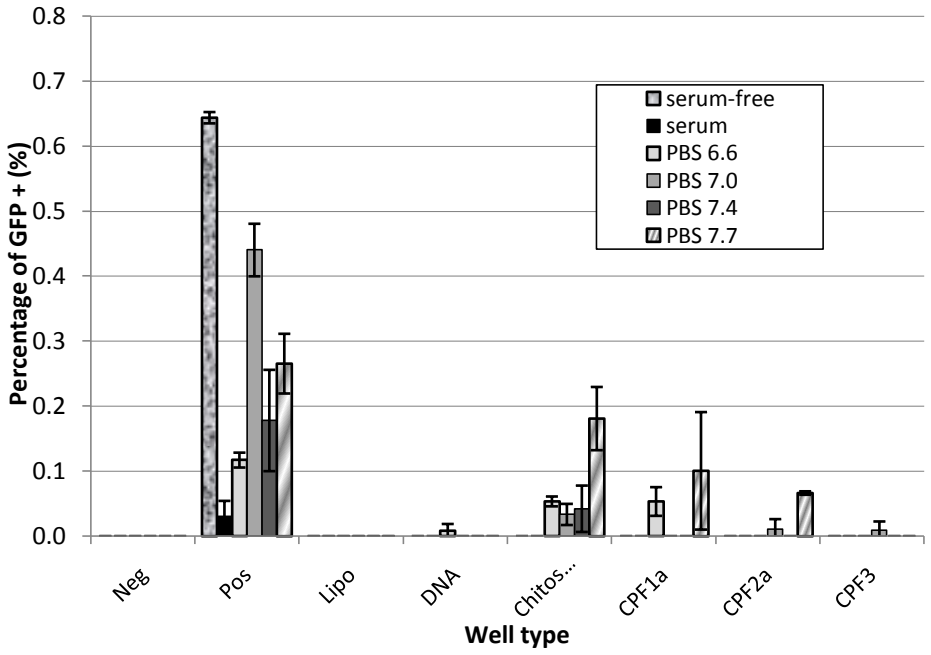

Figure 30 Summary of GFP+ population from media trial in Caov-3 cells.
Data is expressed as a percentage of GFP+ cells on live population 48 hours post-transfection for cells incubated with 7µg of pEGFP-C3 for 4 hours in six types of media with various chitosan/alginate nanoparticle. Error bars represent standard deviation of the mean. Each condition was replicated in duplicate (n= 2).

In general, there was little to no transfection in all media types for chitosan and chitosan-PEG-folate samples. There was minimal transfection in Lipofectamine positive controls, with a maximum of 0.64 % GFP+ on live in serum-free media. Un-modified chitosan and modified chitosan-PEG-folates 1a and 2a showed some GFP+ signal after transfection in PBS at pH of 7.7. Cell death as assessed by propidium iodide staining is displayed in Figure 31.

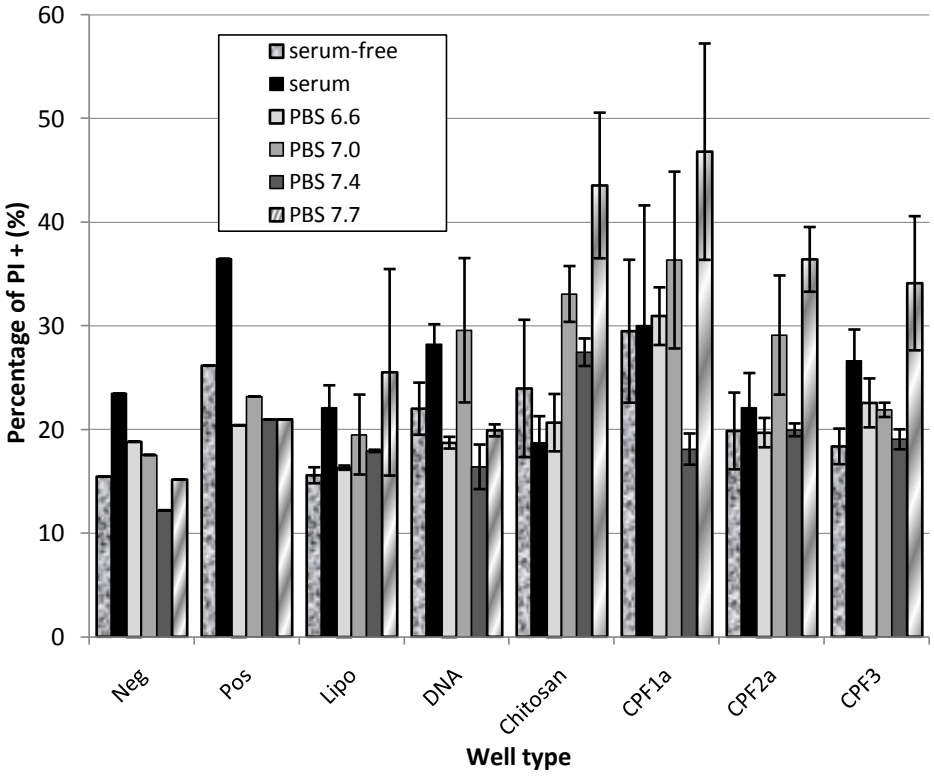

Figure 31 Summary of PI+ population from media trial in Caov-3 cells.
Data is expressed as a percentage of PI+ cells 48 hours post-transfection after incubation with 7μg of pEGFP-C3 for 4 hours in six types of media with various chitosan/alginate nanoparticle. Error bars represent standard deviation of the mean. Negative and positive controls have have n =1 and therefore no associated error, due to one sample being left unstained with PI. All other conditions were replicated in duplicate (n= 2).

Cell death was high in all conditions, with a minimum of 12.1% PI+ in negative control in PBS 7.4. Positive controls and chitosan samples displayed PI+ percentages between 15.6% and 46.8%.

6.3.2.4 MDA-MB-231 cells

Media trials were undertaken with MDA-MB-231 cells, under the same conditions as for Caov-3 cells. In every type of media, the GFP+ signal was nonexistent, even in Lipofectamine-treated wells therefore a graphical summary is not presented here. Representative plots, as analyzed on Flowjo, illustrating the gates used, are depicted in Figure 32. Lipofectamine-treated cells incubated with serum-free media showed evidence of autofluorescence, which should not be mistaken for successful transfection. Cell death reached a maximum of 8.3 ± 0.6 % PI+ for chitosan samples in PBS 7.4 (data not shown).

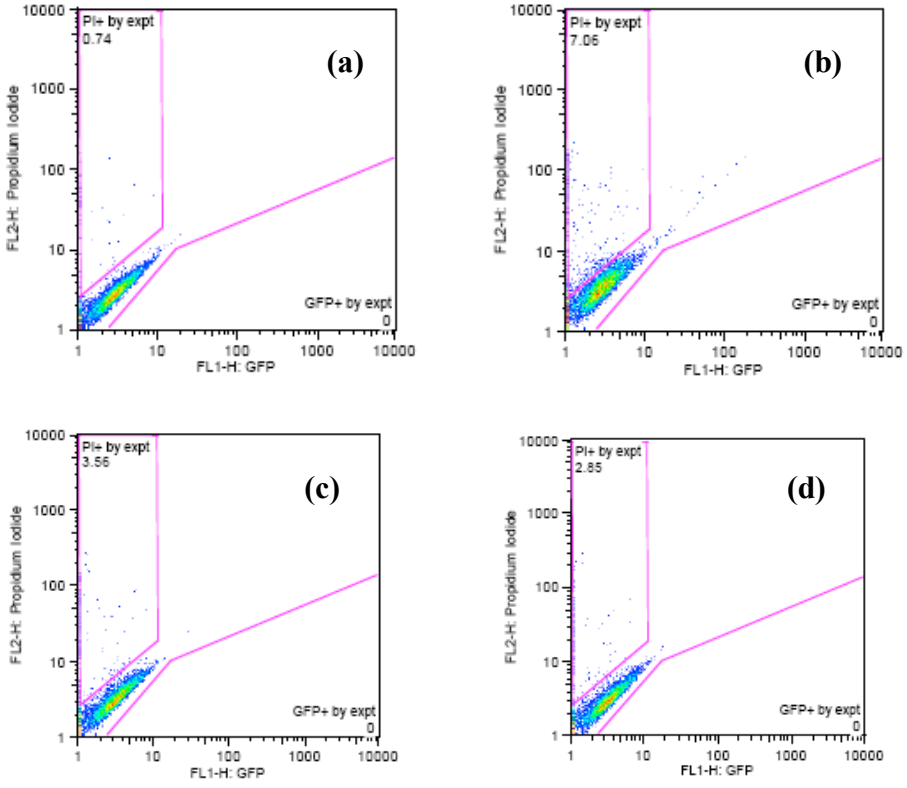

Figure 32 Selected plots for transfection of MDA-MB-231 cells using 7 µg pEGFP-C3 in serum-free media. (a) negative control (b) Lipofectamine positive control (c) chitosan-10 (d) chitosan-PEG-FA1a-10

CHAPTER 7
DISCUSSION

7.1 SYNTHETIC METHODS

Although the published protocol of Chan *et al.* was followed as closely as possible, there were several reasons for which this synthetic protocol was abandoned as a method of production of chitosan-PEG-folate. In brief, concerns were raised around the removal of DMSO during the synthesis, potential side reactions that could occur using this method, and insufficient purification of intermediate products. Low product yield and nanoparticles that could not be formed with the desired size and charge characteristics led to our search for another means of production.

We were fortunate in being able to consult with Xingping Qiu (University of Montreal) about a revised protocol for the production of chitosan-PEG-folate. Modified from a published protocol (Cho et al., 2005) for the synthesis of folate-PEG-PEI, this alternative synthetic scheme was able to address some of our main concerns with the previous method.

7.1.2 Chi-PEG-FA (Chan)

A major issue encountered during synthesis using the Chan method was the removal of DMSO after the folate activation step. DMSO has a boiling point of 189 ^{o}C and under vacuum, should be removed at lower temperatures. Unfortunately, in this setup, it was not possible to completely remove DMSO without reaching very high temperatures (> 180 ^{o}C as measured outside of the flask), thus possibly degrading our samples. These high temperatures also caused the reactants to caramelize, turning a very dark brown/black in color. Attempts to improve DMSO removal, including pre-drying of DMSO and the use of a mixture of solvents to lower the temperature at which it would evaporate, were unsuccessful. Removal of DMSO by dialysis was also suggested but not pursued due to the prohibitively large volumes used.

NMR analysis of chitosan-PEG-folate (Chan) did display the relevant peaks of chitosan, PEG and folate, however additional peaks that were not expected also appeared on the spectra. These peaks potentially represent breakdown products of the synthesis that were

not removed by dialysis as well as unwanted side products due to the chemical scheme followed.

The folate molecule contains two potentially reactive carboxyl groups (α and γ), which can be carbodiimide activated. The first folate-activation step of the Chan protocol may therefore result in 1) activation at the distal γ carboxyl group, our desired results; 2) reaction at the α carboxyl group; or 3) an empty reaction, with no activation. As the α carboxyl group is more sterically hindered due to its mid-chain position, reaction conditions may be chosen to limit reaction at this site. Once activated and thiolated, however, the very active thiol molecules may come together to form disulfide bridges and can also react with carboxyl groups, causing potential linking reactions to other folate molecules, rather than producing chitosan-PEG-maleimide. If these undesirable products are indeed formed, an additional problem is encountered in that there is no purification step at this point. Dialysis of the reactants would not be feasible due to the relatively small size of the folate molecule. The lack of purification step at this point in the procedure may have contributed to some of the unidentified peaks in the NMR spectra.

Not surprisingly, when characterizing nanoparticles formed from the chitosan-PEG-folate produced via this reaction and alginate, a positive surface charge was very difficult to obtain, even at higher chitosan/alginate charge ratios. Those particles that did display positive surface charges were larger than desired. Additional syntheses performed with chitosan with varying average chain molecular masses did not improve the situation.

Another contributing factor in the decision to abandon this synthetic procedure was the low yield of the reaction. While the researchers who initially published this protocol may have obtained higher yields, each synthesis performed in this study yielded only between 20 to 50 mg of chitosan-PEG-folate, much of which was lost in characterization. The material proved to be prone to static, as chitosan is normally, but in the low amounts and with high volumes of solution to be lyophilized, the resulting product was easily lost when transferred or weighed out. Attempts were made to reduce the volume of solution with vacuum evaporation prior to lyophilization to decrease the "fluffiness" of the product and while they helped somewhat, the samples produced did not last long enough for full characterization, much less transfection. Additional syntheses were carried out,

and the reaction was scaled up to three times the stated amounts but while the overall mass of product was increased, the reaction still suffered from high temperatures in the DMSO removal step. As the particles produced from the product still did not meet our criteria of small sizes and positive surface charge, this synthetic procedure was abandoned in favour of the one presented below.

7.1.2 Chi-PEG-FA (Qiu)

In order to address the issue of potential side reactions raised in the first reaction scheme, when developing the new protocol, folate was activated by NHS/DCC chemistry in a 1.5 folate/NHS ratio. This served to limit the amount of NHS available for reaction and therefore drive the reaction preferentially towards the less sterically hindered carboxyl group. After activation of the folate-NHS ester, we assumed that folate was approximately 66% activated and calculated a 3-fold lesser amount of NH_2-PEG-COOH. Using a limited amount of PEG ensured that the reaction would proceed via the more sterically convenient route, at the distal end of the folate molecule. Further carbodiimide chemistry can target either the α carboxyl group on folate or the carboxyl at the end of PEG. Due to the bulky PEG chain and the fact that the α carboxyl group already exists in a mid-chain position on folate, reaction at this site even more sterically hindered and less likely to occur. Thus it was not necessary in this step to limit our reagent and a greater amount of NHS was used to maximise production. Protection of folate from reaction at the α carboxyl is therefore maximized using this scheme and there is less likelihood of unwanted side reactions. No reactive thiol group exists in this new protocol, thus eliminating the possibility of disulfide bond formation or further carboxyl group reactions.

Purification of folate-NHS was achieved by precipitation with a mixture of acetone and ether to remove un-reacted folate. Unlike in the previous reaction scheme, further purification of the folate-PEG-COOH intermediate product was achieved by dialysis, as the long PEG chain was conjugated directly to the relatively smaller folate molecule, and their relative size difference was enough to make this a viable option. This step also helped to facilitate the final purification, which was dialysis of chitosan-PEG-folate against deionized water to remove any un-reacted components. At this final step, the

desired product was more soluble in water, due to its conjugation to the long PEG chain, and was therefore more easily purified by dialysis.

As for the removal of DMSO, much smaller volumes of solvent were used in this synthetic procedure, thus allowing for its easy removal by dialysis. Higher yields of chitosan-PEG-folate were obtained using this new synthetic protocol, and the resulting particles formed using this product exhibited the small sizes and positive surface charges desired.

7.2 ANALYSIS OF SYNTHESIZED PRODUCT

7.2.1 Degrees of substitution of PEG and folate

The values for degrees of substitution of PEG and folate were calculated from NMR and UV spectrophotometric analysis, respectively. The degrees of substitution of PEG were found to be close to, or higher than, those intended in our reaction scheme. The amount of folate-PEG-COOH used in the conjugation reaction with chitosan was calculated based upon our intended degree of substitution, and several assumptions regarding the efficiency of this reaction were made. Since the measured degree of substitution closely matched or exceeded expectations, our assumptions appear to have been close and we may have underestimated the success of the reaction. The reasons for which the reactions for chitosan-PEG-folate2b and -3 were more successful are not entirely clear.

Results from UV spectrophotometry give us an indication of the degree of folate substitution achieved. This analysis was repeated twice to confirm our readings. As the degree of folate substitution did not match the degrees of PEG substitution, our assumption that each molecule of PEG carried one molecule of folate after reaction and purification of folate-PEG-COOH was clearly incorrect. These results indicate that conjugation of folate to NH_2-PEG-COOH did not proceed with 100% efficiency.

7.2.2 Molecular mass

The average molecular weight of chitosan and chitosan-PEG-folate samples was assessed by gel permeation chromatography. The secondary analysis of light scattering measurements alone was performed due to the very high polydispersity of the samples, as

determined via both refractive index and light scattering. Although this form of analysis reduces the apparent polydispersity, it is known that light scattering measurements tend to disregard smaller weights. It is clear that our samples include a broad range of average chain molecular weights and that they became more polydisperse after synthesis. This increase in the number of small chains may be due to product breakdown during our synthetic procedure.

7.3 NANOPARTICLE FORMATION AND CHARACTERIZATION

7.3.1 Particle size and surface charge

As described previously, particle sizes were assessed using DLS software. Results are given as z-average size, which is the most stable measurement produced through DLS, but depends on samples being monomodal, approximately spherical and relatively monodisperse. For samples that do not meet these criteria, results should only be compared with other measurements made using DLS, and not, for example, with sizes analyzed by microscopy methods. The values presented include mean value for size as well as a value for polydispersity. In general, it is recommended by the instrument literature that samples having a polydispersity index of 0.1 or less can be compared to other means of size measurement. In the case of all nanoparticles produced in this study, polydispersity was above 0.1, therefore further indicating that these size measurements cannot be reliably compared to those obtained by other methods.

Both un-modified chitosan and chitosan-PEG-FA were able to form complexes with alginate, resulting in particles with sizes in our desired range, around 250 nm and below. It is clear from Figure 10 that particle size increases dramatically at certain charge ratios (data for nanoparticles formed at 1:1 charge ratio not shown, as the measured size for un-modified chitosan was in excess of 20 μm and could not be feasibly represented), and that the particular charge ratio at which this occurs is not the same for every chitosan formulation.

From Figure 11, the apparent surface charge of nanoparticles was positive for all formulations having an excess of chitosan. Nanoparticles formed by a 1:1 charge ratio of

theoretical positive amino groups to theoretical negative carboxyl groups were negatively charged. It should be noted that modified chi-PEG-FA nanoparticles exhibited more highly positive charges than those produced with un-modified chitosan at the same charge ratios. This trend was encouraging, as we would expect that more positively charged nanoparticles can better complex and retain pDNA

7.3.2 Scanning electron microscopy

Attempts were made to visualize the nanoparticles by FEG SEM. Unfortunately, clear images showing discrete particle size and shapes were difficult to obtain, due to changes in particle structure that resulted from sample drying, which is necessary for SEM analysis. While it was expected that the effective size of dried particles would be smaller than those analyzed by DLS (due to swelling and the hydrodynamic layer surrounding particles in solution), the effect of drying also caused particles to not only aggregate, but also to merge into one another. Many of the nanoparticle samples imaged could not be differentiated into discrete particles of regular size, as they had dried together to form films or masses. The images presented in Figure 12 and Figure 13 most clearly show that particles that were once separate entities seem to have merged together, a phenomenon that is more apparent for chitosan-15 samples, where the borders between particles as they connect can be seen. While the size of apparent particles formed by chitosan-PEG-folate3-15 appeared to be in the expected size range, those formed by un-modified chitosan were much larger than predicted by DLS. Though it was previously noted that sizes as measured by DLS analysis cannot be reliably compared to other methods, we did not expect such a large difference. This may indicate that chitosan-15 nanoparticles had already merged due to drying in the image shown and were not in fact discrete entities. Different drying strategies were attempted, with direct drying on silicium slides, drying on PLL-coated slides, and freeze-drying of samples, but the best images were those obtained on PLL-coated slides. Even under these conditions, it was difficult to find areas where particles had not merged. Obtaining images of samples in their swollen state, as they exist in solution, might be possible using cryogenic transmission electron microscopy (cryo-TEM), which allows for visualization of nanomaterials in fluids (Won, 2004).

7.4 IN VITRO ANALYSIS

7.4.1 Fluorescence microscopy

To qualitatively compare the transfection efficiency of complexes, each experiment was screened via fluorescence microscopy before flow cytometry analysis. In general, fluorescence images were not taken of each experiment, in order to decrease the effect of photobleaching on quantitative measurements. Some transfection experiments were performed for the express purpose of obtaining fluorescence images. While the images presented are not quantitative, it is quite clear that transfection using the liposomal vector Lipofectamine achieved better transfection based on the number of cells that fluoresce and the distribution of cells transfected. The difference in transfection efficiency by un-modified chitosan and chitosan-PEG-FA is harder to discern from these images, which is why for the most part, all analyses were performed quantitatively by flow cytometry.

7.4.2 Cell lines

Three cell lines were chosen in order to assess the transfection potential of synthesized chitosan-PEG-folate. As time became an issue in experimental design, transfection was first optimized in HEK 293T cells, a cell line that has been extensively studied in gene delivery literature and has been shown to be transfected by chitosan and chitosan-based vectors. Since approximately 90% of ovarian cancer cell lines are known to overexpress folate (Parker et al., 2005), Caov-3 cells were also used to evaluate whether the addition of the folate ligand did indeed improve transfection targeting. Folate receptors are also known to be expressed in some breast cancer cell lines and therefore MDA-MB-231 cells, as derived from breast adenocarcinoma tissue, were chosen for evaluation from the cancer cell lines available to us. In the initial design of this project, quantification of folate-receptor expression on cell lines for which we could achieve efficient transfection was a goal. However, as both cancer cell lines were not effectively transfected in preliminary trials, this analysis was not performed. Although both KB and HeLa cells are known to express the α isoform of the folate receptor at far higher levels than either Caov-3 or MDA-MB-231 cells, these cell lines are designated as biosafety level 2, due to contamination by papovavirus. Although both KB and HeLa cells are known to express the α isoform of the folate receptor at far higher levels than either Caov-3 or MDA-MB-

231 cells, these cell lines are designated as biosafety level 2, due to contamination by papovavirus. In addition, HeLa cells are rather notorious for cross contamination of other cell lines in culture due to their aggressive nature (Masters, 2002a; Masters, 2002b; Macleod et al., 1999). Indeed KB cells may themselves have been contaminated by HeLa cells (Lacroix, 2008). It was hoped that the cancer cells we had available for use would be amenable to transfection by our modified vector.

7.4.3 Transfection procedures

Initial transfection studies were performed in PBS at a pH 6.6, based on previously work in our laboratory on chitosan-based transfection vectors. After initial flow cytometry analysis indicated low transfection efficiencies, media trials were carried out in PBS solutions of varying pH as well as in full media and serum-free media. It was clear that in this particular system, transfection was optimized at pH 7.7, which was used for subsequent analyses. Although cell death for some chitosan-PEG-folate samples was also highest when incubated with PBS at pH 7.7, the maximum cell death in these samples was still under 10% and was potentially affected by manipulation of cells prior to analysis. For all experiments, transfection time was 4 hours. This decision was made based on previous work in our lab. After several trials, it became apparent that HEK 293T cells maintained in PBS for 4 hours began to lift off and so longer transfection times were avoided in order to minimize cell loss. Transfection efficiency was analyzed 48 hours post–transfection for all trials. At this time point, cells became confluent and longer incubation times were therefore not used.

Both modified and bare chitosan were analyzed in order to assess whether chitosan-PEG-folate mediated higher levels of transfection as compared to the starting material. Positive controls consisted of cells transfected with the liposomal vector Lipofectamine with comparable amounts of pDNA, while negative controls contained no vector (liposomal or chitosan-based) or DNA. Experiments showed that the transfection procedure seemed to cause a shift in the live cell population, as seen on flow cytometry plots of forward scatter vs. side scatter and therefore additional control wells were included, with only liposomal vector and only DNA. Due to this shift in the live cell population, GFP+ and PI+ gates

were for the most part applied to the entire data set, but were shifted manually for PI-control wells.

7.4.4 HEK 293T cell transfection

Transfection was optimized in HEK 293T cells, using PBS at pH 7.7 as the transfection media and 7 μg of pDNA per well. DNA trials showed that increasing the amount of pDNA per well increased the efficiency of transfection, without much difference in cell death. The highest amount of DNA tested (9 μg) was not used for subsequent trials, as work performed previously by our group gave evidence that higher quantities of DNA mediated an increase in cell death and we therefore sought to avoid this possibility. Using optimized conditions, chitosan-PEG-folate1a, -2a, and -3 were assessed for transfection efficiency at charge ratios ranging from 3 to 15. The best results were found with chitosan-PEG-folate2a samples at a chitosan to alginate ratio of 15, with 8.6 ± 1.87 % GFP+ of live cells, as compared to chitosan-15 at 16.1 ± 1.52 % of live cells and lipofectamine control at 55.1 ±3.7 % of live cells. Transfection efficiency increased with increasing charge ratio of both forms of chitosan, which may be due to the higher surface charges associated with greater amounts of relative chitosan as charge ratio increases. However, transfection achieved by chitosan-PEG-folate samples was consistently less than that achieved by chitosan samples at the same charge ratios. The same trend was also observed in experiments on chitosan-PEG-folate1a and -3. This effect was not expected, as chitosan-PEG-folate samples displayed more highly positive zeta potentials and this would indicate a greater binding capacity of DNA. Since uptake of nanoparticles by HEK 293T cells is expected to occur through non-specific endocytosis, it could be that the addition of folate and PEG to modified chitosan interferes with the interaction of the particle with the cell membrane, potentially due to the shielding capacity of PEG. As HEK 293T cells are not particularly known for overexpressing the folate receptor, our transfection strategy would not mediate targeted, and thus increased, affinity for the cell membrane. It is encouraging to note, however, that modified chitosan-PEG-folate/alginate nanoparticles did not increase cell death, with PI+ percentages equal or lesser than those obtained by un-modified chitosan samples at every charge ratio.

7.4.5 Caov-3 and MDA-MD-231 cell transfection

Transfection of Caov-3 cells using the same conditions as optimized for HEK 293T cells was not very successful. Changing the transfection media did little to improve transfection regardless of the vector type, with very minimal transfection observed even for Lipofectamine controls. Although Caov-3 cells are known to overexpress the folate receptor, no published literature has shown transfection in this cell type, possibly due to this issue of low transfection efficiency. Similarly, MDA-MB-231 cells were also transfected in a variety of different media and showed no evidence of GFP+ cells in any condition, with Lipofectamine controls only displaying autofluorescence. Once again, this cell line has not been reported in transfection literature. Given the scope of this project, further optimization of these cell lines was not possible and our hypothesis, that chitosan-PEG-folate/alginate nanoparticles would improve transfection potential in cancerous cell lines expressing the folate receptor, could not be tested. While it was our aim to assess transfection in cells overexpressing the folate-receptor, it is clear that this cannot be assessed effectively with these cell types. While improvements to transfection efficiency in the Caov-3 cell line may be possible, high rates of cell death and a slow growth rate may render this a difficult task. It would therefore be more valuable for future work with synthesized chitosan-PEG-folate to use those cells that are both known to overexpress the folate receptor in high quantities as well as have shown good transfection potential *in vitro*. These cell types would include both HeLa and KB cells, which are again, at a biosafety level of 2 and potentially prone to cross contamination of other cell stocks.

CHAPTER 8
CONCLUSIONS AND FUTURE WORK

Following two separate synthetic strategies, samples of chitosan-PEG-folate with differing degrees of PEG and folate substitution were produced. NMR results confirmed conjugation of PEG and showed that assumptions made regarding the efficiency of the PEG conjugation reaction were sound. UV spectrophotometry results verified the presence of folate in each sample and implied that folate and PEG were not associated in a 1:1 ratio as assumed. GPC results for average chain molecular mass indicated that the chitosan-PEG-folate samples produced displayed a high polydispersity, which may change the formation of particles.

Chitosan-PEG-folate was able to associate with the secondary polymer alginate and form particles in the nano-scale size range, depending on the charge ratio used. Surface charges of modified chitosan particles were more highly positive than those formed with un-modified chitosan, which is promising for complexation with the negatively charged phosphates of DNA.

Field emission gun scanning electron microscopy was used to visualize nanoparticles when dried, however, drying seemed to cause particle aggregation and reorganization. Further work can therefore be undertaken to maintain the stability of nanoparticles with drying, potentially with the use of a sucrose gradient. Additional imaging methods that maintain the integrity of the particles, such as cryo-TEM imaging, should also be explored.

While transfection in HEK 293T cells was achieved with chitosan-PEG-folate/alginate particles, efficiencies did not improve upon results obtained with un-modified chitosan/alginate particles and did not match those of Lipofectamine positive controls. As our hypothesis presumed that modified chitosan-PEG-folate/ alginate nanoparticles would perform better in cells overexpressing the folate receptor, initial screening was carried out in two cancerous cell lines, Caov-3 and MDA-MB-231. Unfortunately, preliminary transfection trials in these cell lines were not successful, regardless of the

parameters tested. While Caov-3 cells may be more amenable to transfection, MDA-MB-231 cells displayed no transfection, even with positive controls.

Within the scope of this project, further optimization of transfection in Caov-3 cells as well as attempts to evaluate different cancer cell lines was not possible. Further work in Caov-3 cell transfection could be attempted, as it was possible to obtain some GFP+ cells, although in very small percentages. It would perhaps be more valuable to examine transfection in other cancer cell lines, particularly KB and HeLa cells, which have shown good transfection potential with folate targeting strategies. While it was not within the reach of this project, folate receptor binding capacity of synthesized chitosan-PEG-folate may be assessed by surface plasmon resonance measurements.

The initial objectives of this project were successfully achieved, as synthesized chitosan-PEG-folate was produced and found to form nanoparticles with alginate with a positive surface charge. The final objective, which was to evaluate these nanoparticles in HEK 293T cells as well as in cancer cells, was also met, but with results that do not yet confirm our project hypothesis. While the synthesized chitosan-PEG-folate particles should in theory offer improved transfection as compared to bare chitosan in cell lines that over-express the folate receptor, this could not be effectively evaluated, since the cell lines chosen were not amenable to transfection.

The use of chitosan-PEG-folate as a targeted DNA delivery vehicle remains one of some promise, whose potential could not be fully evaluated within the scope of this project.

REFERENCES CITED

1. Anderson, J. & Akkina, R. (2005). CXCR4 and CCR5 shRNA transgenic CD34+cell derived macrophages are functionally normal and resist HIV-1 infection. *Retrovirology, 2*.

2. Antony, A. C. (1996). Folate receptors. *Annu.Rev.Nutr., 16,* 501-521.

3. Bae, Y., Nishiyama, N., Fukushima, S., Koyama, H., Yasuhiro, M., & Kataoka, K. (2005). Preparation and biological characterization of polymeric micelle drug carriers with intracellular pH-triggered drug release property: Tumor permeability, controlled subcellular drug distribution, and enhanced in vivo antitumor efficacy. *Bioconjugate Chemistry, 16,* 122-130.

4. Beduneau, A., Saulnier, P., & Benoit, J. P. (2007). Active targeting of brain tumors using nanocarriers. *Biomaterials, 28,* 4947-4967.

5. Borchard, G. (2001). Chitosans for gene delivery. *Advanced Drug Delivery Reviews, 52,* 145-150.

6. Boussif, O., Lezoualc'h, F., Zanta, M. A., Mergny, M. D., Scherman, D., Demeneix, B. et al. (1995). A versatile vector for gene and oligonucleotide transfer into cells in culture and in vivo: polyethylenimine. *Proc.Natl.Acad.Sci.U.S.A, 92,* 7297-7301.

7. Brigger, I., Dubernet, C., & Couvreur, P. (2002). Nanoparticles in cancer therapy and diagnosis. *Advanced Drug Delivery Reviews, 54,* 631-651.

8. Cambridge Isotope Laboratories (2009). NMR Solvents. Cambridge Isotopes Laboratories [On-line]. Available: http://www.isotope.com/cil/products/listproducttypes.cfm?prodtypeid=41

9. CarrenoGomez, B. & Duncan, R. (1997). Evaluation of the biological properties of soluble chitosan and chitosan microspheres. *International Journal of Pharmaceutics, 148,* 231-240.

10. Chan, P., Kurisawa, M., Chung, J. E., & Yang, Y. Y. (2006). Synthesis and characterization of chitosan-g-poly(ethylene glycol)-folate as a non-viral carrier for tumor-targeted gene delivery. *Biomaterials*.

11. Chandy, T. & Sharma, C. P. (1990). Chitosan - As A Biomaterial. *Biomaterials Artificial Cells and Artificial Organs, 18,* 1-24.

12. Cho, K. C., Jeong, J. H., Chung, H. J., Joe, C. O., Kim, S. W., & Park, T. G. (2005). Folate receptor-mediated intracellular delivery of recombinant caspase-3 for inducing apoptosis. *Journal of Controlled Release, 108,* 121-131.

13. Chrai, S. S., Murari, R., & Ahmad, I. (2001). Liposomes (a review) - Part one: Manufacturing issues. *Biopharm-the Applied Technologies of Biopharmaceutical Development, 14,* 10-+.

14. Coney, L. R., Mezzanzanica, D., Sanborn, D., Casalini, P., Colnaghi, M. I., & Zurawski, V. R. (1994). Chimeric Murine Human-Antibodies Directed Against Folate Binding-Receptor Are Efficient Mediators of Ovarian-Carcinoma Cell-Killing. *Cancer Research, 54,* 2448-2455.

15. Corsi, K., Chellat, F., Yahia, L., & Fernandes, J. C. (2003). Mesenchymal stem cells, MG63 and HEK293 transfection using chitosan-DNA nanoparticles. *Biomaterials, 24,* 1255-1264.

16. Couzin, J. & Kaiser, J. (2006). As Gelsinger Case Ends, Gene Therapy Suffers Another Blow. Science [On-line].

17. Danielsen, S., Maurstad, G., & Stokke, B. T. (2005). DNA-polycation complexation and polyplex stability in the presence of competing polyanions. *Biopolymers, 77,* 86-97.

18. Dastan, T. & Turan, K. (2004). In vitro characterization and delivery of chitosan-DNA microparticles into mammalian cells. *Journal of Pharmacy and Pharmaceutical Sciences, 7,* 205-214.

19. De, S. & Robinson, D. (2003). Polymer relationships during preparation of chitosan-alginate and poly-l-lysine-alginate nanospheres. *J.Control Release, 89,* 101-112.

20. Douglas, K. L. (2006). *Non-viral gene therapy: Design and characterisation of novel non-viral vectors for improved cellular transfection.* McGill University.

21. Douglas, K. L. & Tabrizian, M. (2005). Effect of experimental parameters on the formation of alginate-chitosan nanoparticles and evaluation of their potential application as DNA carrier. *J.Biomater.Sci.Polym.Ed, 16,* 43-56.

22. Erbacher, P., Zou, S. M., Bettinger, T., Steffan, A. M., & Remy, J. S. (1998). Chitosan-based vector/DNA complexes for gene delivery: Biophysical characteristics and transfection ability. *Pharmaceutical Research, 15,* 1332-1339.

23. Gabizon, A., Horowitz, A. T., Goren, D., Tzemach, D., Mandelbaum-Shavit, F., Qazen, M. M. et al. (1999). Targeting folate receptor with folate linked to extremities of poly(ethylene glycol)-grafted liposomes: In vitro studies. *Bioconjugate Chemistry, 10,* 289-298.

24. Gabizon, A., Shmeeda, H., Horowitz, A. T., & Zalipsky, S. (2004). Tumor cell targeting of liposome-entrapped drugs with phospholipid-anchored folic acid-PEG conjugates. *Advanced Drug Delivery Reviews, 56,* 1177-1192.

25. Gao, X., Kim, K. S., & Liu, D. X. (2007). Nonviral gene delivery: What we know and what is next. *Aaps Journal, 9,* E92-E104.

26. Garnett, M. C. & Kallinteri, P. (2006). Nanomedicines and nanotoxicology: some physiological principles. *Occupational Medicine-Oxford, 56,* 307-311.

27. Gaumet, M., Vargas, A., Gurny, R., & Delie, F. (2008). Nanoparticles for drug delivery: The need for precision in reporting particle size parameters. *European Journal of Pharmaceutics and Biopharmaceutics, 69,* 1-9.

28. Godbey, W. T. & Mikos, A. G. (2001). Recent progress in gene delivery using non-viral transfer complexes. *J.Control Release, 72,* 115-125.

29. Hattori, Y. & Maitani, Y. (2005). Folate-linked lipid-based nanoparticle for targeted gene delivery. *Curr.Drug Deliv., 2,* 243-252.

30. Hilgenbrink, A. R. & Low, P. S. (2005). Folate receptor-mediated drug targeting: From therapeutics to diagnostics. *Journal of Pharmaceutical Sciences, 94,* 2135-2146.

31. Hirano, S., Tsuchida, H., & Nagao, N. (1989). N-Acetylation in Chitosan and the Rate of Its Enzymic-Hydrolysis. *Biomaterials, 10,* 574-576.

32. Hofland, H. E. J., Masson, C., Iginla, S., Osetinsky, I., Reddy, J. A., Leamon, C. P. et al. (2002). Folate-targeted gene transfer in vivo. *Molecular Therapy, 5,* 739-744.

33. Howling, G. I., Dettmar, P. W., Goddard, P. A., Hampson, F. C., Dornish, M., & Wood, E. J. (2001). The effect of chitin and chitosan on the proliferation of human skin fibroblasts and keratinocytes in vitro. *Biomaterials, 22,* 2959-2966.

34. Hwang, H. Y., Kim, I. S., Kwon, I. C., & Kim, Y. H. (2008). Tumor targetability and antitumor effect of docetaxel-loaded hydrophobically modified glycol chitosan nanoparticles. *Journal of Controlled Release, 128,* 23-31.

35. Illum, L., Farraj, N. F., & Davis, S. S. (1994). Chitosan As A Novel Nasal Delivery System for Peptide Drugs. *Pharmaceutical Research, 11,* 1186-1189.

36. Ishii, T., Okahata, Y., & Sato, T. (2001). Mechanism of cell transfection with plasmid/chitosan complexes. *Biochim.Biophys.Acta, 1514,* 51-64.

37. Jeon, S. I., Lee, J. H., Andrade, J. D., & Degennes, P. G. (1991). Protein Surface Interactions in the Presence of Polyethylene Oxide .1. Simplified Theory. *Journal of Colloid and Interface Science, 142,* 149-158.

38. Jiang, X., Dai, H., Leong, K. W., Goh, S. H., Mao, H. Q., & Yang, Y. Y. (2006). Chitosan-g-PEG/DNA complexes deliver gene to the rat liver via intrabiliary and intraportal infusions. *Journal of Gene Medicine, 8,* 477-487.

39. John Wiley and Sons Ltd. (2009). Gene Therapy Clinical Trials Worldwide. The Journal of Gene Medicine [On-line]. Available: http://www.wiley.co.uk/genmed/clinical/

40. Kabanov, A. V. & Kabanov, V. A. (1995). DNA complexes with polycations for the delivery of genetic material into cells. *Bioconjug.Chem., 6,* 7-20.

41. Kim, I. Y., Seo, S. J., Moon, H. S., Yoo, M. K., Park, I. Y., Kim, B. C. et al. (2008). Chitosan and its derivatives for tissue engineering applications. *Biotechnology Advances, 26,* 1-21.

42. Kim, T. H., Park, I. K., Nah, J. W., Choi, Y. J., & Cho, C. S. (2004). Galactosylated chitosan/DNA nanoparticles prepared using water-soluble chitosan as a gene carrier. *Biomaterials, 25,* 3783-3792.

43. Koping-Hoggard, M., Tubulekas, I., Guan, H., Edwards, K., Nilsson, M., Varum, K. M. et al. (2001). Chitosan as a nonviral gene delivery system. Structure-property relationships and characteristics compared with polyethylenimine in vitro and after lung administration in vivo. *Gene Ther., 8,* 1108-1121.

44. Koping-Hoggard, M., Varum, K. M., Issa, M., Danielsen, S., Christensen, B. E., Stokke, B. T. et al. (2004). Improved chitosan-mediated gene delivery based on easily dissociated chitosan polyplexes of highly defined chitosan oligomers. *Gene Ther., 11,* 1441-1452.

45. Lacroix, M. (2008). Persistent use of "false" cell lines. *International Journal of Cancer, 122,* 1-4.

46. Leamon, C. P. & Low, P. S. (1994). Selective Targeting of Malignant-Cells with Cytotoxin-Folate Conjugates. *Journal of Drug Targeting, 2,* 101-112.

47. Leamon, C. P., Low, P. S., & Turek, J. J. (1992). Cytotoxicity of Folate-Momordin Conjugates in Cultured Human-Cells. *Molecular Biology of the Cell, 3,* A117.

48. Leamon, C. P., Pastan, I., & Low, P. S. (1993). Cytotoxicity of Folate-Pseudomonas Exotoxin Conjugates Toward Tumor-Cells - Contribution of Translocation Domain. *Journal of Biological Chemistry, 268,* 24847-24854.

49. Leong, K. W., Mao, H. Q., Truong-Le, V. L., Roy, K., Walsh, S. M., & August, J. T. (1998). DNA-polycation nanospheres as non-viral gene delivery vehicles. *J.Control Release, 53,* 183-193.

50. Li, Q. J., Sun, X. L., & Antony, A. C. (1996). Regulation of folate receptors in human cervical carcinoma cells by the extracellular folate concentration:

Evidence for dominant modulation at the translational level associated with homeostatic changes. *Journal of Investigative Medicine, 44,* A203.

51. Li, S. & Huang, L. (2000). Nonviral gene therapy: promises and challenges. *Gene Ther., 7,* 31-34.

52. Li, X. B., Tushima, Y., Morimoto, M., Saimoto, H., Okamoto, Y., Minami, S. et al. (2000). Biological activity of chitosan-sugar hybrids: Specific interaction with lectin. *Polymers for Advanced Technologies, 11,* 176-179.

53. Liu, W. G. & De Yao, K. (2002). Chitosan and its derivatives - a promising non-viral vector for gene transfection. *Journal of Controlled Release, 83,* 1-11.

54. Lode, K., Fichtner, I., Kreuter, J., Berndt, A., Diederichs, J. E., & Reszka, R. (2001). Influence of surface-modifying surfactants on the pharmacokinetic behavior of C-14-poly (methylmethacrylate) nanoparticles in experimental tumor models. *Pharmaceutical Research, 18,* 1613-1619.

55. MacLaughlin, F. C., Mumper, R. J., Wang, J., Tagliaferri, J. M., Gill, I., Hinchcliffe, M. et al. (1998). Chitosan and depolymerized chitosan oligomers as condensing carriers for in vivo plasmid delivery. *J.Control Release, 56,* 259-272.

56. Macleod, R. A. F., Dirks, W. G., Matsuo, Y., Kaufmann, M., Milch, H., & Drexler, H. G. (1999). Widespread intraspecies cross-contamination of human tumor cell lines arising at source. *International Journal of Cancer, 83,* 555-563.

57. Mansouri, S., Cuie, Y., Winnik, F., Shi, Q., Lavigne, P., Benderdour, M. et al. (2006). Characterization of folate-chitosan-DNA nanoparticles for gene therapy. *Biomaterials, 27,* 2060-2065.

58. Mansouri, S., Lavigne, P., Corsi, K., Benderdour, M., Beaumont, E., & Fernandes, J. C. (2004). Chitosan-DNA nanoparticles as non-viral vectors in gene therapy: strategies to improve transfection efficacy. *European Journal of Pharmaceutics and Biopharmaceutics, 57,* 1-8.

59. Mao, H. Q., Roy, K., Troung-Le, V. L., Janes, K. A., Lin, K. Y., Wang, Y. et al. (2001). Chitosan-DNA nanoparticles as gene carriers: synthesis, characterization and transfection efficiency. *J.Control Release, 70,* 399-421.

60. Mao, S. R., Shuai, X. T., Unger, F., Simon, M., Bi, D. Z., & Kissel, T. (2004). The depolymerization of chitosan: effects on physicochemical and biological properties. *International Journal of Pharmaceutics, 281,* 45-54.

61. Masters, J. R. (2002a). False cell lines: The problem and a solution. *Cytotechnology, 39,* 69-74.

62. Masters, J. R. (2002b). HeLa cells 50 years on: the good, the bad and the ugly. *Nature Reviews Cancer, 2,* 315-319.

63. Min, K. H., Park, K., Kim, Y. S., Bae, S. M., Lee, S., Jo, H. G. et al. (2008). Hydrophobically modified glycol chitosan nanoparticles-encapsulated camptothecin enhance the drug stability and tumor targeting in cancer therapy. *Journal of Controlled Release, 127,* 208-218.

64. Morimoto, M., Saimoto, H., Usui, H., Okamoto, Y., Minami, S., & Shigemasa, Y. (2001). Biological activities of carbohydrate-branched chitosan derivatives. *Biomacromolecules, 2,* 1133-1136.

65. Murata, J., Ohya, Y., & Ouchi, T. (1997a). Design of quaternary chitosan conjugate having antennary galactose residues as a gene delivery tool. *Carbohydrate Polymers, 32,* 105-109.

66. Murata, J., Ohya, Y., & Ouchi, T. (1997b). Design of quaternary chitosan conjugate having antennary galactose residues as a gene delivery tool. *Carbohydrate Polymers, 32,* 105-109.

67. Muzzarelli, R. A. A. (1993). Biochemical Significance of Exogenous Chitins and Chitosans in Animals and Patients. *Carbohydrate Polymers, 20,* 7-16.

68. Muzzarelli, R. A. A. (1997). Human enzymatic activities related to the therapeutic administration of chitin derivatives. *Cellular and Molecular Life Sciences, 53,* 131-140.

69. Muzzarelli, R. A. A. & Muzzarelli, C. (2005). Chitosan chemistry: Relevance to the biomedical sciences. *Polysaccharides 1: Structure, Characterization and Use, 186,* 151-209.

70. Park, E. K., Kim, S. Y., Lee, S. B., & Lee, Y. M. (2005). Folate-conjugated methoxy poly(ethylene glycol)/poly(epsilon-caprolactone) amphiphilic block copolymeric micelles for tumor-targeted drug delivery. *J.Control Release, 109,* 158-168.

71. Park, J. H., Lee, S., Kim, J. H., Park, K., Kim, K., & Kwon, I. C. (2008). Polymeric nanomedicine for cancer therapy. *Progress in Polymer Science, 33,* 113-137.

72. Park, Y. K., Park, Y. H., Shin, B. A., Choi, E. S., Park, Y. R., Akaike, T. et al. (2000). Galactosylated chitosan-graft-dextran as hepatocyte-targeting DNA carrier. *Journal of Controlled Release, 69,* 97-108.

73. Parker, N., Turk, M. J., Westrick, E., Lewis, J. D., Low, P. S., & Leamon, C. P. (2005). Folate receptor expression in carcinomas and normal tissues determined by a quantitative radioligand binding assay. *Analytical Biochemistry, 338,* 284-293.

74. Prego, C., Torres, D., Fernandez-Megia, E., Novoa-Carballal, R., Quinoa, E., & Alonso, M. J. (2006). Chitosan-PEG nanocapsules as new carriers for oral peptide delivery - Effect of chitosan pegylation degree. *Journal of Controlled Release, 111,* 299-308.

75. Reddy, J. A., Abburi, C., Hofland, H., Howard, S. J., Vlahov, I., Wils, P. et al. (2002). Folate-targeted, cationic liposome-mediated gene transfer into disseminated peritoneal tumors. *Gene Therapy, 9,* 1542-1550.

76. Richardson, S. C., Kolbe, H. V., & Duncan, R. (1999). Potential of low molecular mass chitosan as a DNA delivery system: biocompatibility, body distribution and ability to complex and protect DNA. *Int.J.Pharm., 178,* 231-243.

77. Rothberg, K. G., Ying, Y. S., Kolhouse, J. F., Kamen, B. A., & Anderson, R. G. W. (1990). The Glycophospholipid-Linked Folate Receptor Internalizes Folate Without Entering the Clathrin-Coated Pit Endocytic Pathway. *Journal of Cell Biology, 110,* 637-649.

78. Roy, K., Mao, H. Q., Huang, S. K., & Leong, K. W. (1999). Oral gene delivery with chitosan--DNA nanoparticles generates immunologic protection in a murine model of peanut allergy. *Nat.Med., 5,* 387-391.

79. Rubanyi, G. M. (2001). The future of human gene therapy. *Mol.Aspects Med., 22,* 113-142.

80. Sashiwa, H., Shigemasa, Y., & Roy, R. (2001). Preparation and lectin binding property of chitosan-carbohydrate conjugates. *Bulletin of the Chemical Society of Japan, 74,* 937-943.

81. Shmeeda, H., Mak, L., Tzemach, D., Astrahan, P., Tarshish, M., & Gabizon, A. (2006). Intracellular uptake and intracavitary targeting of folate-conjugated liposomes in a mouse lymphoma model with up-regulated folate receptors. *Mol.Cancer Ther., 5,* 818-824.

82. Stella, B., Arpicco, S., Peracchia, M. T., Desmaele, D., Hoebeke, J., Renoir, M. et al. (2000). Design of folic acid-conjugated nanoparticles for drug targeting. *Journal of Pharmaceutical Sciences, 89,* 1452-1464.

83. Storm, G., Belliot, S. O., Daemen, T., & Lasic, D. D. (1995). Surface Modification of Nanoparticles to Oppose Uptake by the Mononuclear Phagocyte System. *Advanced Drug Delivery Reviews, 17,* 31-48.

84. Sudimack, J. & Lee, R. J. (2000). Targeted drug delivery via the folate receptor. *Advanced Drug Delivery Reviews, 41,* 147-162.

85. Sugimoto, M., Morimoto, M., Sashiwa, H., Saimoto, H., & Shigemasa, Y. (1998). Preparation and characterization of water-soluble chitin and chitosan derivatives. *Carbohydrate Polymers, 36,* 49-59.

86. Thanou, M., Florea, B. I., Geldof, M., Junginger, H. E., & Borchard, G. (2002). Quaternized chitosan oligomers as novel gene delivery vectors in epithelial cell lines. *Biomaterials, 23,* 153-159.

87. Toffoli, G., Cernigoi, C., Russo, A., Gallo, A., Bagnoli, M., & Boiocchi, M. (1997). Overexpression of folate binding protein in ovarian cancers. *International Journal of Cancer, 74,* 193-198.

88. Wagner, E., Cotten, M., Mechtler, K., Kirlappos, H., & Birnstiel, M. L. (1991). Dna-Binding Transferrin Conjugates As Functional Gene-Delivery Agents - Synthesis by Linkage of Polylysine Or Ethidium Homodimer to the Transferrin Carbohydrate Moiety. *Bioconjugate Chemistry, 2,* 226-231.

89. Weitman, S. D., Lark, R. H., Coney, L. R., Fort, D. W., Frasca, V., Zurawski, V. R. et al. (1992a). Distribution of the Folate Receptor Gp38 in Normal and Malignant-Cell Lines and Tissues. *Cancer Research, 52,* 3396-3401.

90. Weitman, S. D., Weinberg, A. G., Coney, L. R., Zurawski, V. R., Jennings, D. S., & Kamen, B. A. (1992b). Cellular-Localization of the Folate Receptor - Potential Role in Drug Toxicity and Folate Homeostasis. *Cancer Research, 52,* 6708-6711.

91. Won, Y. Y. (2004). Imaging nanostructured fluids using cryo-TEM. *Korean Journal of Chemical Engineering, 21,* 296-302.

92. Yoo, H. S. & Park, T. G. (2004). Folate-receptor-targeted delivery of doxorubicin nano-aggregates stabilized by doxorubicin-PEG-folate conjugate. *Journal of Controlled Release, 100,* 247-256.

93. Yoshida, T., Oide, N., Sakamoto, T., Yotsumoto, S., Negishi, Y., Tsuchiya, S. et al. (2006). Induction of cancer cell-specific apoptosis by folate-labeled cationic liposomes. *Journal of Controlled Release, 111,* 325-332.

94. You, J. O., Liu, Y. C., & Peng, C. A. (2006). Efficient gene transfection using chitosan-alginate core-shell nanoparticles. *International Journal of Nanomedicine, 1,* 173-180.

95. Zhang, L., Guo, J., Peng, X. H., & Jin, Y. (2004). Preparation and release behavior of carboxymethylated chitosan/alginate microspheres encapsulating bovine serum albumin. *Journal of Applied Polymer Science, 92,* 878-882.

96. Zhang, Q., Xiang, G. Y., Zhang, Y. J., Yang, K. Y., Fan, W., Lin, J. L. et al. (2006). Increase of doxorubicin sensitivity for folate receptor positive cells when given as the prodrug N-(phenylacetyl) doxorubicin in combination with folate-conjugated PGA. *Journal of Pharmaceutical Sciences, 95,* 2266-2275.

97. Zhao, H. Z., Yue, L., & Yung, L. (2008). Selectivity of folate conjugated polymer micelles against different tumor cells. *International Journal of Pharmaceutics, 349,* 256-268.

98. Zhao, X. B. & Lee, R. J. (2004). Tumor-selective targeted delivery of genes and antisense oligodeoxyribonucleotides via the folate receptor. *Adv.Drug Deliv.Rev., 56,* 1193-1204.

APPENDIX A
NMR SPECTRA

^{1}H NMR spectra for the folate molecule as well as chitosan-PEG-folate samples as prepared by the protocol designed by Qiu are depicted below, as they were not included in results. Folate appears in Appendix A Figure 1, while spectra for chitosan-PEG-folate2a, -3, -1b, -2b, and -5 follow as Appendix A Figures 2 through 6.

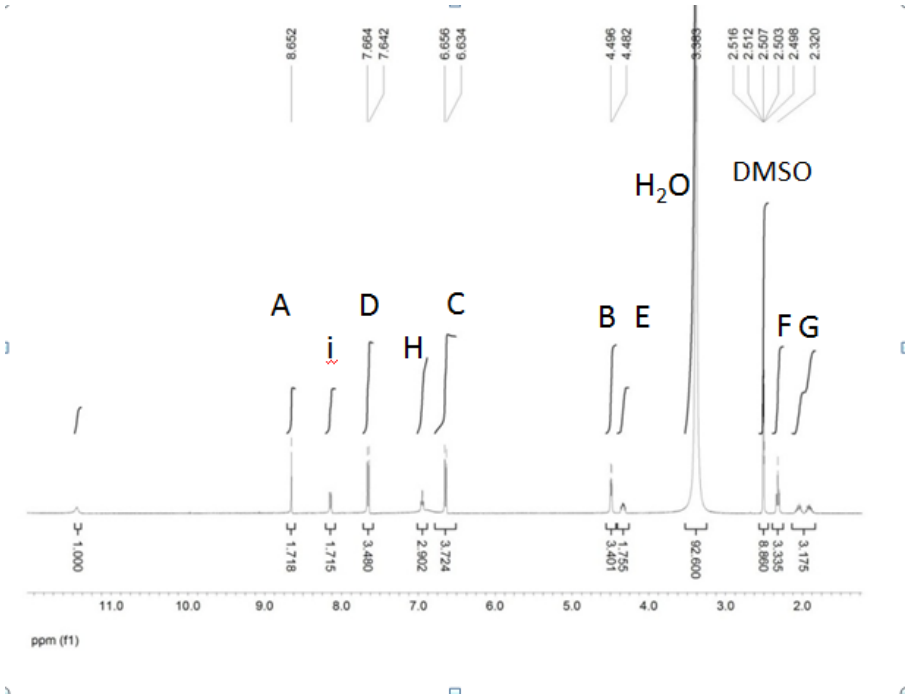

Appendix A Figure 1 ^{1}H NMR spectrum of folate. Solvent is deuterated DMSO.

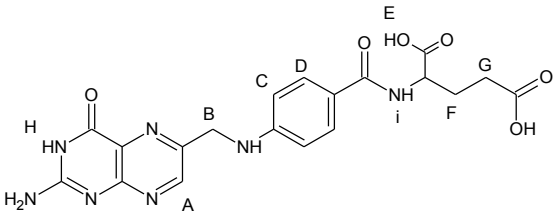

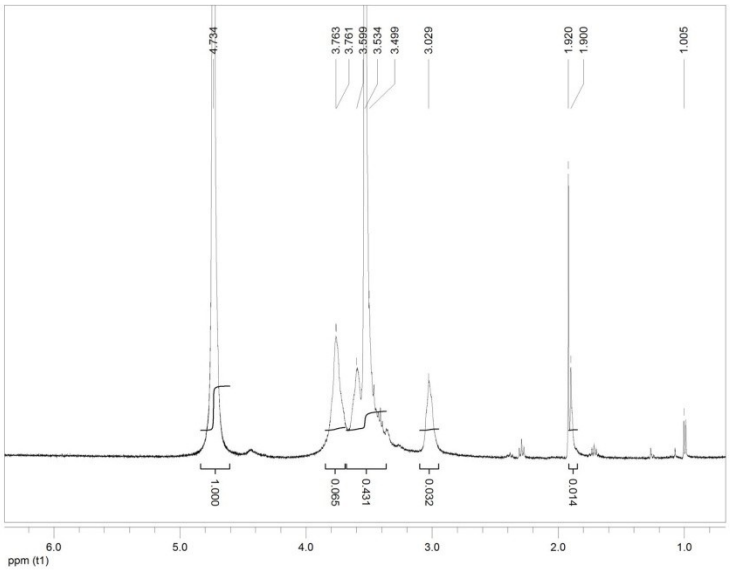

Appendix A Figure 2 ^{1}H NMR spectrum of chitosan-PEG-folate 2a in 1%DCl in D_2O

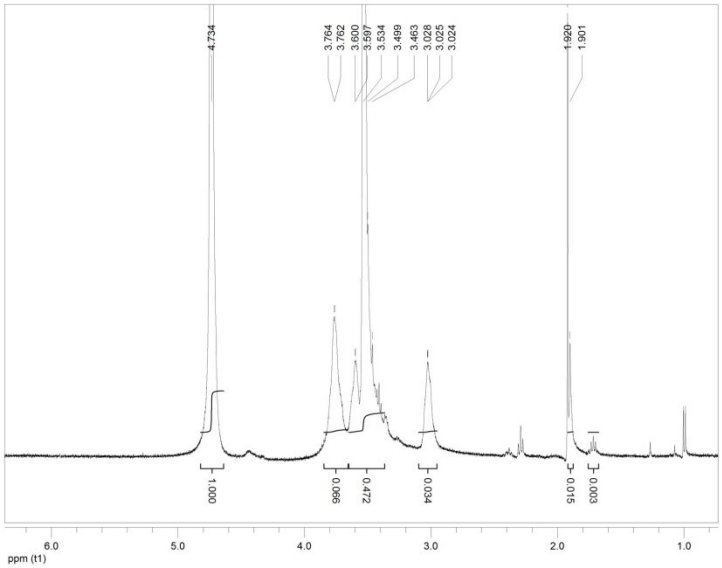

Appendix A Figure 3 ^{1}H NMR spectrum of chitosan-PEG-folate3 in 1%DCl in D_2O

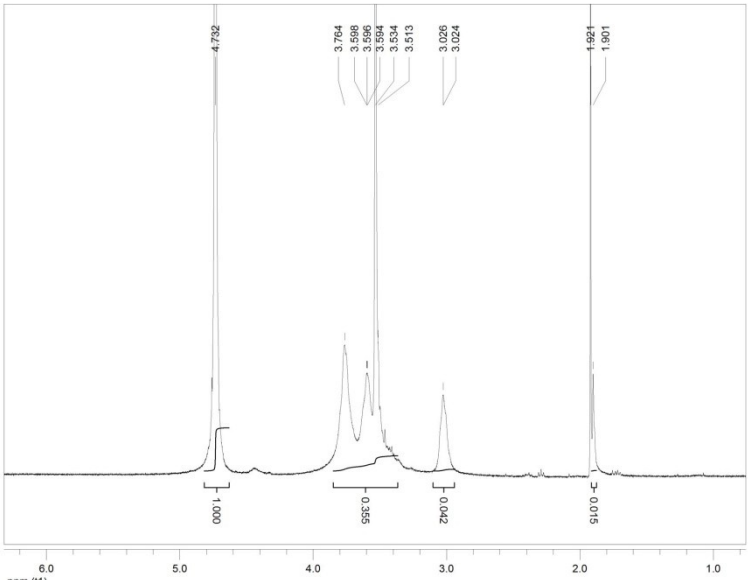

Appendix A Figure 4 ^{1}H NMR spectrum of chitosan-PEG-folate1b in 1%DCl in D_2O

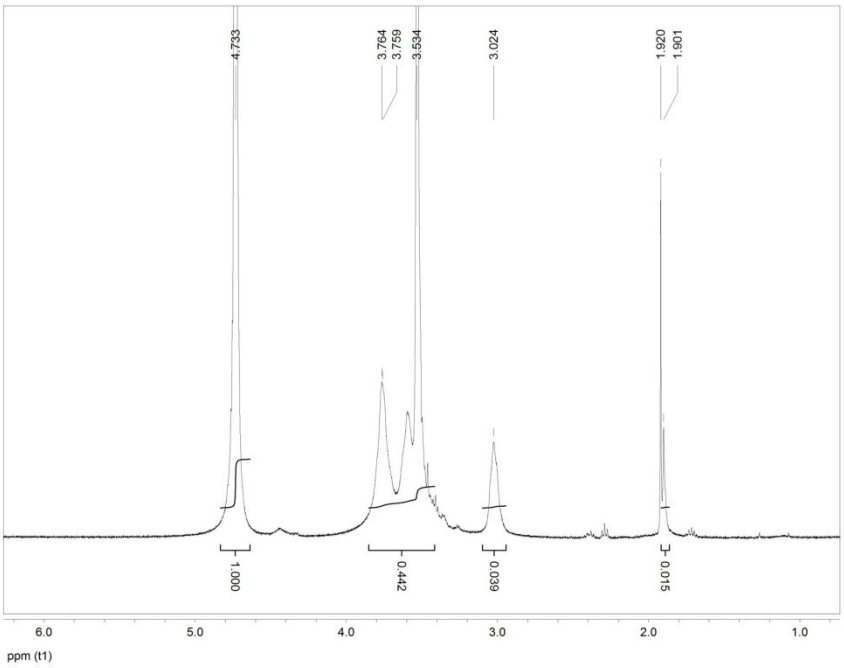

Appendix A Figure 5 ^{1}H NMR spectrum of chitosan-PEG-folate2b in 1%DCl in D_2O

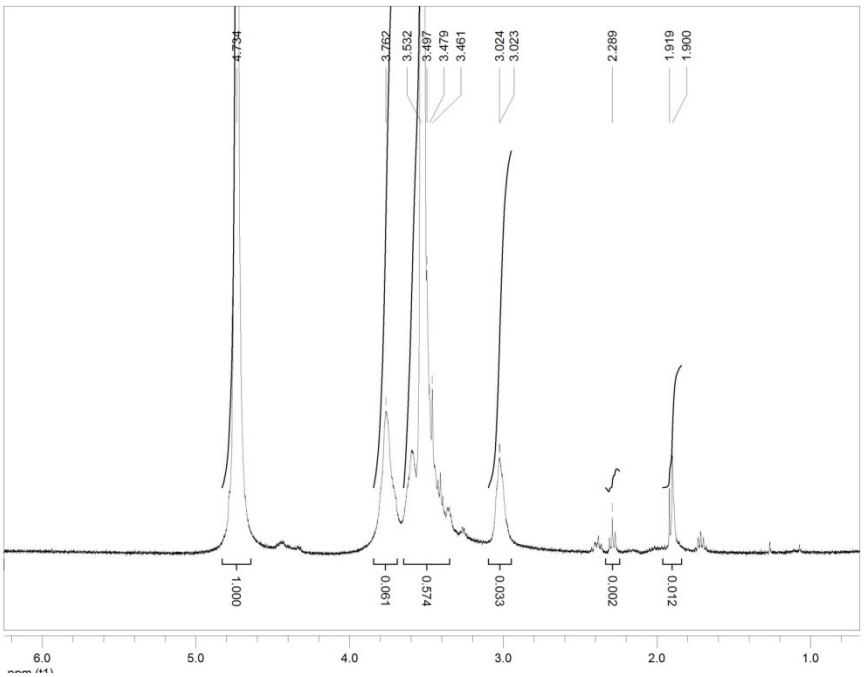

Appendix A Figure 6 ^{1}H NMR spectrum of chitosan-PEG-folate5 in 1% DCl in D_2O

A summary of peak integrations appears below in Appendix A Table 1.

*Note that all integrations for H3-6 include the peak of PEG at 3.7 ppm, with the exception of un-modified chitosan sample.

Appendix A Table 1 Peak assignment for chitosan-PEG-folate (Qiu) samples.

	H_{ACETYL}	H-2	*H3-6
Sample ID	**2.0ppm**	**3.0ppm**	**3.3-4.0ppm**
chitosan	3.359	11.421	67.339
ChiPEGFA1a	0.016	0.042	0.335
ChiPEGFA1b	0.015	0.042	0.355
ChiPEGFA2a	0.014	0.032	0.496
ChiPEGFA2b	0.015	0.039	0.442
ChiPEGFA3	0.015	0.034	0.538
ChiPEGFA5	0.012	0.033	0.635

Representative ^{1}H NMR of chitosan-PEG-folate samples as prepared through the protocol designed by Chan *et al*., are depicted as Appendix A Figure 7 and Appendix A Figure 8,

and serve to display the difference in clarity of signal and presence of un-identified peaks, as compared to those samples prepared through the protocol designed by Qiu.

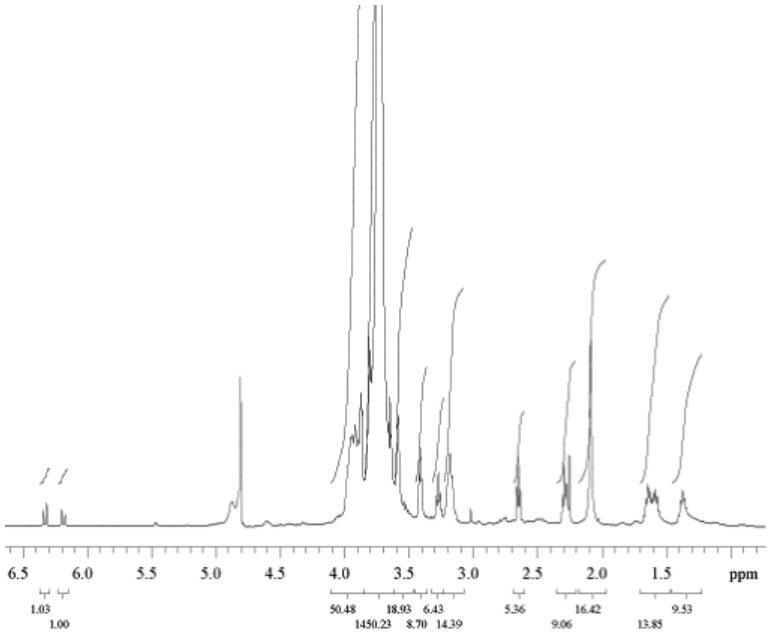

Appendix A Figure 7 ^{1}H NMR spectrum of chitosan-PEG-folate9.1 in D_2O with acetic acid-d_6, synthesized via the Chan protocol.

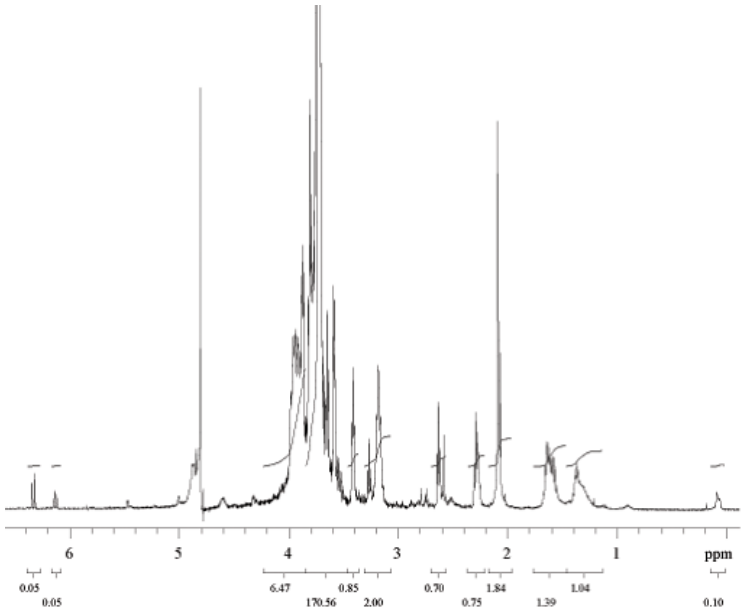

Appendix A Figure 8 ^{1}H NMR spectrum of chitosan-PEG-folate7.25 in D_2O with acetic acid-d_6, as synthesized by the Chan protocol.